REPORT DOCUMENTATION PAGE

1. REPORT DATE (DD-MM-YYYY) 30-Apr-2006	2. REPORT TYPE Final	3. DATES COVERED (From - To) –

4. TITLE AND SUBTITLE	5a. CONTRACT NUMBER
Comparison of Predicted and Measured Wavefields for Model 5365 Hull Form	5b. GRANT NUMBER
	5c. PROGRAM ELEMENT NUMBER

6. AUTHOR(S)	5d. PROJECT NUMBER
Wesley Wilson	5e. TASK NUMBER
Thomas Fu	
Anne Pence	5f. WORK UNIT NUMBER

7. PERFORMING ORGANIZATION NAME(S) AND ADDRESS(ES) AND ADDRESS(ES)	8. PERFORMING ORGANIZATION REPORT NUMBER
Naval Surface Warfare Center Carderock Division 9500 Macarthur Boulevard West Bethesda, MD 20817-5700	NSWCCD-50-TR-2006/014

9. SPONSORING / MONITORING AGENCY NAME(S) AND ADDRESS(ES)	10. SPONSOR/MONITOR'S ACRONYM(S)
Attn ONR Chief of Naval Research Ballston Centre Tower One 800 North Quincy Street Arlington, VA 22217-5660	
	11. SPONSOR/MONITOR'S REPORT NUMBER(S)

12. DISTRIBUTION / AVAILABILITY STATEMENT
Approved for public release; distribution unlimited.

13. SUPPLEMENTARY NOTES

14. ABSTRACT
David Taylor Model Basin Model 5365 (R/V Athena) was chosen by the Office of Naval Research (ONR) to be used to establish the current state of Computational Fluid Dynamics (CFD) capability in predicting ship generated wave fields. CFD solutions for two cases: 1) FrL=0.25, U=1.88 m/s (6.17 ft/s), and 2) FrL=0.43, U=3.22 m/s (10.58 ft/s) were generated by several organizations and submitted to the workshop. The codes and organizations are as follows: Das Boot – SAIC, Naval Hydrodynamics Group, La Jolla, CA, Numerical Flow Analysis (NFA) – SAIC, Naval Hydrodynamics Group, La Jolla, CA and Massachusetts Institute of Technology, CFDSHIP-IOWA, Fluent, and Comet – NSWCCD, Code 5400, and CFDSHIP-IOWA – University of Iowa, Iowa Institute of Hydraulic Research. These predictions were compared to measurements of the wave field performed by NSWCCD, Code 5600 and reported in Fu et al (2005). This report will document these comparisons and summarize the results and conclusions of the workshop.

15. SUBJECT TERMS
Hydrodynamics   Free Surface   RANS   Wave Breaking   VOF

16. SECURITY CLASSIFICATION OF:			17. LIMITATION OF ABSTRACT	18. NUMBER OF PAGES	19a. NAME OF RESPONSIBLE PERSON Wesley M. Wilson
a. REPORT UNCLASSIFIED	b. ABSTRACT UNCLASSIFIED	c. THIS PAGE UNCLASSIFIED	SAR	80+vi	19b. TELEPHONE NUMBER (include area code) (301) 227-5407

CONTENTS

FIGURES

TABLES

ABSTRACT

David Taylor Model Basin Model 5365 (R/V Athena) was chosen by the Office of Naval Research (ONR) to be used to assess the current state of Computational Fluid Dynamics (CFD) capability in predicting ship generated wave fields. CFD solutions for two cases: 1) Fr_L=0.25, U=1.88 m/s (6.17 ft/s), and 2) Fr_L=0.43, U=3.22 m/s (10.58 ft/s) were generated by several organizations and submitted to the workshop. The codes and organizations are as follows: Das Boot - SAIC, Naval Hydrodynamics Group, La Jolla, CA, Numerical Flow Analysis (NFA) - SAIC, Naval Hydrodynamics Group, La Jolla, CA and Massachusetts Institute of Technology, CFDSHIP-IOWA, Fluent, and Comet – NSWCCD, Code 5400, and CFDSHIP-IOWA – University of Iowa, Iowa Institute of Hydraulic Research. These predictions were compared to measurements of the wave field obtained by NSWCCD, Code 5600 and reported in Fu, *et al.* (2005)[1]. This report will document these comparisons and summarize the results and conclusions of the workshop.

ADMINISTRATIVE INFORMATION

---

[1] References are listed on page 78.

INTRODUCTION

Computational Fluid Dynamics (CFD) codes have demonstrated increasing fidelity in predicting the large-scale Kelvin wave structure for a variety of craft. However, except perhaps for computationally-intensive high-resolution models constructed specifically for that purpose, CFD codes do not, in general, reproduce the short-scale surface evolution or the energy dissipation and turbulence of the breaking wave regions of ship generated wave fields. Since the energy in breaking and other nonlinear events is not redistributed in a consistent manner, wave amplitudes can be over predicted. In the past, the regions of breaking predicted by codes were, in fact, dependent on the specific empirically-based breaking criteria assumed. More recently developed higher-order CFD codes, utilizing level-set and volume-of-fluid schemes to handle the free-surface, may in fact, when run with sufficient resolution, be able to predict these breaking regions.

In order to improve the correspondence of CFD code predictions to the full-scale phenomena (while keeping the computational load tractable), we must focus on understanding how the extent of breaking and nonlinear events may be better accommodated within the existing model framework and, ultimately, on how the crucial aspects of energy redistribution can best be reproduced. By employing model-scale measurements in a controlled environment, we can bridge the gap between CFD predictions and full-scale behavior in the wake region. That is, model-scale measurements can be utilized to characterize the mean elevation and surface roughness in the Kelvin wave system, and thereby to deduce the distribution of wave-breaking and energy dissipation. This in turn can be compared to CFD predictions: first, to evaluate how various breaking criteria employed in potential flow codes either increase or decrease the correspondence of predicted breaking regions to the model-scale measurements of breaking; and second, to evaluate how higher-order CFD predictions provide a better match when applied in nonlinear regions of the wake. It is this strategy that the Office of Naval Research (ONR) Ship Wavebreaking and Bubbly Wake Program has undertaken in 2004-2005, and the work described herein is part of that effort.

In 2004, as part of the ONR Ship Wavebreaking Workshop & Review, a focused effort was made to assess the CFD capability as applied to ship generated waves and wave breaking. Predictions of the wave field around Model 5365 were made by four separate groups, utilizing five CFD codes. One code, CFDSHIP-IOWA (Paterson, Wilson and Stern, 2003)[2], was run by two different groups utilizing two distinct grids. All together, seven separate solution sets were submitted for each of the test conditions requested. Model testing was also performed and used to assess code performance and aid in code development. This report describes the CFD capabilities assessment. Further details regarding the model testing are provided in Fu, *et al.* (2005)[1].

Model 5365 was chosen as the hull form geometry to be utilized in this code evaluation and assessment effort. Model 5365 is a 1/8.25-scale model of the R/V Athena. The R/V Athena is a converted PG-84 Asheville-class patrol gunboat. It is capable of greater than 18 m/s (59 ft/s), or 35 knots, and has a high speed transom stern. This choice of geometry allowed for data to be obtained over a large Froude number range. The

Froude Number is defined as

$$Fr_L \; ? \; \frac{V}{\sqrt{g \, ? L}} \tag{1}$$

where V is the ship velocity, g is the acceleration due to gravity, and L is the ship length. The high-speed transom stern provided the opportunity to test and predict the wave field for both wet and dry transom conditions. Utilizing the Model 5365 hull form also enables comparison with full-scale phenomena, as there is also an ONR effort utilizing the R/V Athena I as a test platform, establishing a database of both qualitative and quantitative information at a variety of ship speeds. To correspond closely to this full-scale work, model-scale measurements have been made at 5.4, 9.3, 13.3, and 15.4 m/s (17.7, 30.4, 43.5, and 50.6 ft/s) or 10.5, 18.0, 25.8, and 30.0 knots. The model was tested unpropelled and unappended to simplify the CFD prediction task.

The objectives of the model test were to:

?   Measure the mean wave elevation and characterize the extent of breaking around Model 5365.

?   Measure the total resistance and sinkage and trim of the hullform.

?   Measure the far-field longitudinal wave field and compute wave resistance.

3

MODEL DESCRIPTION

Model 5365 is a wood and fiberglass model of the R/V Athena, first tested in 1979 as part of the First Workshop on Ship Wave-Resistance Computations. Due to the age and condition of the model, the model was patched, re-painted and measured to determine its actual geometry. A photograph of the *R/V Athena I* is shown in Figure 1, and the model and full-scale hullform characteristics are shown in Table 1. The model was tested unappended at a displacement which matched the displacement of the *R/V Athena I* during the 2004 ONR field test of that ship[1], during which the ship was tested at a light load condition.

Figure 1. The *R/V Athena I*.

The detailed measurement of the model revealed an asymmetry in the hull near the bow. This asymmetry, which can be seen in Figure 2, is shallow (< 1 mm (0.04 in)), but is found near the bow on the starboard side of the model. The actual, as tested, detailed surface geometry of Model 5365 is available from NSWCCD by request. Figure 3 shows the transom and bow regions of the model. The model was painted black on the starboard side, to minimize laser reflections, and yellow on the port side, to aid in visualizing the breaking bow wave. Station markings and waterlines were also marked.

Table 1: Model 5365 and Full-Scale (R/V Athena) Hull Form Characteristics

	Model Scale	Full Scale
Displacement	397 kg (875 lbs)*	229 metric tons (225 long tons)
Draft (hull)	0.19 m (0.618 ft)*	1.7 m (5.5 ft)
Max. Draft (overall)		3.2 m (10.5 ft)
Maximum Beam	0.84 m (2.74 ft)	6.9 m (22.6 ft)
Transom Beam	0.70 m (2.3 ft)	5.8 m (19.0 ft)
LBP	5.69 m (18.67 ft)	46.9 m (154.0 ft)
Scale Ratio	8.25	

*As tested (model was ballasted to match the 2004 ONR Athena Field Test displ.).

4
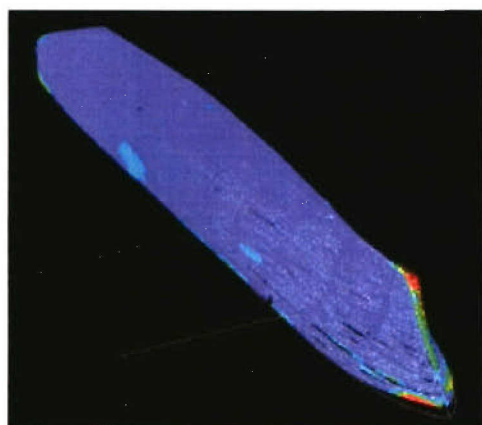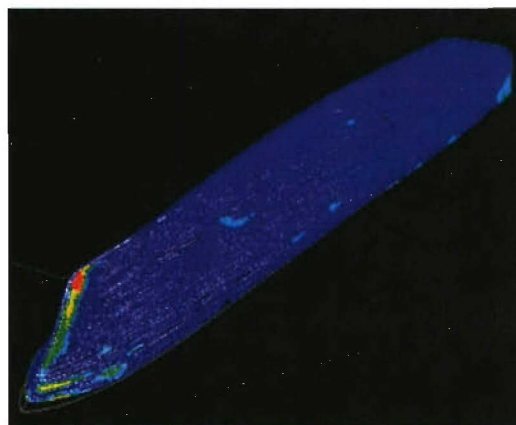
a) Port side.

b) Starboard side.

Figure 2: Contour maps of the deviation (Blue =0.0, Red =1.0 mm (0.04 in)) from the design geometry for Model 5365.
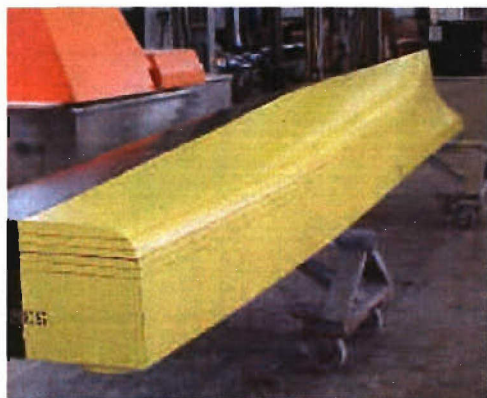
a) Port side.

b) Transom
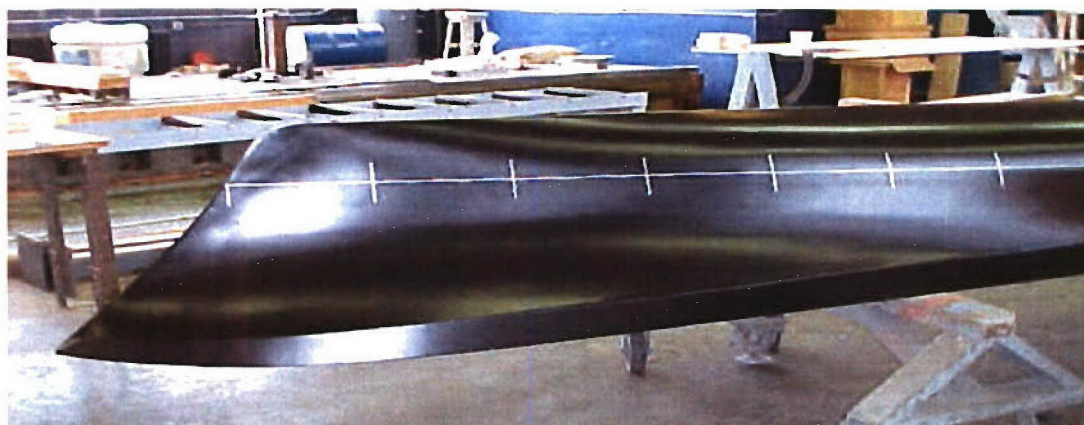
c) Bow region – starboard side.

Figure 3: Images of Model 5365 showing the yellow and black paint scheme, waterlines, and station lines.

MEASUREMENT METHODS

This section provides a brief explanation of the methods used to acquire the experimental measurements. Further details regarding these methods, including calibration and experimental setup, are provided in Fu, *et al.* (2005)[1].

Wave Cut Capacitance Probes (Longitudinal Wave Height Measurement)

Capacitance probes were used to determine wave heights. Wave cuts were obtained using a modified and strengthened capacitance wave probe system that was previously evaluated in the Circulating Water Channel at NSWC, Carderock Division.

Theory of Operation

The sensing element of the capacitance probe is a 30-gauge (AWG) solid silver-plated copper wire with 0.11 mm (0.045 in) kynar insulation, approximately 91 cm (36 in) in length. Attached to the sensing element is a weighted 1.2 m (4 ft) length of Mylar fishing line, used to provide probe stability in waves. The sensing element is suspended with half its length submerged in the basin. The basin water provides the ground reference for the sensing elements on the circuit card. With the copper wire completely insulated from the water, the sensing element behaves as a capacitor with one plate being the copper wire, the second plate the water, and the wire insulation acting as a dielectric. As waves in the basin change the submerged height of the sensing element, they change the effective capacitor plate size, which results in a change in capacitance. The change in capacitance is proportional to the wave height, which can then be calculated. By attaching the wave wire, a varying capacitor, to a timing circuit, a DC voltage is generated that is directly proportional to the capacitance of the probe and therefore, the wave height.

Conductivity Finger Probes (Stern Topography)

Finger probes, which measure the height of the free-surface, were used to measure the stern topography behind the model.

Theory of operation

Conductivity finger probes were developed by Steve McGuigan at NSWCCD and are routinely used to characterize wave heights on the free surface. The finger probe is a vertically oriented, mechanized probe that continuously searches for the free surface. The sensing element of the probe is a 0.038 cm (0.015 in) diameter, 5 cm (2 in) long stainless steel wire. The wire is mounted into a copper tube, which makes up the body of the probe. A geared rack, attached to the probe body, allows the probe to be driven up and down in the vertical plane by a servomotor. Electrical continuity through the probe is sensed by an electronic circuit, which drives the servomotor. When the probe is not in contact with the water surface, there is no electrical continuity through the probe and the servomotor drives the probe toward the surface of the water. Once contact is made between the probe and the surface of the water (circuit ground), electrical continuity is sensed and the probe is driven up out of the water. This process is continuously repeated, causing the probe to oscillate at the free surface at approximately 10 Hz. The probe is

also geared to a potentiometer to track its position along the z-axis (wave height). Probe position is only recorded by a sample and hold circuit during the instant the probe makes initial contact with the water surface. This manner of sampling probe position alleviates position error, from meniscus effects due to surface tension.

Quantitative Visualization (Free-Surface Elevation Mapping)

A non-intrusive optical technique, Quantitative Visualization (QViz), has been developed to measure the free-surface disturbances occurring in regions commonly inaccessible to more traditional measurement methods, i.e. near wake flows, bow sheets and breaking waves. These regions are generally difficult to quantify due to the multiphase aspect of the flow as well as their very unsteady nature. However, the unsteady surfaces, droplets and bubbles in these regions are effective scatterers and allow for optical imaging of the deformations of the surface. Initially used to measure the wave field around ship models[3], this technique has been used extensively to measure free-surface elevations and breaking waves [4,5].

Technique Description

In QViz the free-surface is illuminated by a laser light sheet, generated by a scanning mirror or cylindrical lens, and imaged using a monochrome progressive scan camera (see Figure 4). The recorded digital images are then corrected for distortion and calibrated. The corrected images are then processed to provide the free-surface elevation in the image plane of the camera. The free-surface elevation is determined by utilizing several edge detection image processing techniques.
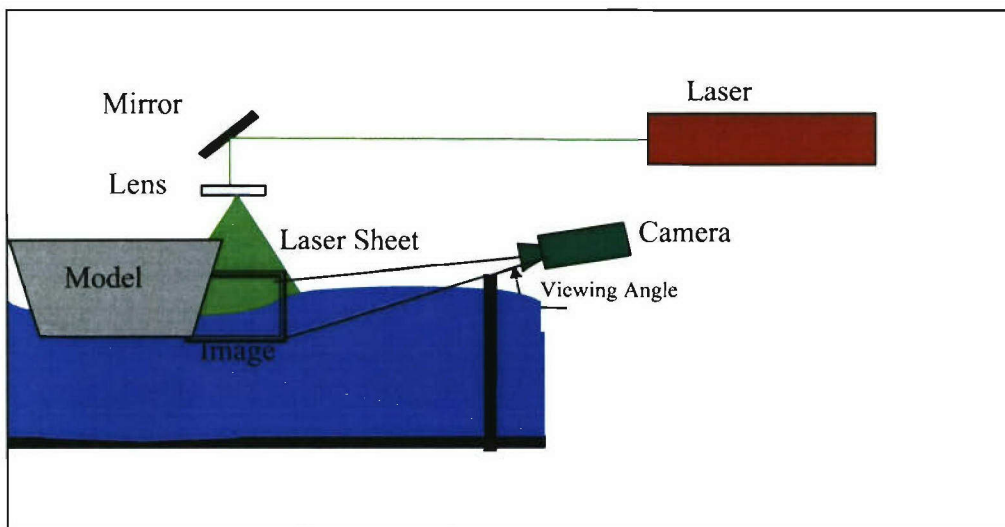
Figure 4: Sketch showing the generalized QViz set-up. The laser sheet can be generated from a cylindrical lens or scanning mirror.

Block Gages & String Potentiometers (Resistance, Sinkage & Trim)

Two calibrated 10-cm (4-in)ch block gages, one 45-kg (100-lb) and one 9-kg (20-lb), were used to measure the drag and side force, respectively.

<u>Experimental Setup</u>

A 91-kg (200-lb) tow post was positioned at station 5 in the model and a grasshopper was attached to the stern (see Figure 5). Mounted to the tow post was a 45-kg (100-lb), 10-cm (4-inch), block gage to measure drag and a 9-kg (20-lb), 10-cm (4-inch) block gage to measure side force. A pitch-roll gimbal (with fixed roll) joined the block gages to the model. Trim was measured using string potentiometers located at the bow and stern of the model. The distance between the string pots was 4.991 m (196.5 in). The forward string pot was located 0.552 m (21.75 in) aft of the Forward Perpendicular and the aft string pot was located 0.146 m (5.75 in) forward of the Aft Perpendicular.
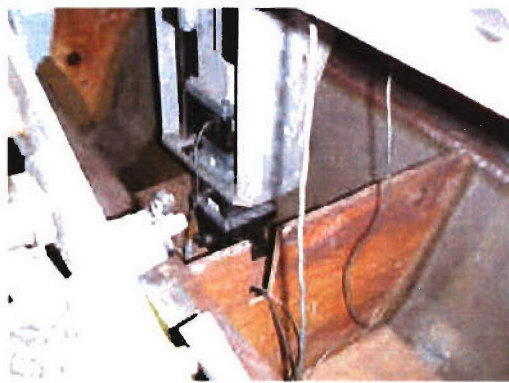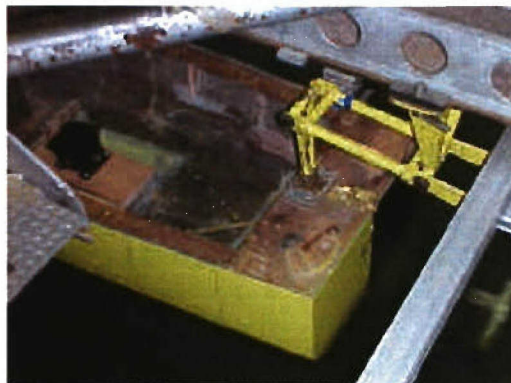
(a)   (b)

Figure 5: Images of Model 5365 rigged with a) a 91-kg (200-lb) tow post and b) a stern Grasshopper for sinkage and trim measurements.

TEST DESCRIPTION

The test was conducted 5-16 November, 2004, on Carriage 1, in the Shallow Water Towing Basin at NSWCCD. The tow tank is approximately 256 m (840 ft) long, 15.5 m (50.9 ft) wide, and 7 m (22 ft) deep. Carriage 1 has a speed range of 0.3 to 9.3 m/s (0.8 to 30.4 ft/s), or 0.5 to 18.0 knots, and the speed was monitored and recorded for each run, for the entire run. The model was newly painted and run without appendages (rudders, shafts, struts and propellers) or a trip wire.

Due to the number of desired measurements, there is significant risk in requiring simultaneous measurements, because the probability of a successful run is the product of all of the individual success rates for each system involved. Additionally, there are conflicting parameters between the instrumentation systems; for example, to increase the signal to noise ratio in the QViz images, low ambient light levels are desired, but light is needed for the standard video cameras used to visually characterize the wave field. Since the objective was time-averaged data, it was prudent to divide the test into the following three parts.

Part 1: Measurement of Resistance and Sinkage and Trim

With the model rigged to be free to sink and trim, resistance and sinkage and trim were measured for model speeds ranging from 1.1 to 6.2 m/s (3.5 to 20.5 ft/s,) corresponding to full-scale speeds of 3.1 to 18 m/s (10.1 to 59.1 ft/s), or 6 to 35 knots. At least two runs were made at each speed.

Part 2: Wave Field Topography

The wave field topography measurements were made at four speeds. The 91-kg (200-lb) tow post and grasshopper were replaced by adjustable tow posts, allowing for the model to be run at fixed sinkage and trim. For each speed, the model was fixed at the sinkage and trim measured in Part 1 of the test for that speed. Specifying and setting the sinkage and trim provided for more control of the run to run variability and allowed for the finger probes to be positioned more closely to the transom, since the model could not move into the probes as is possible when the model is free. At least two complete mappings were made at each of the four model speeds, 1.88, 3.22, 4.62, and 5.37 m/s (6.17, 10.58, 15.16, and 17.63 ft/s), corresponding to full-scale speeds of 5.4, 9.3, 13.3, and 15.4 m/s (17.7, 30.4, 43.5, and 50.6 ft/s), or 10.5, 18, 25.8 and 30 knots.

Part 3: Wave Cuts and Visual Characterization

Similar to Part 2, the model was held fixed in the correct position for each speed (the same four speeds as in Part 2) and the longitudinal wave field was measured by four capacitance probes from the wave boom. Three video cameras were also used to provide a visual record of the wave field for each speed.

9

EXPERIMENTAL RESULTS

Resistance and Sinkage and Trim

The measured sinkage and trim and resistance are shown in Figure 6 and Figure 7, respectively, and given in Table 2 and Table 3. Figure 6 also shows Model 5365 resistance data taken in 1979 (Jenkins, 1984)[6] and 1992. The 1979 test was performed with a skeg; the 1992 test was done with the model in a fully-appended configuration, while the current (2004) test was performed on the bare hull. These configuration differences can be seen in the resistance curves and should have less effect on the sinkage and trim. Trim and sinkage are reported as displacement of the forward and aft perpendiculars from their zero speed position.
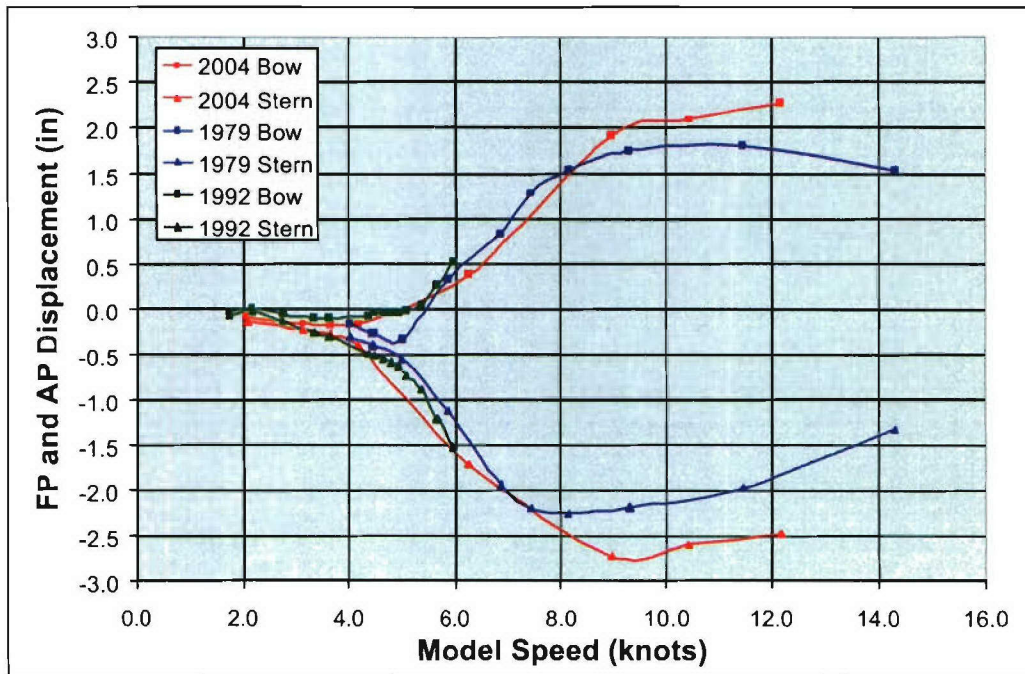
Figure 6: Sinkage and trim for Model 5365, described as the displacement of the Forward and Aft Perpendiculars from their zero speed position.
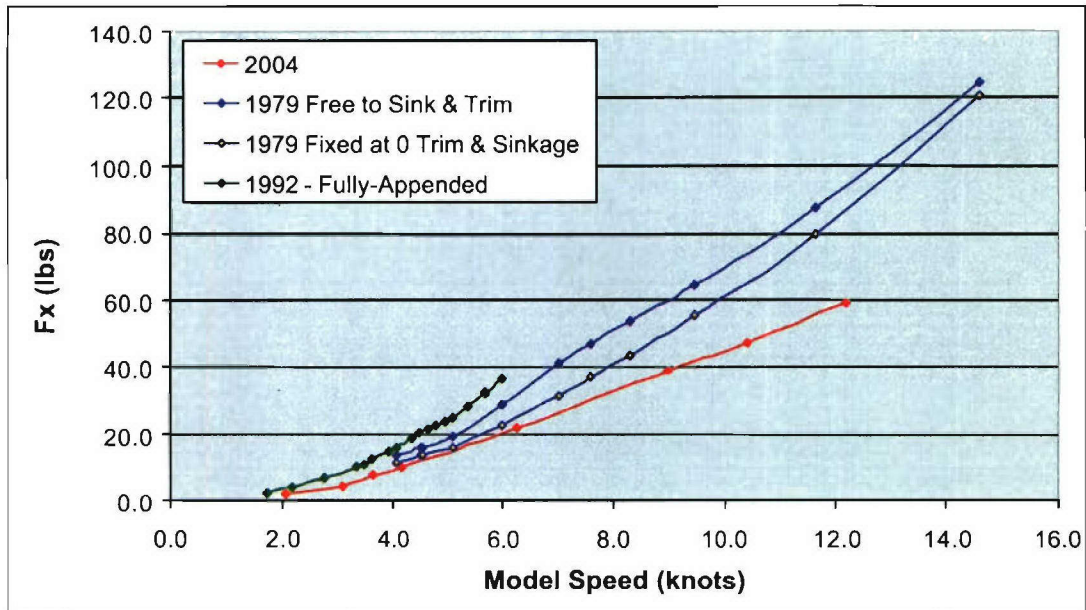
Figure 7: Model 5365 total resistance (lbs) versus speed for three different tests.

It should be noted that the 2004 resistance is significantly lower than the 1979 free to sink and trim data. Since in 2004 the model was tested at a lighter displacement, the zero speed wetted surface areas are different for the two data sets. By computing C_T, the total drag coefficient, we can more meaningfully compare the 2004 to the 1979 data. At 1.88 m/s (6.17 ft/s), $C_T=4.23$ and 5.58, for 2004 and 1979, respectively. So there is a significant difference in the measured resistance between the 1979 and 2004 tests, even when the variation in wetted surface area is accounted for.

Table 2: Model 5365 Trim Data

Full-Scale Speed (m/s (ft/s, knots))	Model-Scale Speed (m/s (ft/s, knots))	Forward Perpendicular Trim (cm (in)) + bow up, - bow down	Aft Perpendicular Trim (cm (in)) + bow up, - bow down
3.1 (10.1, 6.0)	1.08 (3.53, 2.09)	-0.224 (-0.088)	-0.338 (-0.133)
4.6 (15.2, 9.0)	1.62 (5.30, 3.14)	-0.386 (-0.152)	-0.564 (-0.222)
5.4 (17.7, 10.5)	1.88 (6.17, 3.66)	-0.409 (-0.161)	-0.688 (-0.271)
6.2 (20.3, 12.0)	2.15 (7.06, 4.18)	-0.399 (-0.157)	-0.996 (-0.392)
9.3 (30.4, 18.0)	3.22 (10.58, 6.27)	0.983 (0.387)	-4.318 (-1.700)
13.3 (43.5, 25.8)	4.62 (15.16, 8.99)	4.902 (1.930)	-6.909 (-2.720)
15.4 (50.6, 30.0)	5.37 (17.63, 10.45)	5.364 (2.112)	-6.568 (-2.586)
18.0 (59.1, 35.0)	6.27 (20.57, 12.19)	5.812 (2.288)	-6.276 (-2.471)

Table 3: Model 5365 Resistance Data

Full-Scale Speed (m/s (ft/s, knots))	Model-Scale Speed (m/s (ft/s, knots))	Model Drag (N (lbs))	C_T x 1000
3.1 (10.1, 6.0)	1.08 (3.53, 2.09)	9.96 (2.24)	3.75
4.6 (15.2, 9.0)	1.62 (5.30, 3.14)	22.42 (5.04)	3.75
5.4 (17.7, 10.5)	1.88 (6.17, 3.66)	34.38 (7.73)	4.23
6.2 (20.3, 12.0)	2.15 (7.06, 4.18)	44.62 (10.03)	4.20
9.3 (30.4, 18.0)	3.22 (10.58, 6.27)	97.77 (21.98)	4.09
13.3 (43.5, 25.8)	4.62 (15.16, 8.99)	175.88 (39.54)	3.58
15.4 (50.6, 30.0)	5.37 (17.63, 10.45)	212.18 (47.70)	3.19
18.0 (59.1, 35.0)	6.27 (20.57, 12.19)	265.60 (59.71)	2.94

Wave Cut Capacitance Probes

Wave cut data was obtained at model speeds representing full-scale speeds of 5.4, 9.3, 13.3, and 15.4 m/s (17.7, 30.4, 43.5, and 50.6 ft/s), or 10.5, 18, 25.8, and 30 knots. At least two runs were made for each speed. Figure 8 and Figure 9 show typical results. Here, the downstream location, X, and the vertical position above the zero speed water line, H, are normalized by the model length, L. The wave cuts are shown at the four transverse locations, Y, normalized by the maximum beam of the model, B_T.

Wave resistance was computed from this data and C_w is compared to the results from the 1979 and 1992 testing in Figure 10. It can be seen that the all three tests show similar C_w.
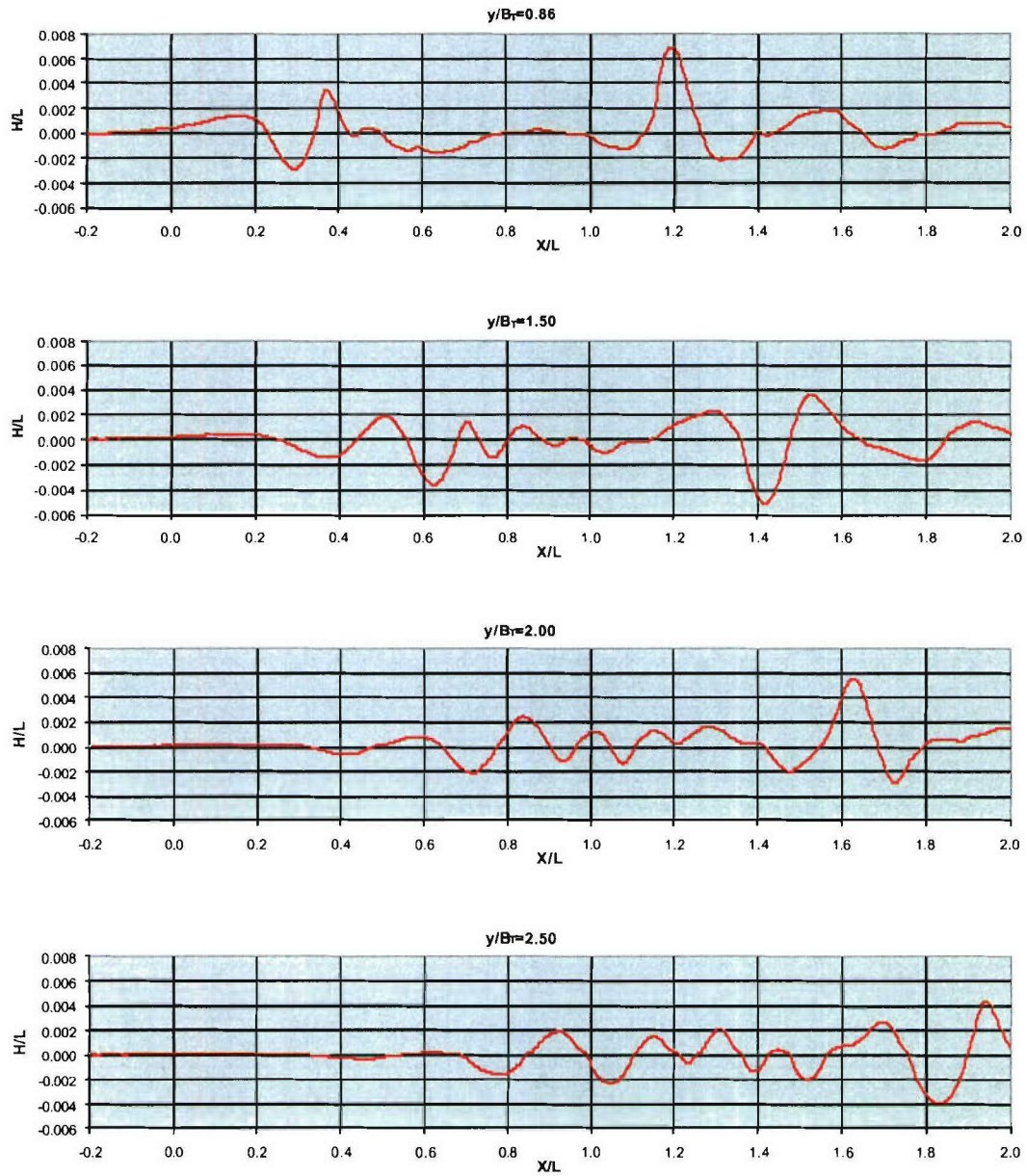
Figure 8: Wave cut records for Model 5365 at 1.88 m/s (6.17 ft/s).
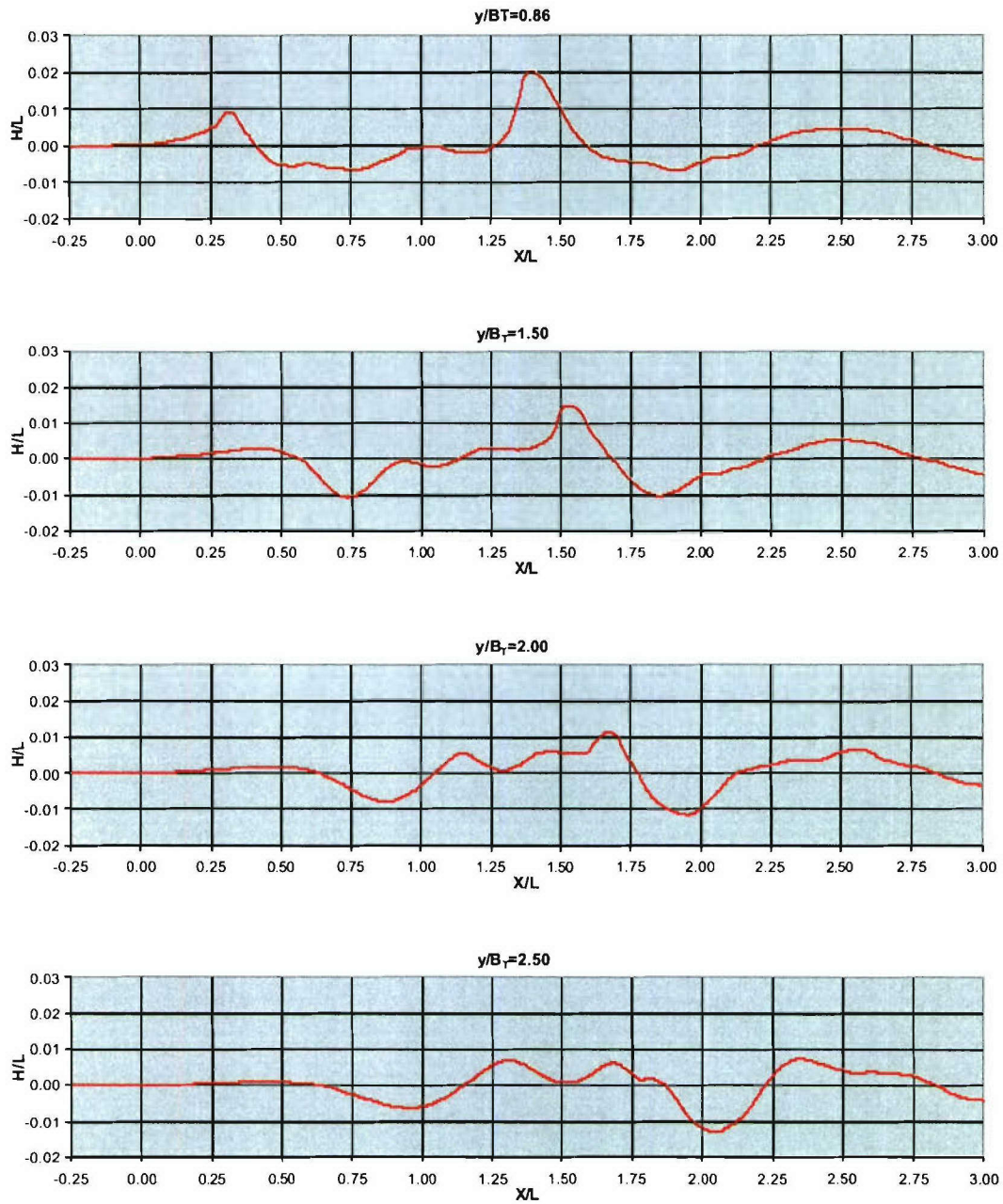
Figure 9: Wave cut records for Model 5365 at 3.22 m/s (10.57 ft/s).

14
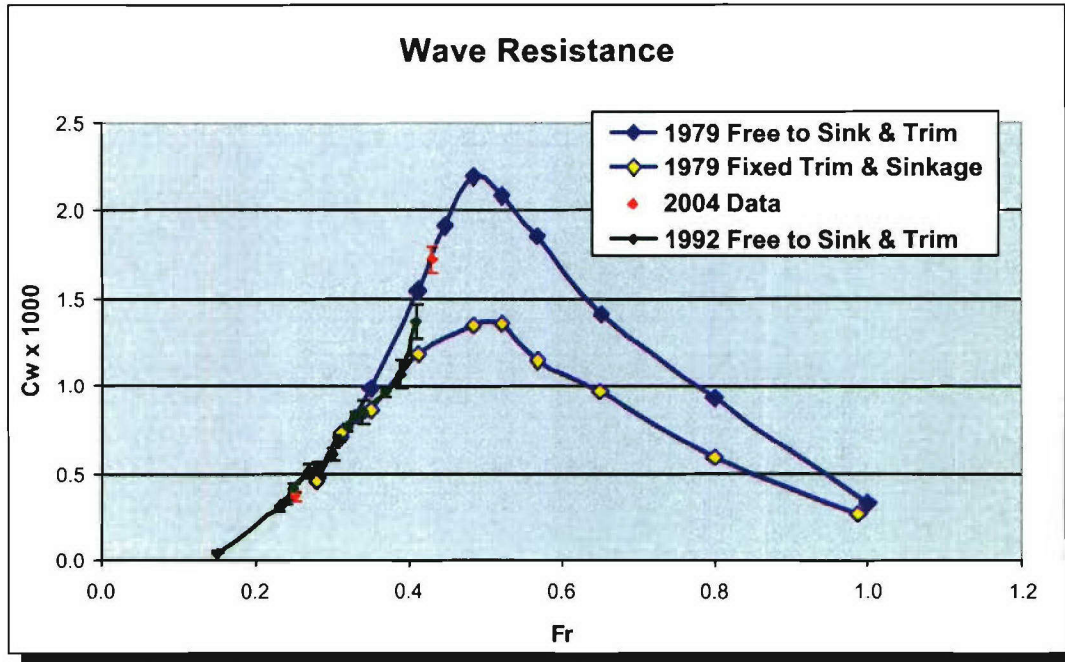
Wave Resistance

Figure 10: Coefficient of wave resistance for a range of Froude numbers.

Free-surface wave field topography

Free-surface wave field topography was generated by combining the QViz and finger probe results. QViz mapped out the region along the starboard side of the hull, while the conductivity probes were used to map out the free-surface wave pattern in the stern region of the model. All length scales in the figures are non-dimensionalized by the length of the model, L. The horizontal axis, "X/L", is zero at the bow stem of the model and positive aft of the model, and the vertical axis, "Y/L", is equal to zero at the model centerline. The zero speed waterline corresponds to Z/L = 0. The data was obtained at speeds corresponding to full-scale speeds of 5.4 and 9.3 m/s (17.7 and 30.4 ft/s), or 10.5 and 18.0 knots. The resulting contour plots are shown in Figure 11 and Figure 12 for the 5.4 m/s and 9.3 m/s case, respectively. Here, the QViz and finger probe data have been mirrored and shown on both sides of the hull.
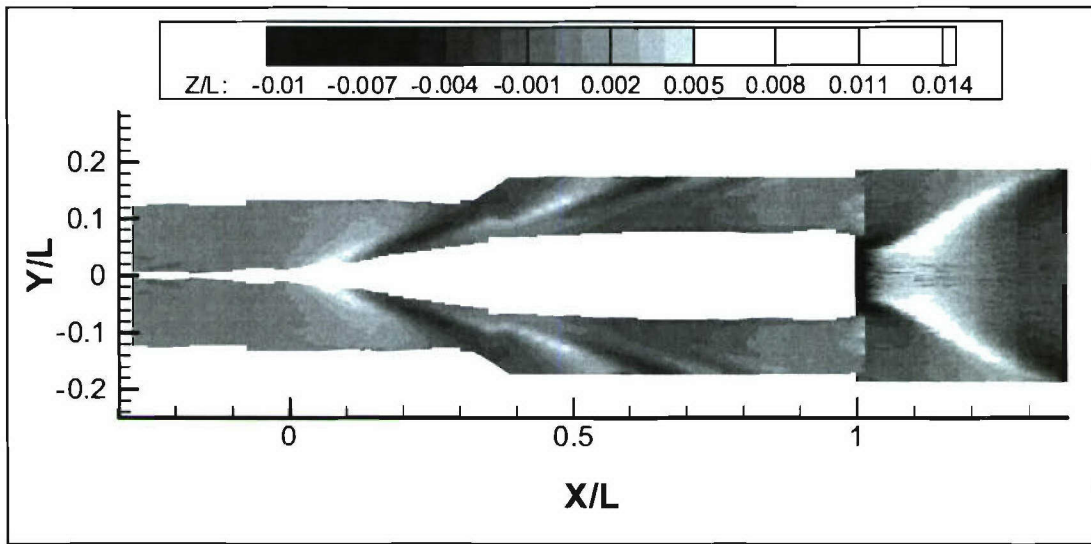
Figure 11: Wave field topography for Model 5365 at 1.88 m/s (6.17 ft/s), corresponding to 5.4 m/s (17.7 ft/s), or 10.5 knots, full-scale.
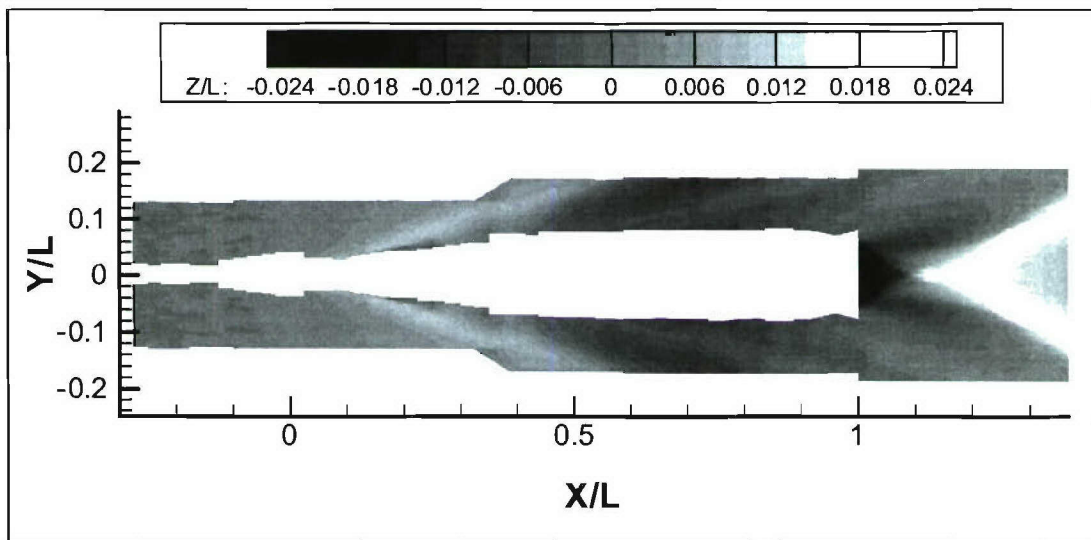
Figure 12: Wave field topography for Model 5365 at 3.22 m/s (10.58 ft/s), corresponding to 9.3 m/s (30.4 ft/s), or 18.0 knots, full-scale.

COMPUTATIONAL METHODS

In this section some details regarding the different computational methods that were used will be discussed. The codes that were used as part of the evaluation and workshop can be broken into four different categories: (1) potential flow methods including a wave breaking model, (2) free surface Reynolds Averaged Navier-Stokes (RANS) solutions using volume of fluid (VOF) method, (3) RANS predictions using the level-set method, and (4) Euler code predictions. A total of five different computational codes were exercised by researchers from four different groups, for a total of seven unique solution sets for the two forward speed conditions as part of this workshop.

The Das Boot program, exercised by engineers at SAIC, is a steady potential flow theory code that includes a wave breaking model. The free surface is predicted using an interface capturing method. This was the only potential flow solution method used for the workshop. Potential flow methods are historically good at predicting farfield wave heights with minimal computational expense; however, a wave breaking model was necessary in order to overcome the limitations of the interface tracking method used, which is unable to handle steep or breaking waves.

The CFD group at NSWCCD utilized two different commercial RANS solvers, Fluent, developed by Fluent, Inc., and Comet, developed by CD-Adapco. Both of these codes use volume of fluid (VOF) free surface methods. In the VOF approach, it is assumed that the volume elements in the domain are filled with a combination of two or more fluids. The volume fraction of each fluid in a control volume must sum to unity. The tracking of the interface is performed by the solution of a continuity equation for the volume fraction. The Fluent predictions use a "realizable" k-? turbulence closure, which includes certain mathematical constraints on the prediction of the normal stresses, and also addresses some deficiencies in the standard k-? turbulence model. The Comet predictions use the Shear-Stress-Transport (SST) k-? turbulence closure.

CFDSHIP-IOWA was exercised by two different groups, one from NSWCCD and one from IIHR, University of Iowa. Previously an interface tracking method was used to resolve the free surface, but recently the code makes use of the level-set technique to model the location of the interface. The level-set approach uses a level-set function (?) to model the gas-liquid interface, where ? < 0 is defined as the gas phase, ? > 0 represents the liquid phase, and ? = 0 represents the interface. Conventional level-set methods include a finite thickness for the interface, which must be reinitialized to prevent distortion or excessive thinning/thickening of the interface. The CFDSHIP-IOWA predictions use a blended k-?/k-? turbulence closure.

The Numerical Flow Analysis (NFA) Navier-Stokes code was exercised by researchers at SAIC and MIT. It uses a Cartesian-grid formulation of the Navier-Stokes equations to model the ship hull and free surface. The gas-liquid interface is modeled using a VOF method. Body-force and finite-volume methods are used to enforce the boundary conditions on the hull. The body-force technique uses a source term in the Navier-Stokes equation to impose a no-slip condition at the solid surface, and the finite-volume technique modifies the Poisson equation to account for fractional cells to impose

free-slip conditions. This code is an Euler solution method, which neglects the viscous fluxes in the Navier-Stokes equations.

Computational Domains

Each of the different computational methods used for the wave predictions has different needs and sensitivities. One aspect is the computational domain space used for the solution. A comparison of the domain sizes used by the different codes is shown in Figure 13. The Fluent and Comet predictions, for example, are performed using a domain that is relatively large, to minimize any influence from the outer boundaries on the flow near the hull. The CFDSHIP-IOWA computations, on the other hand, have relatively small domains due to the use of a numerical beach that avoids wave reflections from the boundaries. The Fluent domain is also shaped with a slanting side boundary. This is to help enforce a positive flux through the boundary, as with a slanted side there will always be an x-component of the fluxed variables. This would not necessarily be the case for parallel sides. Each of the computational grids developed reflect the need to accommodate different perculiarities in each of the codes, as well as certain user preferences based on experience. It is important to recognize these differences amongst the computational methods when comparing ease of use and necessary computational expense (e.g., required CPU time).
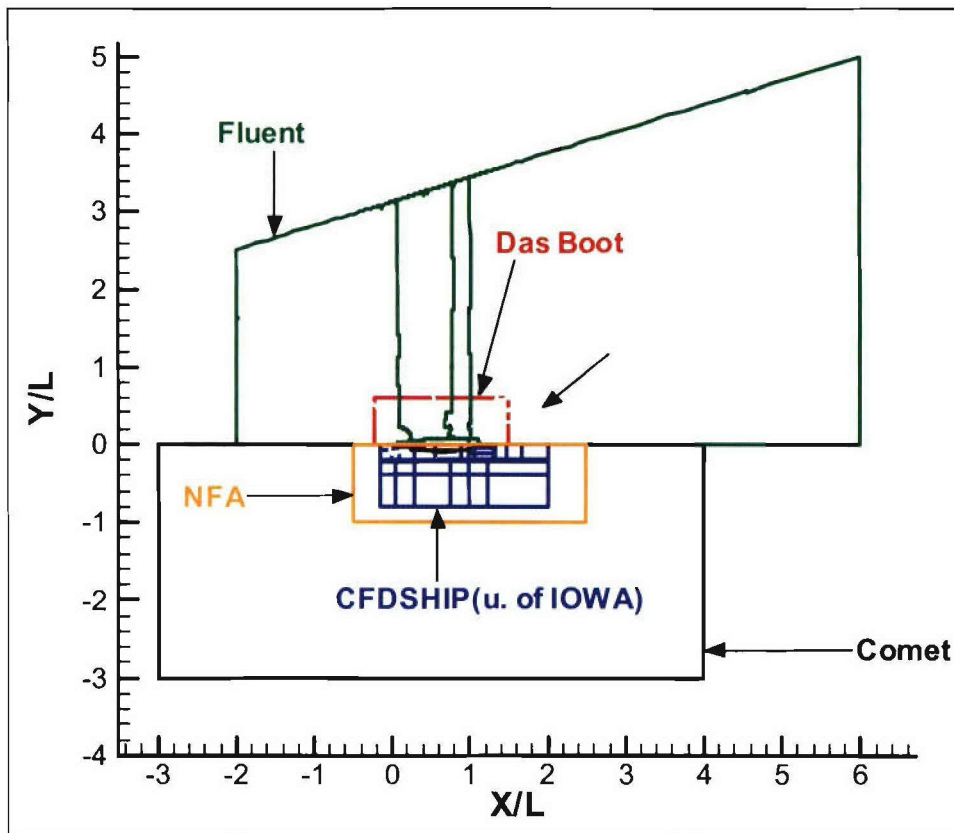
Figure 13: Comparison of computational domains used by different codes.

An overview of the different computational methods is provided in Table 4. The different free surface methods, turbulence models, computational grid sizes, and computational expense for each code are given. As expected, the inviscid method is the fastest and requires the least amount of computational resources. The NFA code, on the other hand, uses the finest grid and requires an enormous amount of computational resources. Additionally, the treatment of the transient nature of the calculations was performed differently in the codes. The Fluent and NFA solutions were performed in a fully time-accurate manner. The Comet predictions were not time-accurate and computed only one inner iteration for each time step. The CFDSHIP-IOWA solutions were performed in a pseudo time accurate manner, with three inner iterations per time step. A comparison of the two commercial codes would seem to indicate that Comet is likely faster than Fluent; however, one must also take into account the added expense in computing a time accurate flow field in the Fluent simulations.

Table 4: Overview of computational methods.

Case	Code	Treatment of Free Surface	Turbulence Model	Grid Size	Computational Expense
1	Das Boot ver. 5.0 beta	Interface Tracking		10.5 knots: Hull ~3,750	~4-8 hours
				Free Surface ~9,000	
				18.0 knots: Hull ~3,750	2 Processor PC
				Free Surface ~11,000	
2	CFDSHIP-IOWA ver. 4 (U. of Iowa)	Level-Set	Blended k-? and DES	10.5 knots: 6.08 million grid points	65-78 hours
				18.0 knots: 7.32 million grid points	64-88 processors Origin 3800
3	CFDSHIP-IOWA ver. 4 (NSWCCD)	Level-Set	Blended k-?/k-?	10.5 knots: 1 million hexahedral cells	~25 hours
				18.0 knots: 1 million hexahedral cells	16 processors IBM P4
4	CFDSHIP-IOWA ver. 4 (w/Chimera)	Level-Set	Blended k-?/k-?	10.5 knots: 1 million cells + 1.3 million chimera	~29 hours
				18.0 knots: 1 million cells + 1.3 million chimera	32 processors IBM P4
5	Fluent	VOF	Realizable k-?	10.5 knots: 2.7 million hexahedral cells	~70-79 hours
				18.0 knots: 2.7 million hexahedral cells	28 processors linux cluster
6	Comet	VOF	k-? SST	10.5 knots: 1 million hexahedral cells	~35 hours
				18.0 knots: 1 million hexahedral cells	10 processors SGI Origin 3800
7	NFA ver. 2.0	VOF	Limited QUICK differencing	10.5 knots: 16.7 million cells	128 processor T3E
				18.0 knots: 11.1 million & 89.1 million cells	256 processor T3E

RESULTS AND DISCUSSION

In this section the results of the different numerical methods will be presented and compared with the model test measurements. In addition, some assessments will be made regarding the differences in the solutions, and potential advantages and disadvantages of each method.

The results presented at the workshop focused on two model test speeds. These were 5.4 m/s (17.71 ft/s) and 9.3 m/s (30.51 ft/s), which corresponded to full-scale speeds of 10.5 and 18.0 knots, respectively based on Froude scaling.

Fr = 0.25 (Full-Scale Speed = 10.5 knots) Wavefields

A comparison of each of the different code predictions with the experimental measurements of the wavefield elevations for Fr = 0.25 is given in Figures 14-27. The streamwise and athwartships coordinate positions (X and Y), as well as the wave heights (Z), have been normalized by the ship length, L.

Das Boot

Comparisons between the experimentally measured and predicted wave elevations using Das Boot[7,8] are shown in Figure 14. The results show an overall good prediction of the Kelvin wake pattern. A more detailed view of the bow and stern regions is given in Figure 15. The bow region shows good prediction of the beginning of the wave train and the wave elevations. The code does a good job predicting the wave trough immediately aft of the outboard section of the transom, but the wave heights aft of the stern appear slightly over-predicted and show a broader wave peak. More detailed quantitative comparison of the predicted wave heights is provided in later sections.
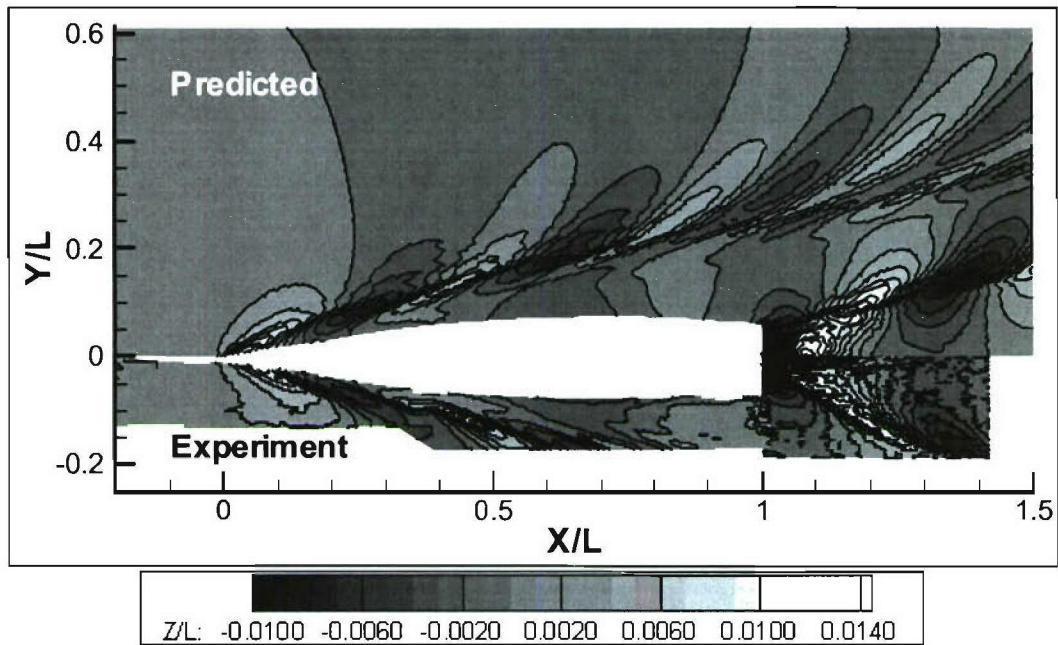
Figure 14: Predicted (Das Boot) normalized wavefield elevations (Z/L) compared with experiment, Fr = 0.25; overall view.

Figure 15: Predicted (Das Boot) normalized wavefield elevations (Z/L) compared with experiment, Fr = 0.25; zoomed view at bow and stern section.

CFDSHIP-IOWA (U. of Iowa)

Predictions made by researchers at the University of Iowa using CFDSHIP-IOWA[9,8] are given in Figure 16 for the overall wave field. Again, the results indicate a good overall prediction of the Kelvin wake over the region that the experimental measurements were available. A more detailed view of the bow and stern regions is given in Figure 17. The results show good agreement in the wave elevations near the bow, and good prediction of the wave heights and topology in the stern region. More detailed quantitative comparison of the wave heights is provided in a later section.

Figure 16: Predicted (CFDSHIP-IOWA, U. of Iowa) normalized wavefield elevations (Z/L) compared with experiment, Fr = 0.25; overall view.

Figure 17: Predicted (CFDSHIP-IOWA, Iowa) normalized wavefield elevations (Z/L) compared with experiment, Fr = 0.25; zoomed view at bow and stern.

25

CFDSHIP-IOWA (NSWCCD)

Predictions were also made by researchers at NSWCCD using the CFDSHIP-IOWA code. Results are provided in Figure 18 for the overall wave field for the baseline computational grid (i.e., no Chimera grid refinement). Again, there appears to be reasonable prediction of the development of the Kelvin wake in the region where the experimental measurements are available. A more detailed view of the bow region in Figure 19 shows qualitatively good prediction of the wave heights. The comparison at the stern, however, shows an over prediction of the wave height. A more quantitative comparison of the wave height predictions is provided in a later section.

Figure 18: Predicted (CFDSHIP-IOWA, NSWCCD) normalized wavefield elevations (Z/L) compared with experiment, Fr = 0.25; overall view.

Figure 19: Predicted (CFDSHIP-IOWA, NSWC) normalized wavefield elevations (Z/L) compared with experiment, Fr=0.25; zoomed view at bow and stern section.

CFDSHIP-IOWA (NSWCCD) with Chimera Grid

This section includes predictions made by NSWCCD using the CFDSHIP-IOWA code with Chimera grid refinement. A comparison of the baseline and Chimera grid is shown in Figure 20. The baseline grid contains approximately 1 million computational cells, while the Chimera grid, which includes the refinement block shown, contains approximately 2.3 million computational cells. The refinement block was positioned in such a way as to provide greater spatial resolution in the region of the bow wave and the resulting wave train.
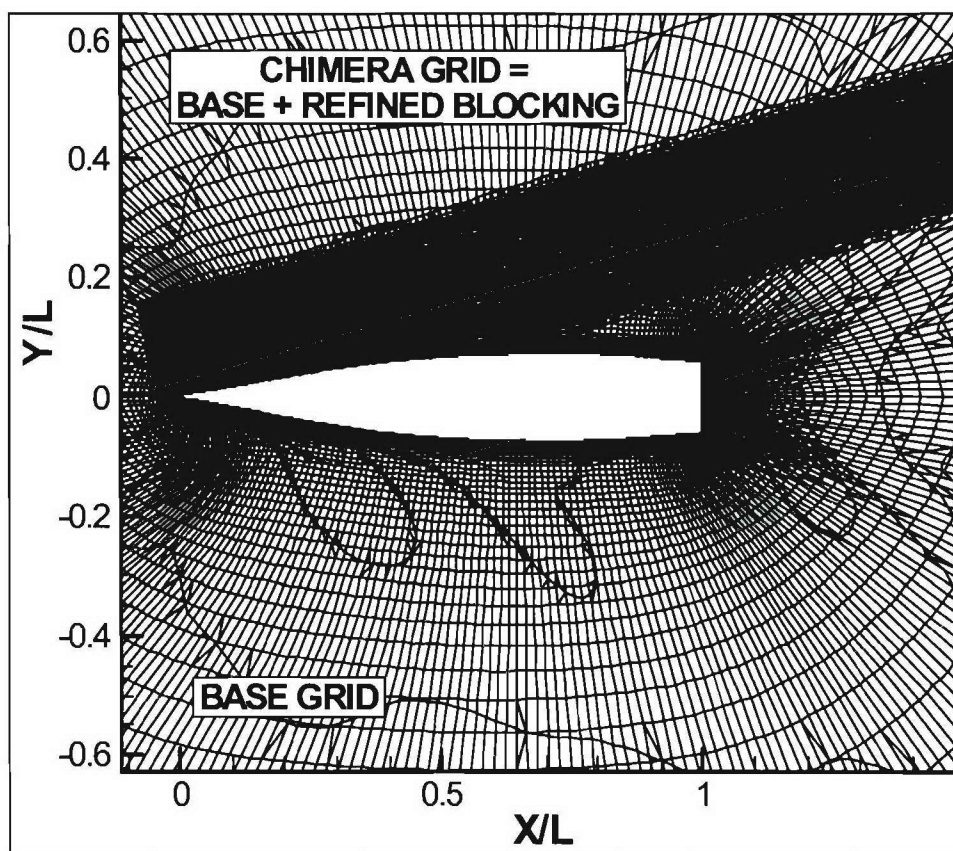
Figure 20: Comparison of baseline and Chimera grid for CFDSHIP-IOWA (NSWCCD) simulations.

The predictions of the overall wave field with the addition of the Chimera refinement block are shown in Figure 21. A comparison of Figure 18 using only the baseline grid and Figure 21 with the addition of the Chimera refinement block shows an enhanced prediction of the bow wake and the resulting wave train, including positions that are far downstream. A more detailed view of the bow and stern regions is shown in Figure 22. No Chimera refinement blocks were included in the stern region; hence, there was no improvement in the over-prediction of the stern wake. More detailed quantitative comparisons of the predicted and measured wave heights are provided in a later section.
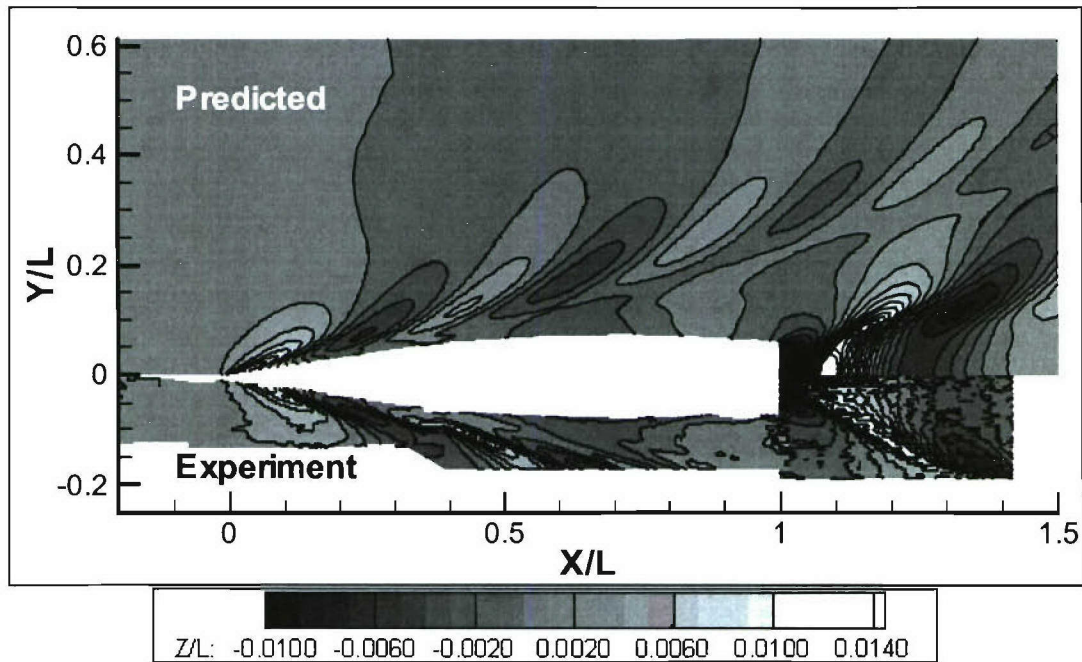
Figure 21: Predicted (CFDSHIP-IOWA, NSWC) normalized wavefield elevations (Z/L) compared with experiment, Fr = 0.25; overall view.
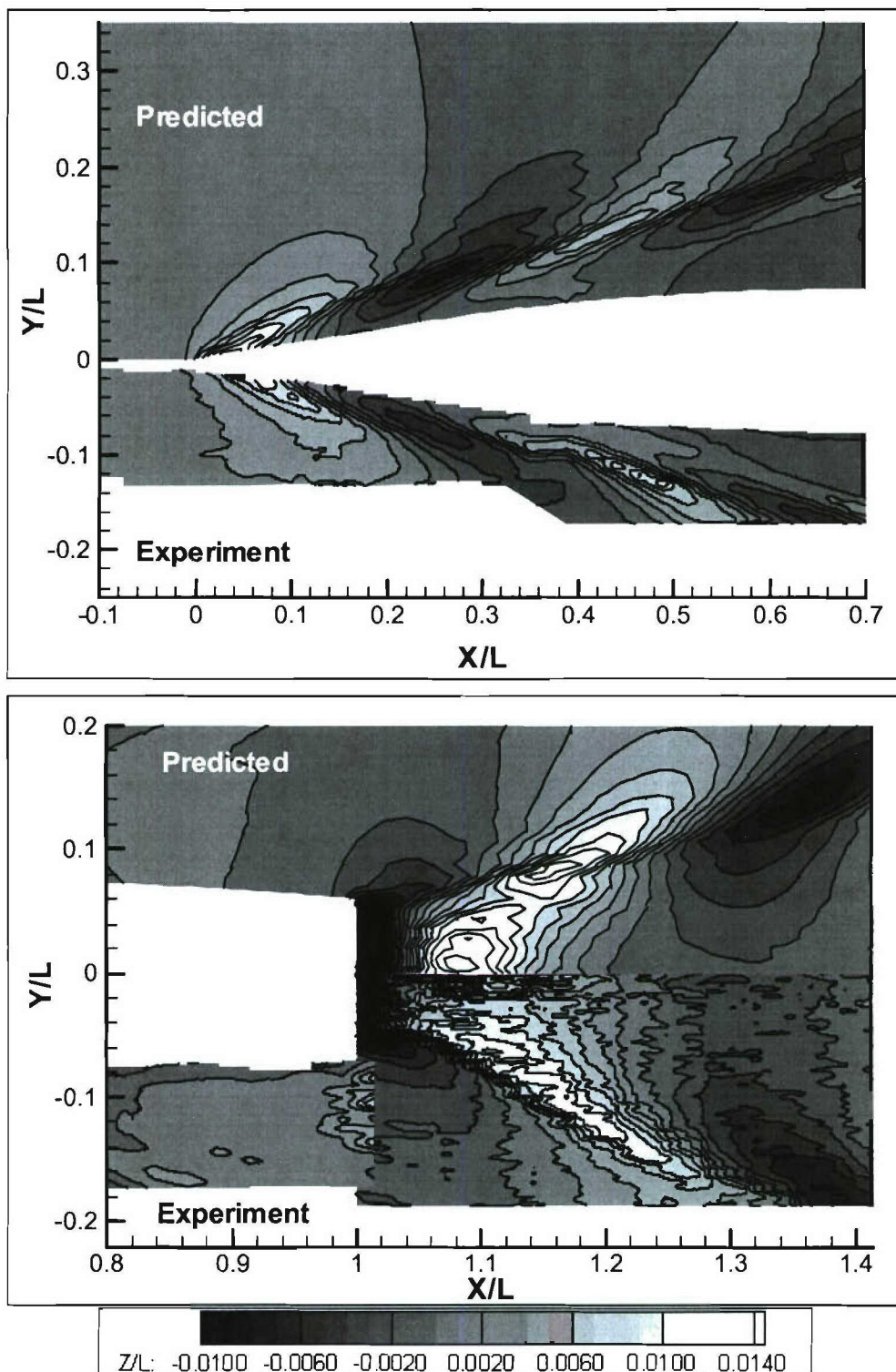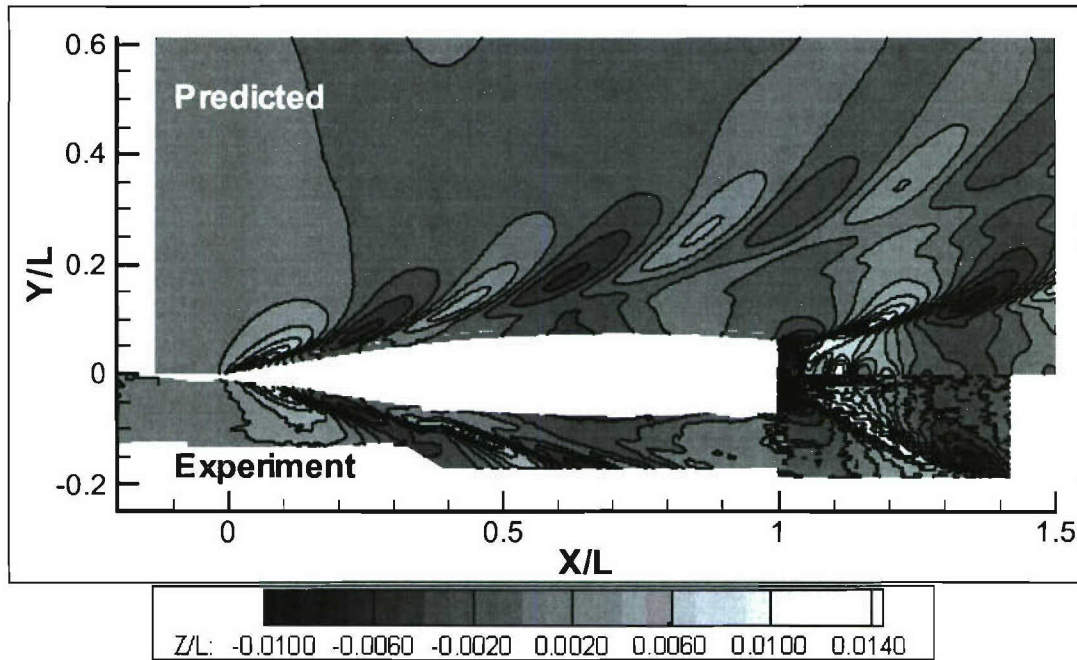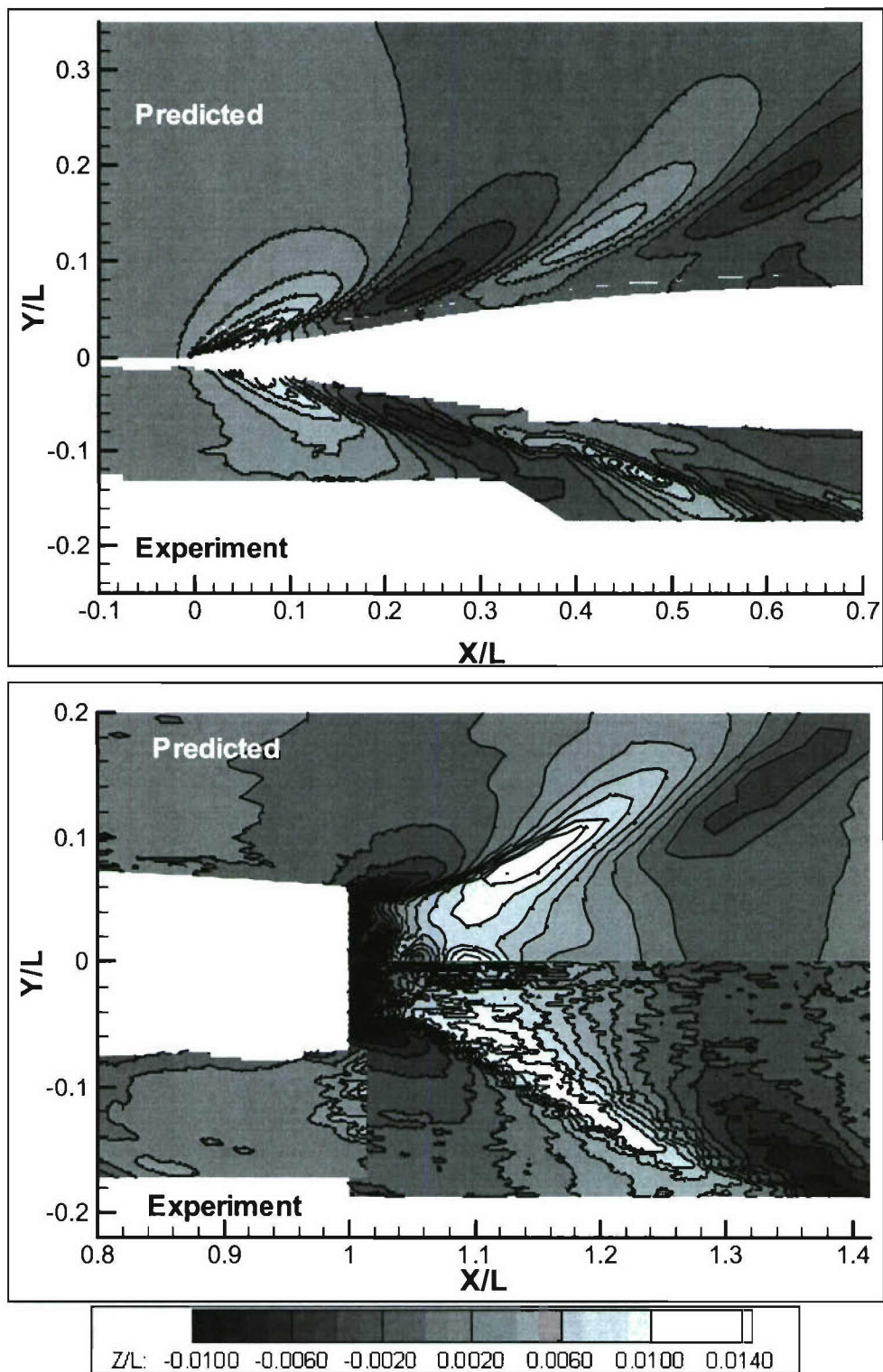
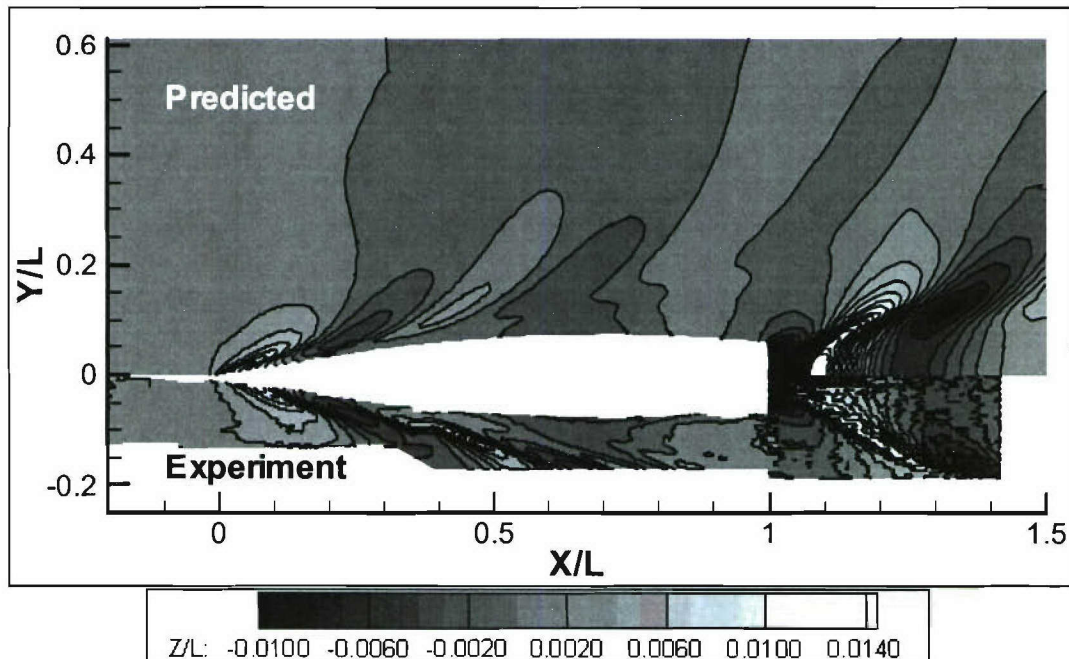**Figure 22: Predicted (CFDSHIP-IOWA, NSWC) normalized wavefield elevations (Z/L) compared with experiment, Fr = 0.25; zoomed view at bow and stern section.**

Fluent

The overall wave field predicted using the commercial solver Fluent is shown in Figure 23. The results indicate a relatively good overall prediction of the Kelvin wake; however, the grid resolution decreases farther downstream and away from the centerline. This results in a lack of definition of the wave topology further downstream. It is anticipated that this could be alleviated by refining the computational grid further, as was demonstrated in the CFDSHIP-IOWA solution with the added Chimera refinement block. A more detailed view of the bow and stern regions is provided in Figure 24. The bow wave appears slightly over-predicted, with an over-predicted wave trough as well. The stern region shows qualitatively good agreement with the measurements, especially in the region very near the transom stern, where the grid resolution is still quite good. A more detailed quantitative comparison of the predicted and measured wave heights in provided in a later section.

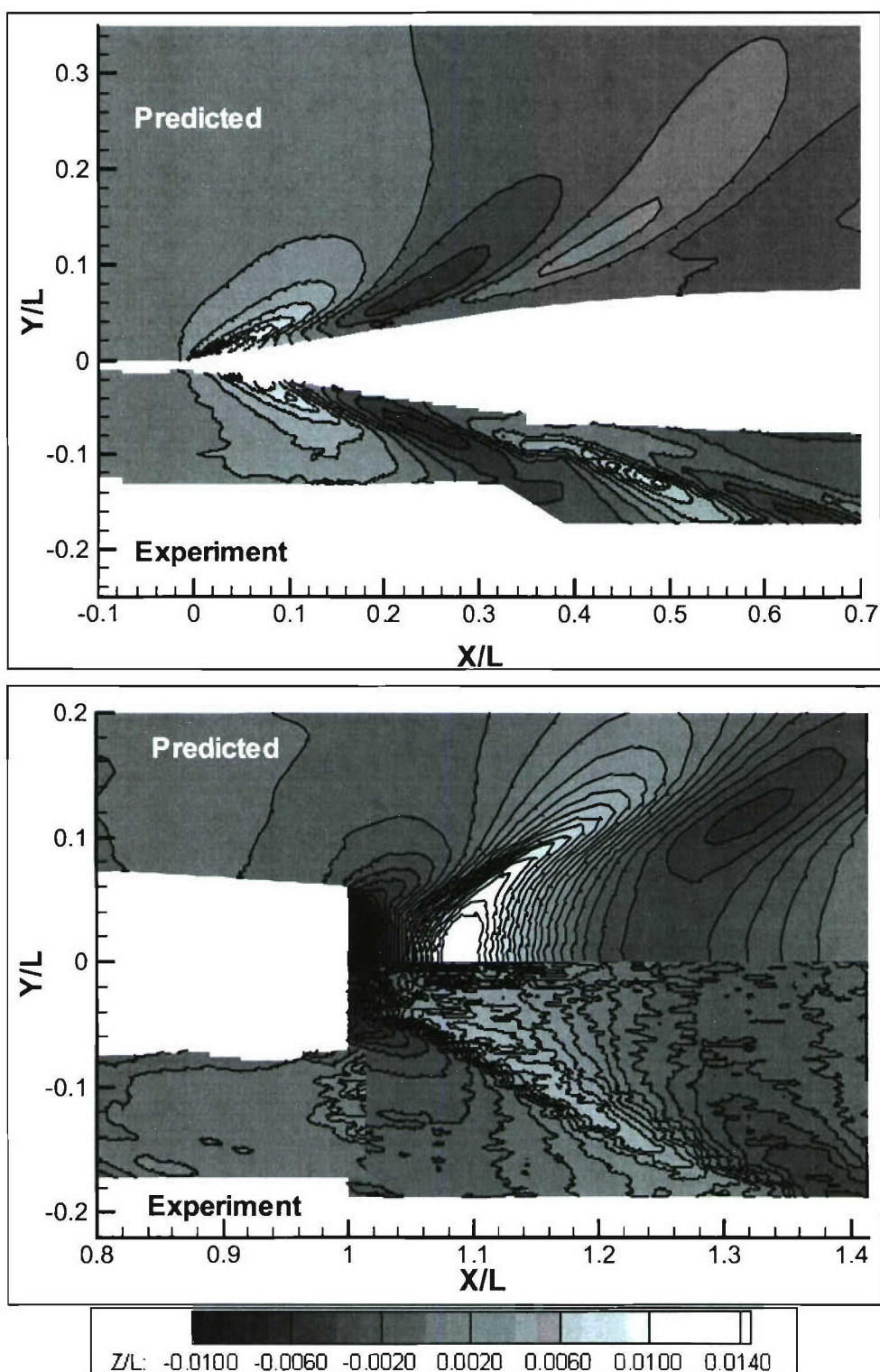**Figure 23: Predicted (Fluent) normalized wavefield elevations (Z/L) compared with experiment, Fr = 0.25; overall view.**

Figure 24: Predicted (Fluent) normalized wavefield elevations (Z/L) compared with experiment, Fr = 0.25; zoomed view at bow and stern section.

Comet

The other commercial CFD solver that was exercised as part of the workshop was Comet. The overall wave field predictions are given in Figure 25. The results show an overall good prediction of the bow wake, but again a lack of grid resolution further downstream prevents a good definition of the wave topology and the wave simply dissipates. A more detailed view of the bow and stern regions is given in Figure 26. The bow wake in the region where the experimental measurements are available appears qualitatively well predicted. In addition, the stern region shows good agreement in the wave heights and the overall stern wave topology. A more detailed quantitative comparison of the predicted and measured wave heights is provided in a later section.

Figure 25: Predicted (Comet) normalized wavefield elevations (Z/L) compared with experiment, Fr = 0.25; overall view.
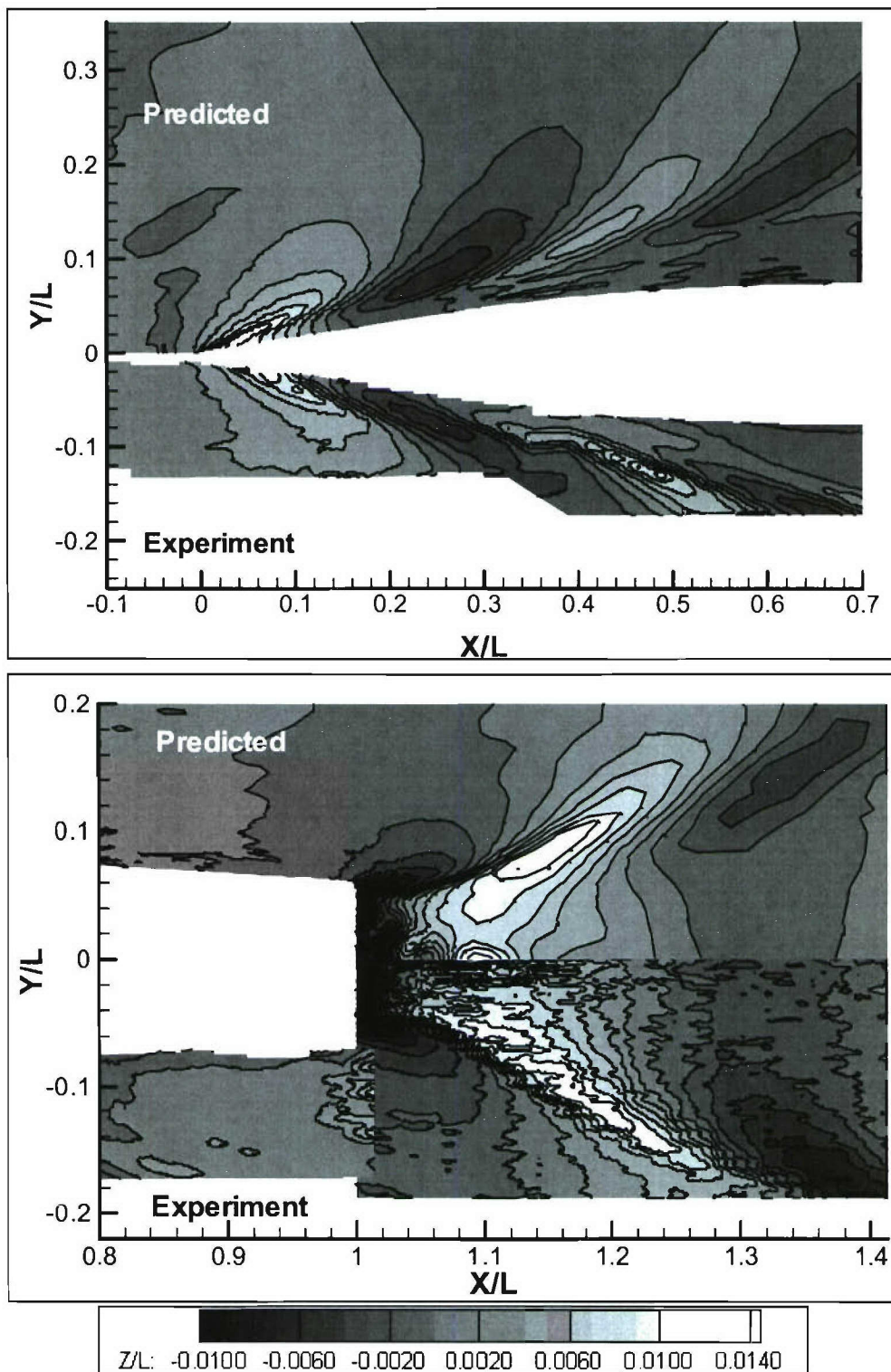
Figure 26: Predicted (Comet) normalized wavefield elevations (Z/L) compared with experiment, Fr = 0.25; zoomed view at bow and stern section.

34

NFA

The overall normalized wave field predictions using NFA version 2.0 [10,8] are shown in Figure 27. The results show a good prediction of the bow wake, with good resolution of the wave topology even far downstream. The results also show that the code picks up secondary wave patterns behind the bow wake even far downstream, which the other codes did not show. These results are not surprising given that the NFA results were generated using the most extensive computational grid and requiring the most computational resources. It is unclear, however, how much of this is physically accurate, as the experimental measurements were not made farther downstream and farther away from the ship model hull. A more detailed view of the bow and stern regions is shown in Figure 28. A comparison of the bow region shows qualitatively good prediction of the wave heights; however, the NFA predictions of the bow wake do not sweep back as much as the experimental measurements. The stern region predictions are excellent, showing a significant amount of small-scale details in the stern wave topology.

Figure 27: Predicted (NFA) normalized wavefield elevations (Z/L) compared with experiment, Fr = 0.25; overall view.

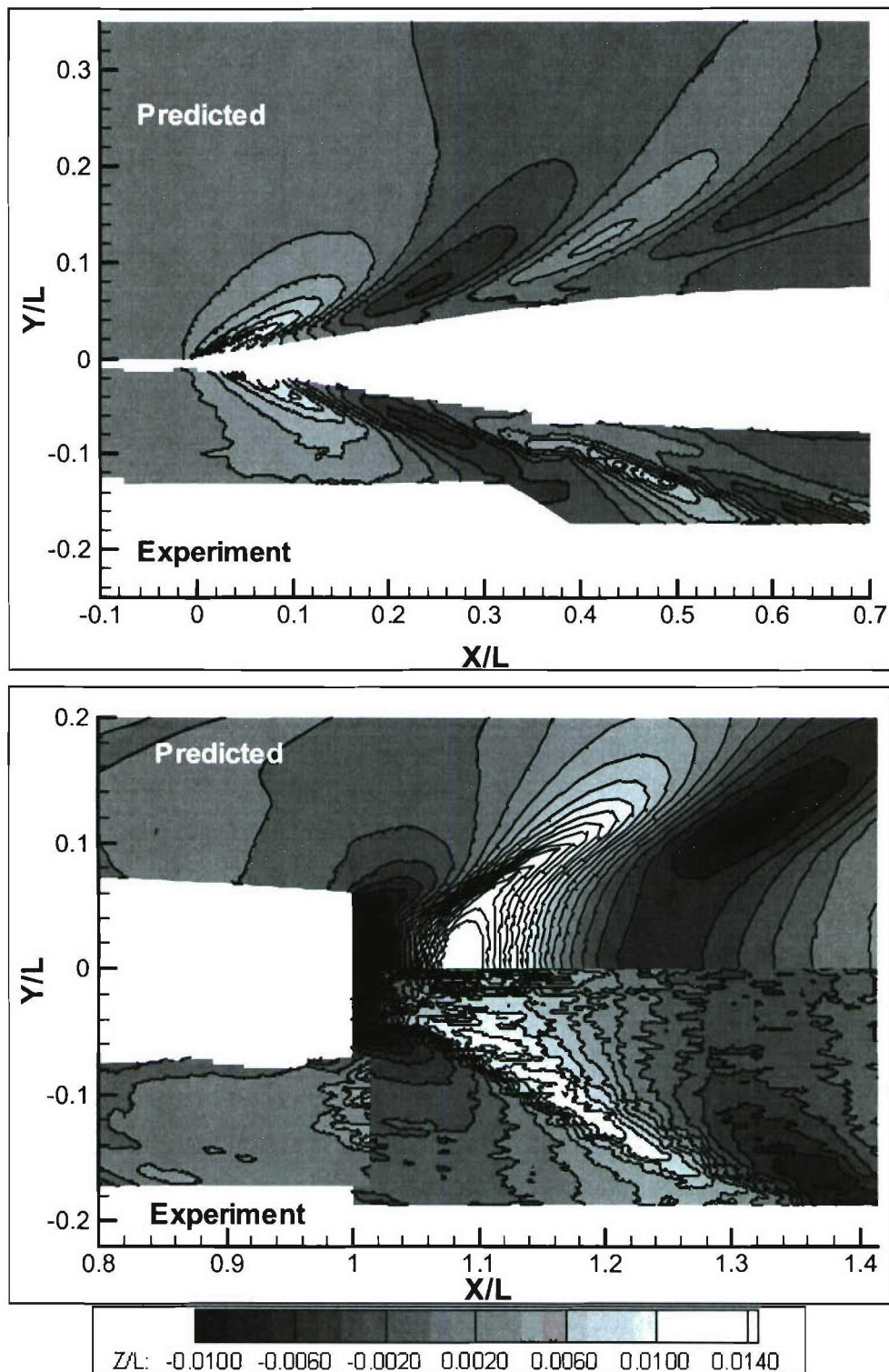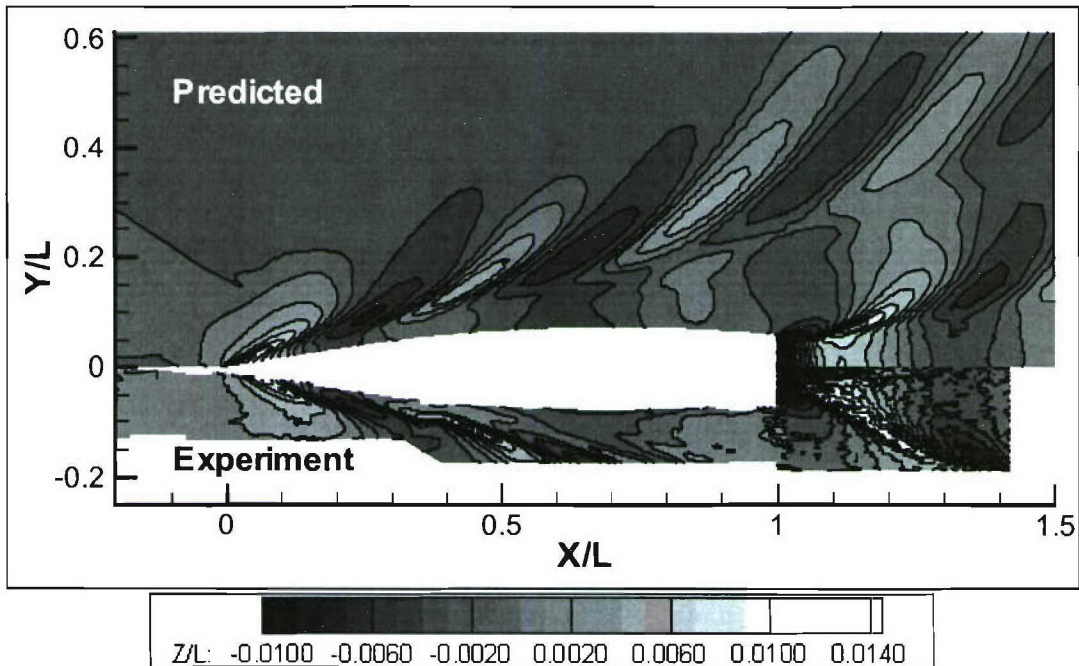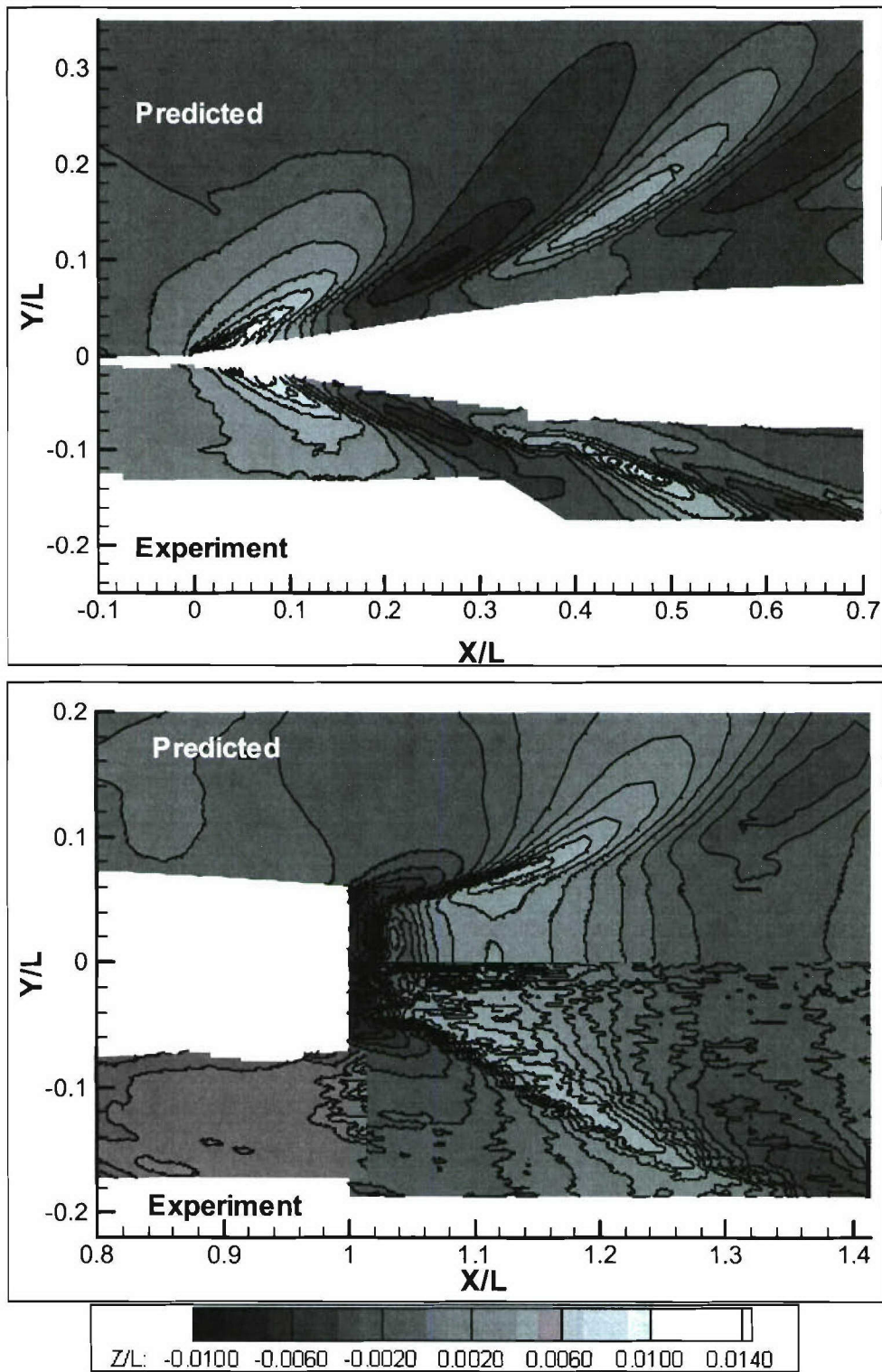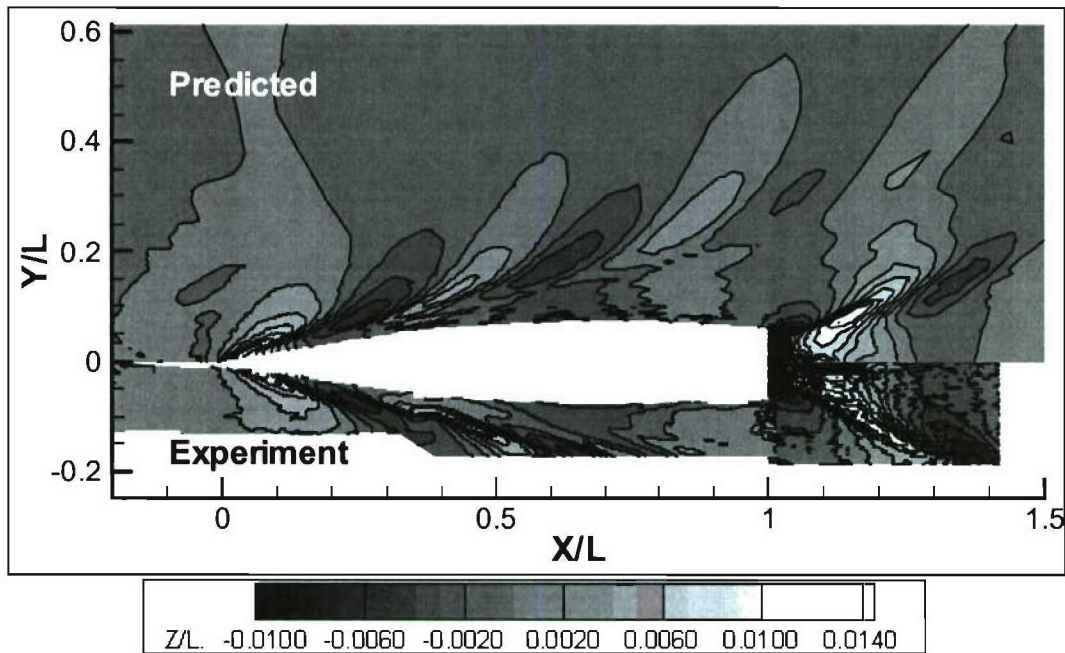**Figure 28: Predicted (NFA) normalized wavefield elevations (Z/L) compared with experiment, Fr = 0.25; zoomed view at bow and stern section.**
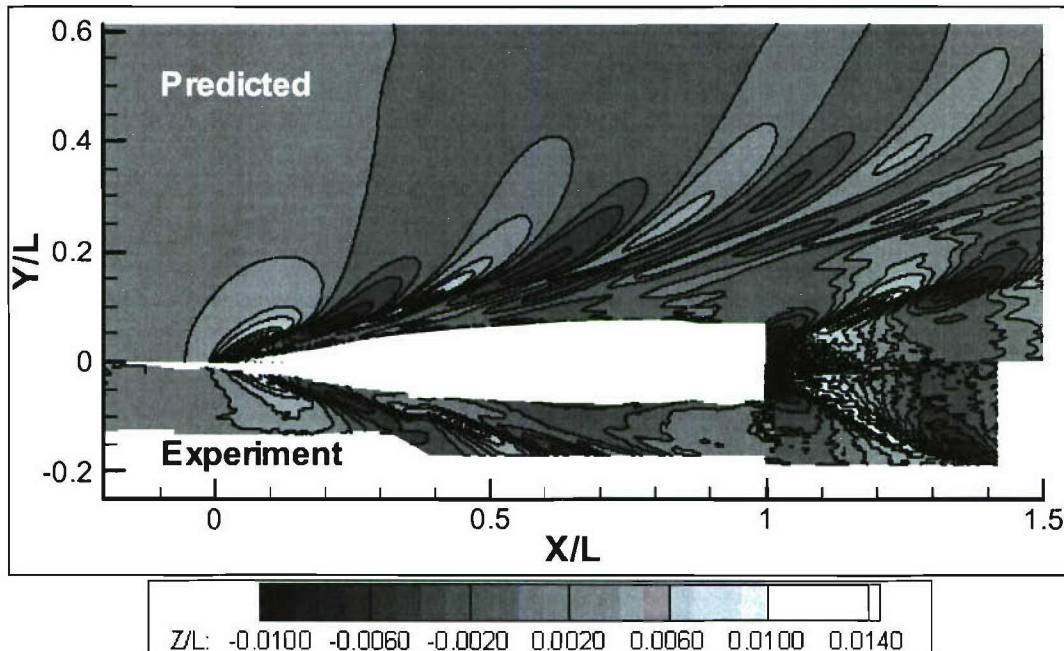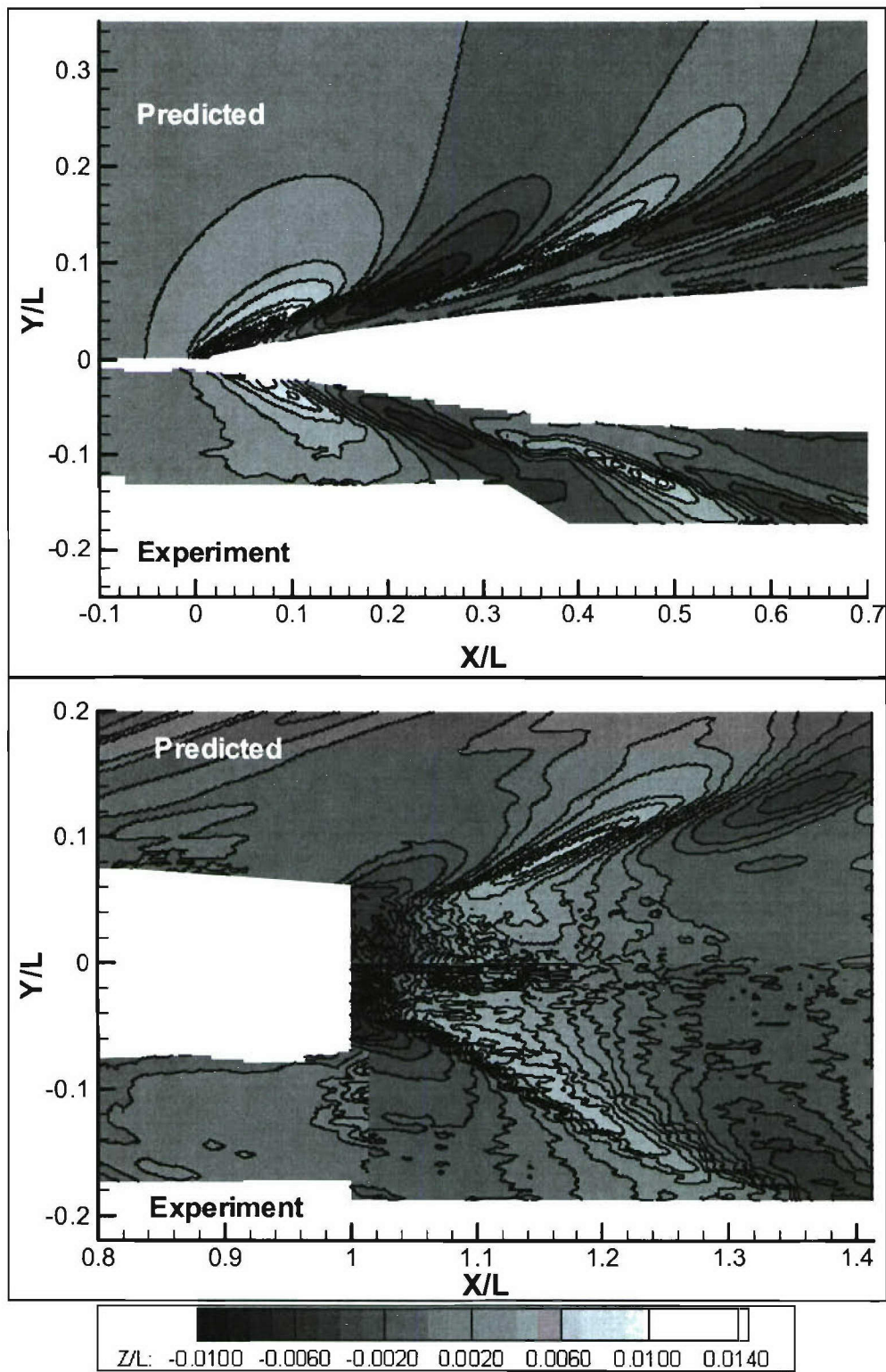
Fr = 0.25 (Full-Scale Speed = 10.5 knots) Wavecuts

This section provides a more quantitative comparison of the wave height predictions of the various solution methods. The wave elevations were recorded in the experiments using capacitance probes at four transverse locations away from the ship hull centerline. These locations were at y/B_T = 0.86, 1.50, 2.0, and 2.5 where B_T is the maximum beam of the model: 0.84 m (2.74 ft).

The comparisons between the measured and predicted wave cuts using the Das Boot program are shown in Figure 29 for all four transverse locations. The predictions overall agree well with the experimental measurements, although there is an over-prediction of the wave trough just aft of the transom ($x/L \sim 1.3$) for y/B_T = 0.86 and over-prediction of the largest wave height for y/B_T = 1.5 ($x/L \sim 1.5$). The code also does a good job of predicting the wave elevations at the locations that are farther away from the ship hull centerline, including the majority of the smaller details in the wave pattern.

The predictions made by the University of Iowa researchers using CFDSHIP-IOWA are compared with the measured wave heights in Figure 30. The results indicate that the code does a good job in predicting the wave elevations of the bow wave as it proceeds out away from the ship model. The first wave crest just aft of the transom is reasonably well predicted for the transverse location closest to the ship model, though the maximum height is under-predicted and the trough following is over-predicted, similar to the Das Boot result in Figure 29. This trend follows through the other transverse wave cut locations as well. The remainder of the wave pattern at y/B_T = 0.86 appears well predicted. The wave cuts at the other transverse locations show that the code does a good job predicting the first wave height, but then misses some of the smaller details in the next several wave heights that follow through the region of the ship model.

The predicted wave heights made by NSWCCD using the CFDSHIP-IOWA code are shown in Figure 31 for the baseline grid with no chimera grid refinement. The results are similar to the U. of Iowa results for the first transverse location, y/B_T = 0.86. The first bow wave is well predicted, and the region in the vicinity of the ship model ($x/L = 0$-1) is reasonably well predicted. The wave height immediately aft of the stern, however, is over predicted, and the following trough is greatly over predicted. The remainder of the transverse locations show a good prediction of the first wave height near the bow region, and an overall okay prediction of the rest of the wave pattern, but misses some of the smaller details, and under predicts the magnitudes of the waves aft of the transom stern. The predictions made with the added chimera grid refinement are shown in Figure 32. The result of the added refinement block produces a significantly better prediction of the wave elevations in the region of the bow at all the transverse wave cut locations. The same results continue at the stern region since there was no refinement block added in that region.

The wave elevations predicted using Fluent are shown in Figure 33. The code does an okay job at the first transverse cut location in predicting the height of the bow wave and the region of the ship model; however, the wave height just aft of the stern is under predicted. The predictions are reasonably good at the second transverse location, y/B_T = 1.5. In moving out to the farther wave cut locations the wave height predictions

are degraded. This is not surprising since the grid becomes relatively coarse away from the ship model. There also is some issue with the predicted mean free surface level, which seems to decrease at the further wave cut locations, but is also seen at $y/B_T = 0.86$. This has the appearance of the upstream free surface level "dropping". This effect was investigated but was not resolved in the time prior to the workshop. It would also seem to be speed dependent, as this effect was not observed for the higher speed case, which is discussed in a later section.

The Comet wave cut predictions are shown in Figure 34. The results show good agreement between the experimental measurements and the Comet predictions for the first transverse location. The region of the bow wave is well predicted; the code was able to pick up some of the small details in the near-bow region, from $x/L = 0.2$ to 0.6. The first wave peak aft of the transom stern is also well predicted; however, the wave amplitudes are well under-predicted for the following waves. This again points out the lack of grid resolution moving away from the ship model. The other transverse locations are fairly well predicted, and the near-bow region is well predicted even at the farthest transverse location. The following wave elevations, however, are under predicted and much of the smaller wave details are "smeared out".

The wave cuts predicted using the NFA Euler code are compared with the experimental wave cuts in Figure 35. The results show an overall good agreement with the experimental measurements. At the first transverse location, $y/B_T = 0.86$, the NFA predictions show very good agreement for the bow wave and the near-bow region, similar to the Comet predictions. The agreement continues past the transom stern, and the code provides good agreement with the experimental measurements for the downstream wave heights as well. The NFA code predicts much of the smaller wave elevation changes for all of the transverse wave cut locations, although the peak wave heights aft of the transom stern region are under predicted in all cases. There is also a curious over prediction of the free surface height upstream of the ship model, which would seem to be the reverse problem of the Fluent results. As in the Fluent results, this problem does not occur for the higher Froude number case.

Das Boot
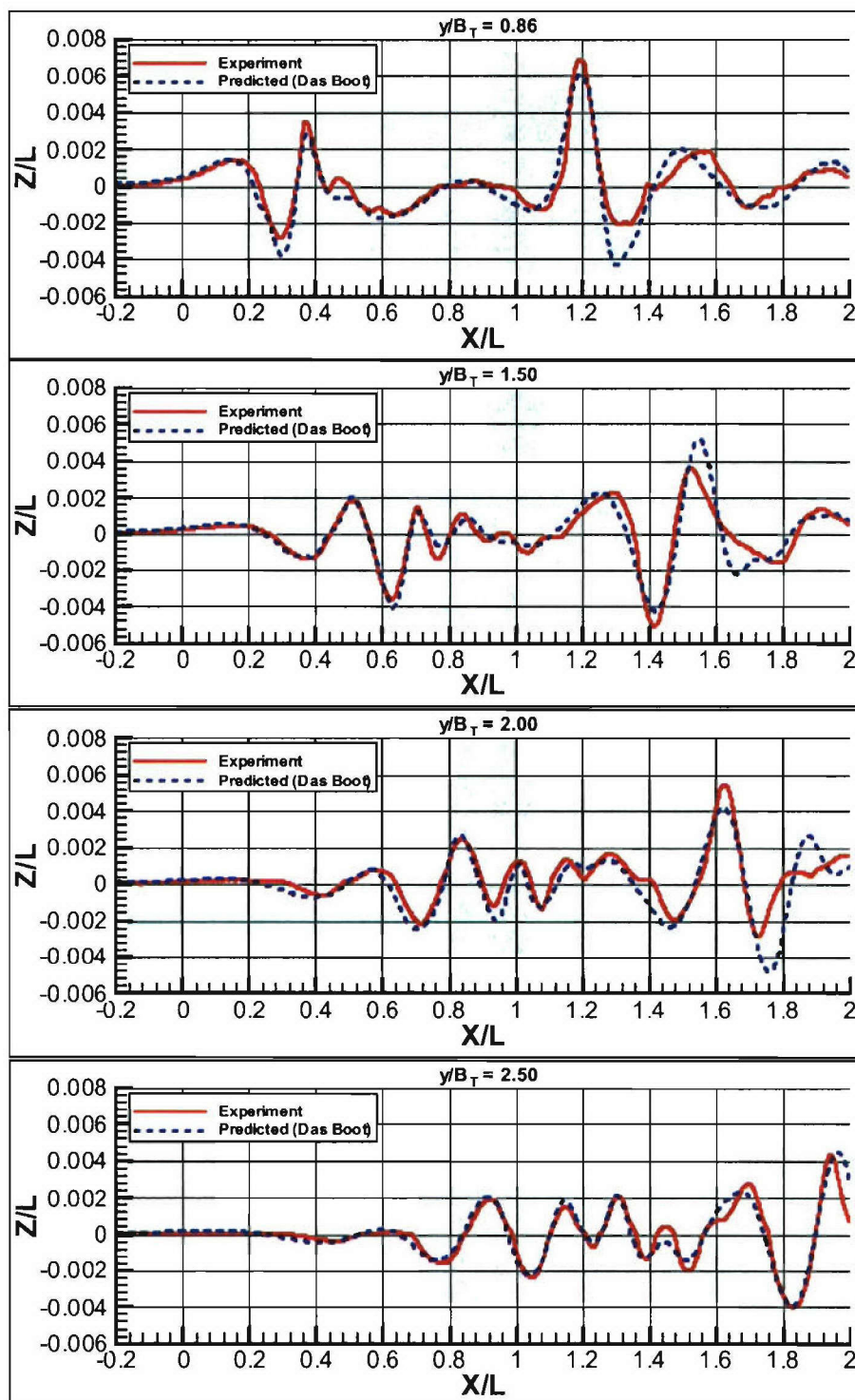
Figure 29: Predicted (Das Boot) and measured wavecuts for Model 5365, Fr = 0.25:
(a) y/B = 0.86, (b) y/B = 1.50, (c) y/B = 2.0, and (d) y/B = 2.50.

CFDSHIP-IOWA (U. of Iowa)
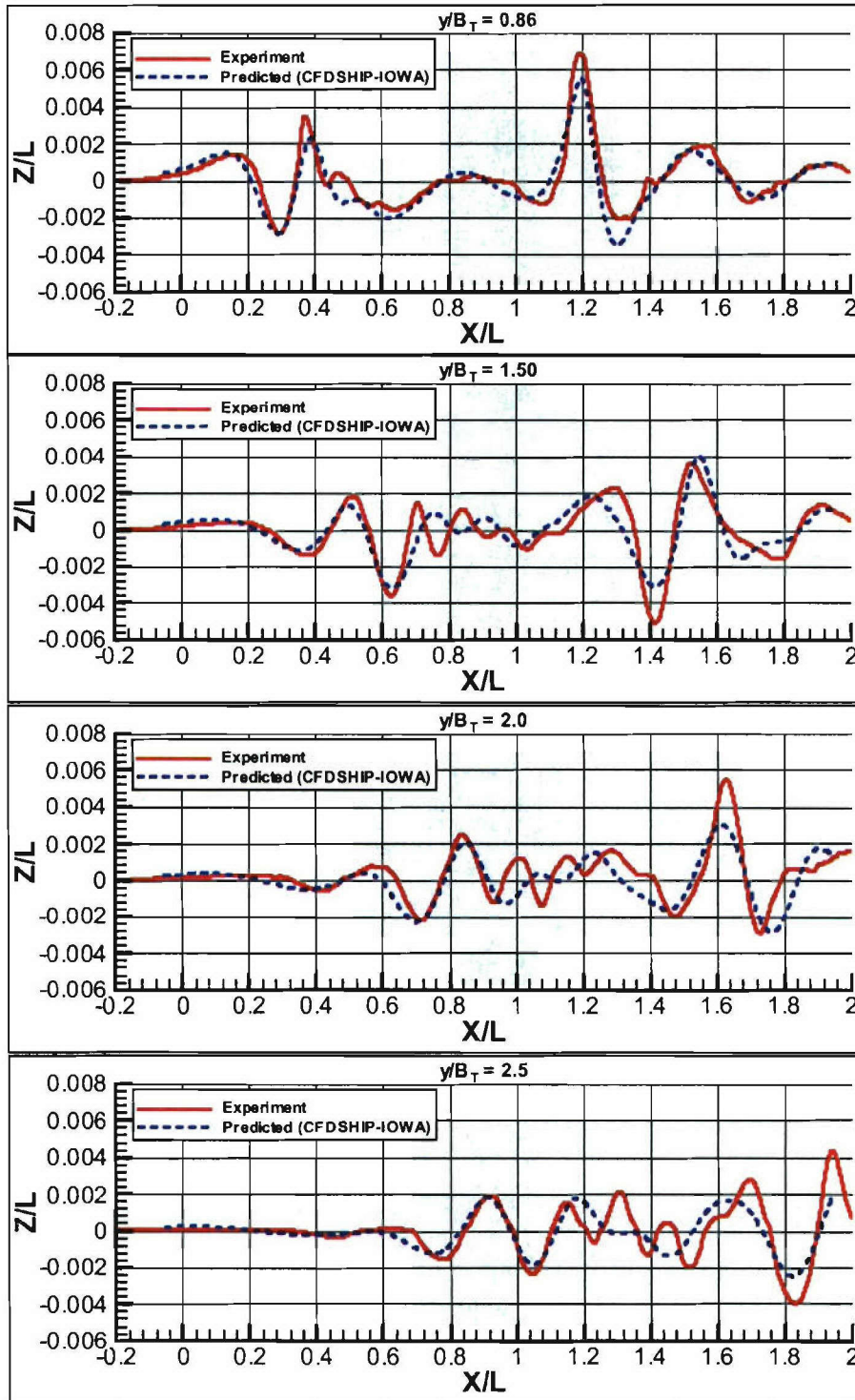
Figure 30: Predicted (CFDSHIP-IOWA, U. of Iowa) and measured wavecuts, Model 5365, Fr = 0.25: (a) y/B=0.86, (b) y/B=1.50, (c) y/B=2.0, (d) y/B=2.50.

CFDSHIP-IOWA (NSWCCD)
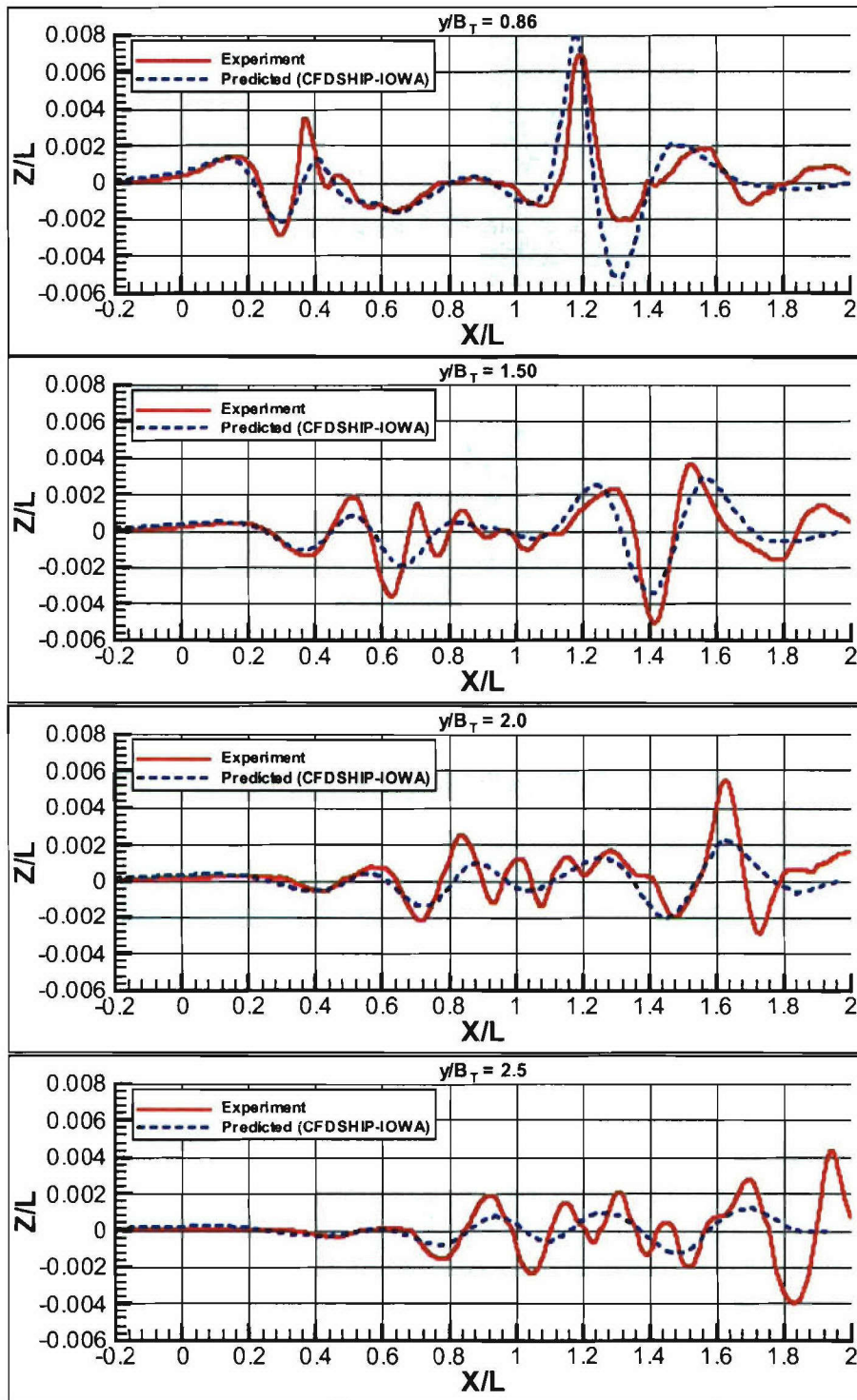
Figure 31: Predicted (CFDSHIP-IOWA, NSWCCD) and measured wavecuts, Model 5365, Fr = 0.25: (a) y/B=0.86, (b) y/B=1.50, (c) y/B=2.0, (d) y/B=2.50.

CFDSHIP-IOWA (NSWWCD) with Chimera Grid Refinement
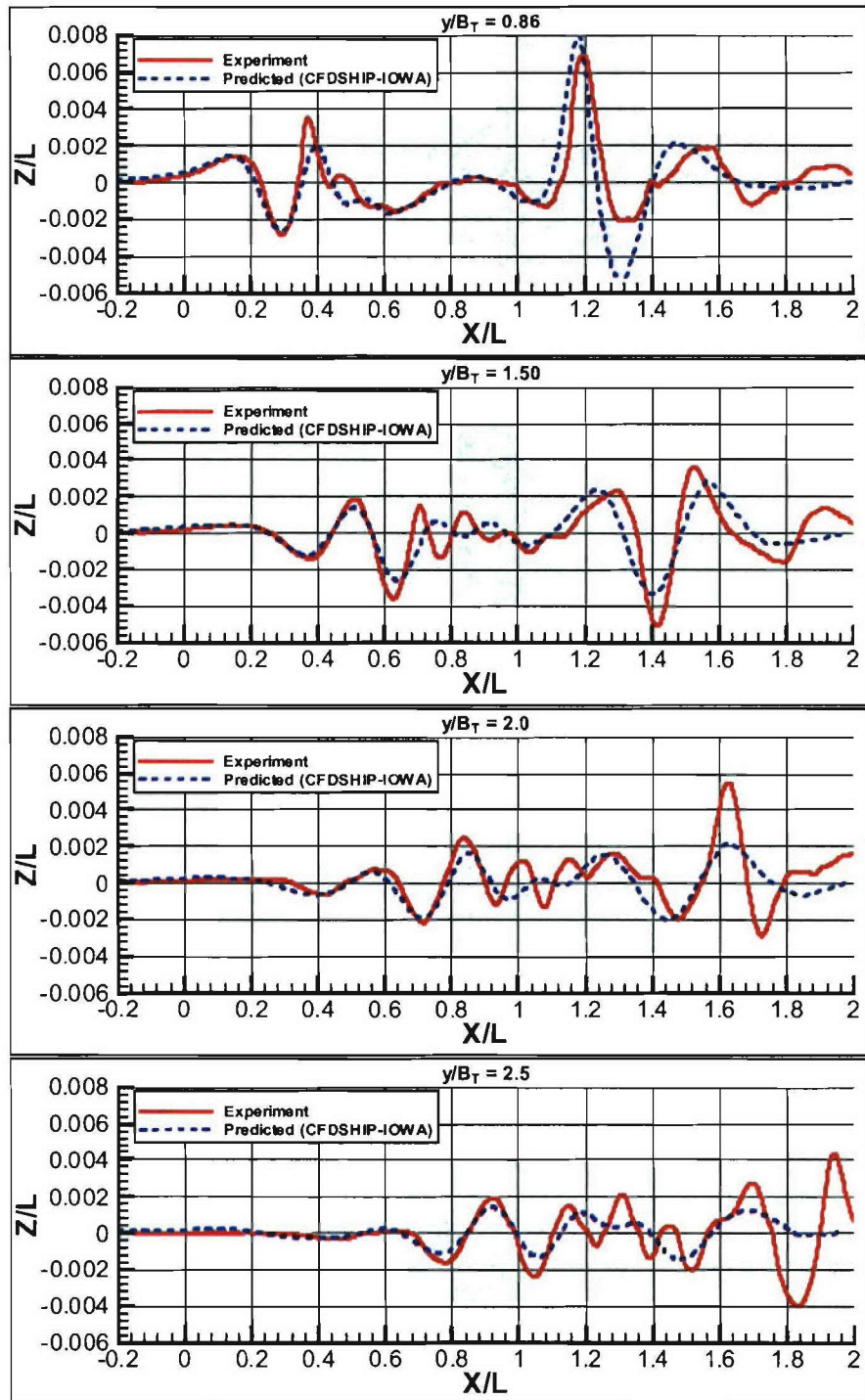
Figure 32: Predicted (CFDSHIP-IOWA, NSWCCD) with chimera grid refinement and measured wavecuts, Model 5365, Fr = 0.25: (a) y/B=0.86, (b) y/B=1.50, (c) y/B=2.0, (d) y/B=2.50.
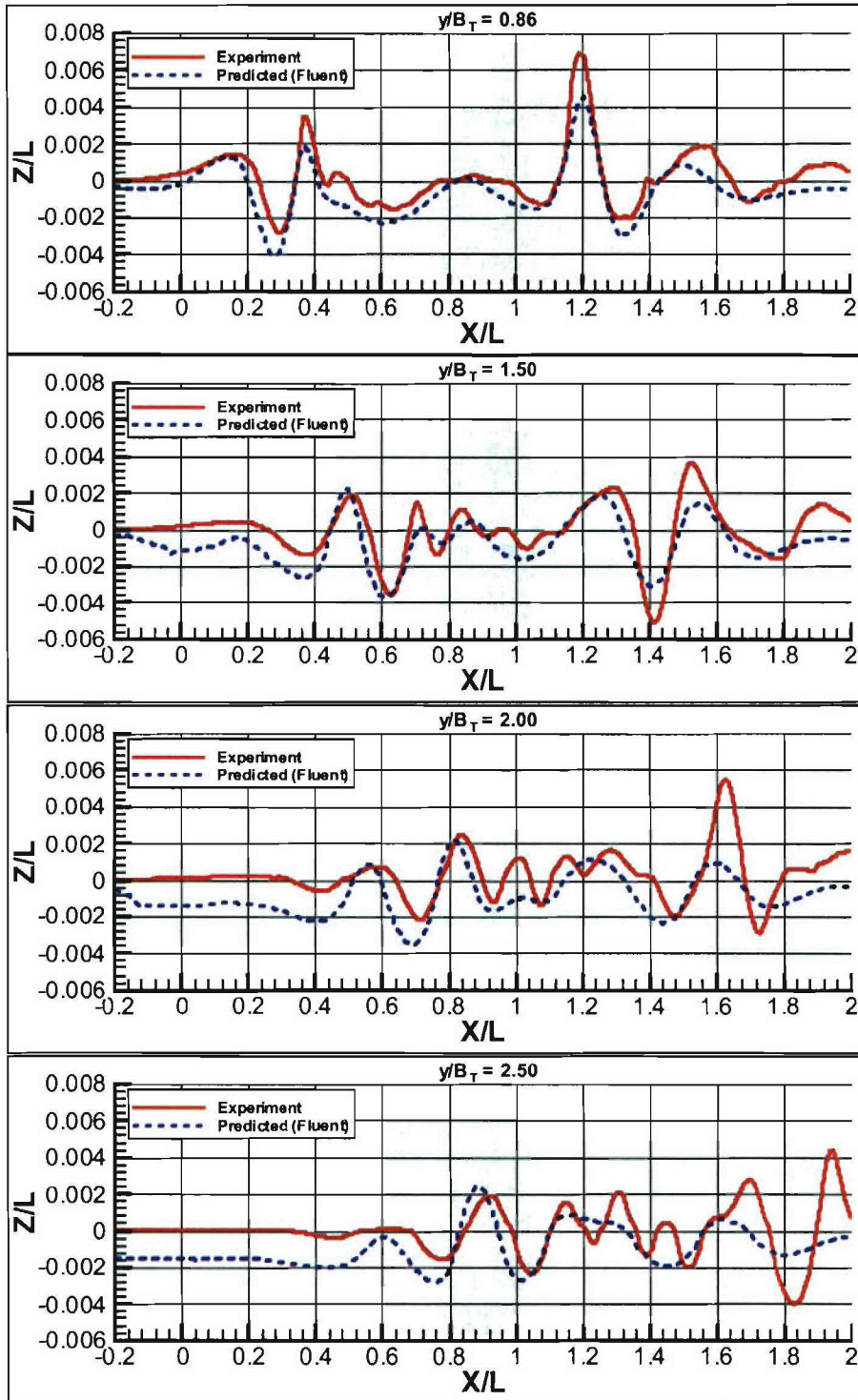
Fluent

Figure 33: Predicted (Fluent) and measured wavecuts for Model 5365, Fr = 0.25: (a) y/B = 0.86, (b) y/B = 1.50, (c) y/B = 2.0, and (d) y/B = 2.50.
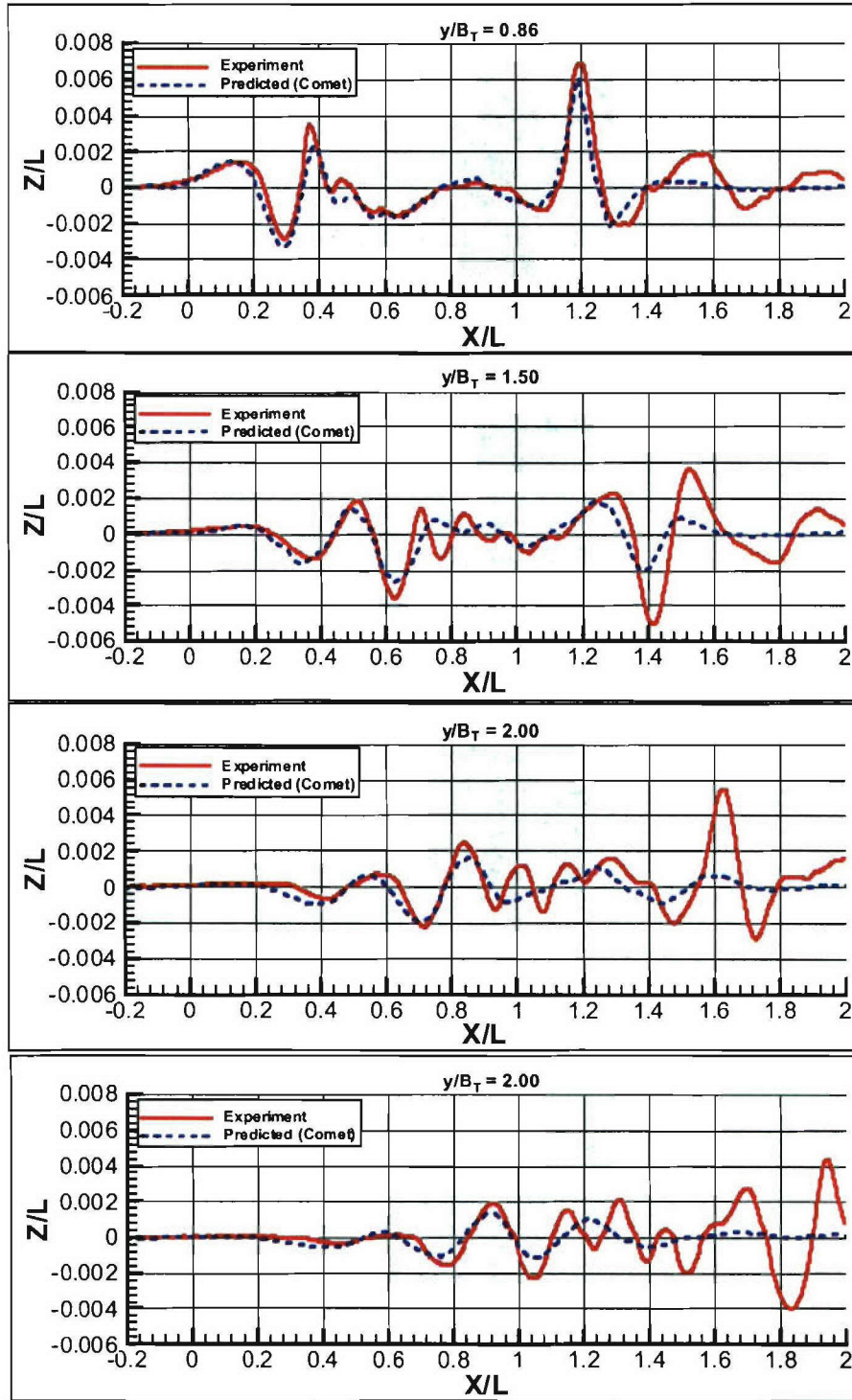
Comet

**Figure 34: Predicted (Comet) and measured wavecuts for Model 5365, Fr = 0.25:
(a) y/B = 0.86, (b) y/B = 1.50, (c) y/B = 2.0, and (d) y/B = 2.50.**

NFA:
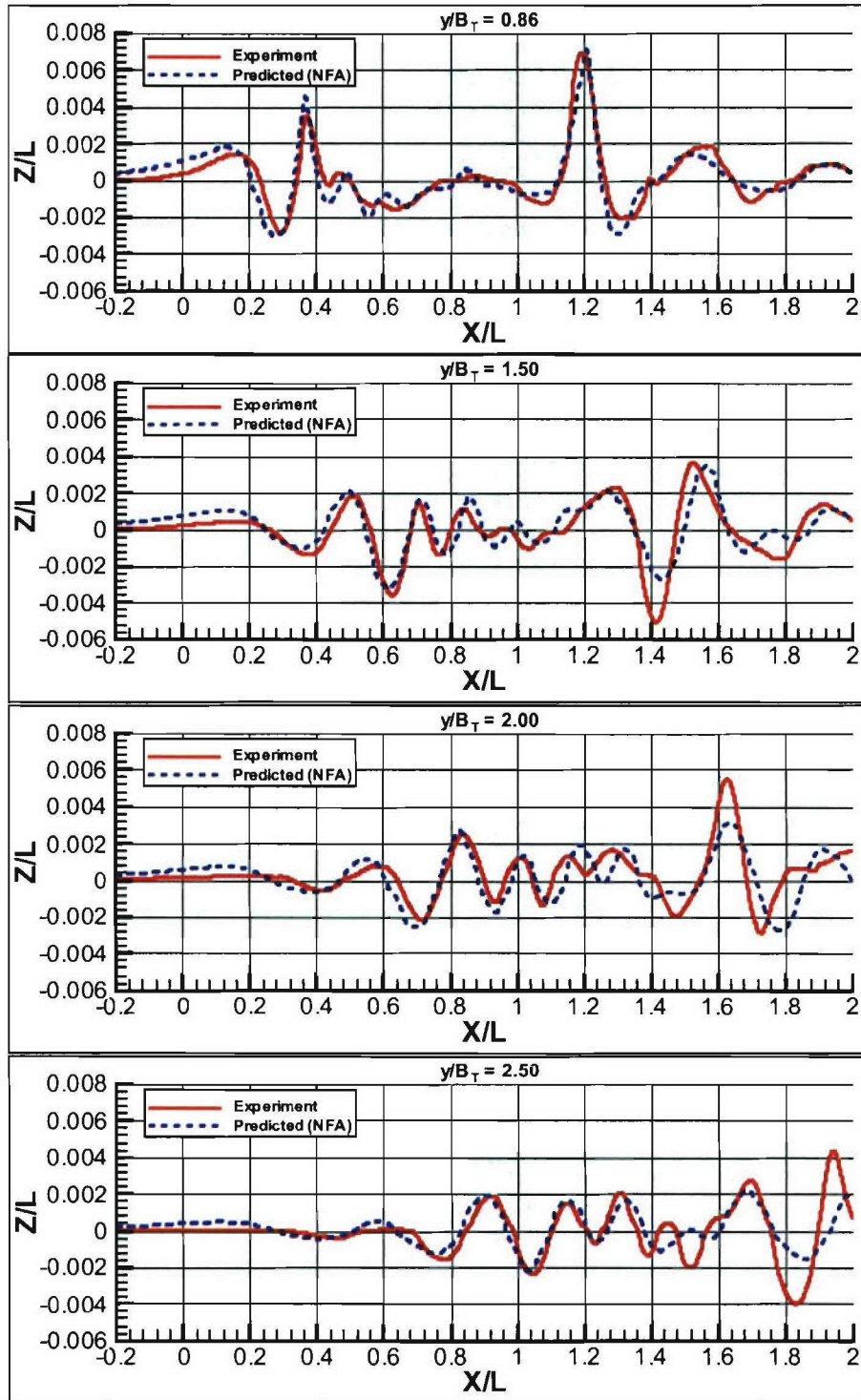
Figure 35: Predicted (NFA) and measured wavecuts for Model 5365, Fr = 0.25:
(a) y/B = 0.86, (b) y/B = 1.50, (c) y/B = 2.0, and (d) y/B = 2.50.

Fr = 0.25 (Full-Scale Speed = 10.5 knots) Summary

The results of the wavefield and wavecut predictions by the various codes is summarized in Table 5. While these comparisons are somewhat subjective, and it is often difficult to distinguish between the different solutions, this provides a useful way to examine the capabilities of the different solution methods.

Table 5: Summary of wavefield and wavecut predictions (Fr = 0.25)

Case	Code	Bow Region	Stern Region	Wave Cuts
1	Das Boot w/Breaking Model	Looks Good	Slightly Overpredicted	Looks Really Good
2	CFDSHIP-IOWA	Looks Good	Looks Really Good	Looks Good
3	CFDSHIP-IOWA (NSWC)	Looks Good	Overpredicted	Looks Okay
4	CFDSHIP-IOWA w/Chimera	Looks Good	Overpredicted	Looks Okay
5	Fluent	Slightly Overpredicted	Looks Good	Looks Okay
6	Comet	Looks Good	Looks Good	Looks Okay
7	NFA v2.0	Looks Good	Looks Really, Really Good	Looks Really Good

Fr = 0.43 (Full-Scale Speed = 18.0 knots) Wavefields

A comparison of each of the different code predictions with the experimental measurements of the wavefield elevations for Fr = 0.43 is given in Figures 36-49. The streamwise and athwartships coordinate positions (X and Y), as well as the wave heights (Z), have been normalized by the ship length, L.

Das Boot

Comparisons between the experimentally measured and predicted wave elevations using Das Boot (Wyatt, 2004)[7,8] are shown in Figure 36. The results show an overall relatively good prediction of the Kelvin wake pattern, at least for as much as was measured in the experiment. A more detailed view of the bow and stern regions is given in Figure 37. The bow region appears to show reasonable prediction of the beginning of the wave train. The stern region shows good agreement just aft of the transom stern including the beginning of the shoulder wave, but the code does not predict the rooster tail well and delays the center wave peak. More detailed quantitative comparison of the predicted wave heights is provided in later sections.
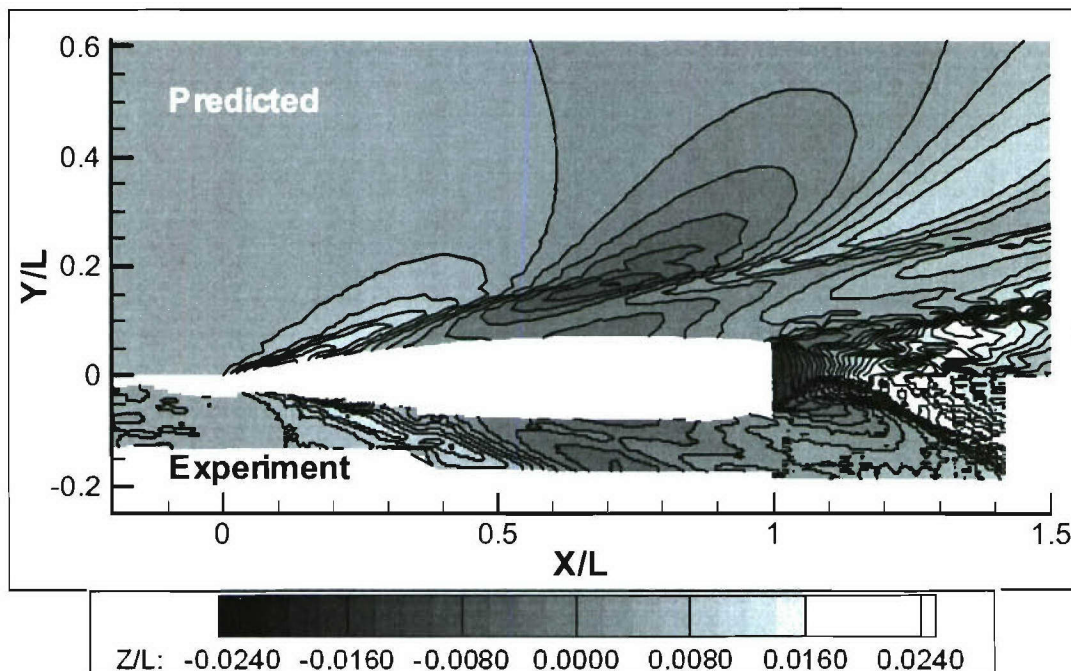
Figure 36: Predicted (Das Boot) normalized wavefield elevations (Z/L) compared with experiment, Fr=0.43; overall view.

Figure 37: Predicted (Das Boot) normalized wavefield elevations (Z/L) compared with experiment, Fr = 0.43; zoomed view at bow and stern section.

CFDSHIP-IOWA (U. of Iowa)

Predictions made by researchers at the University of Iowa[9,8] using CFDSHIP-IOWA are given in Figure 38 for the overall wave field. Again, the results indicate a good overall prediction of the Kelvin wake over the region that the experimental measurements were available. A more detailed view of the bow and stern regions is given in Figure 39. The results show good agreement in the wave elevations near the bow, and good prediction of the wave heights and topology in the stern region, including good prediction of the shoulder wave from the transom, though the maximum wave elevations are somewhat under predicted. More detailed quantitative comparison of the wave heights is provided in a later section.

Figure 38: Predicted (CFDSHIP-IOWA, U. of Iowa) normalized wavefield elevations (Z/L) compared with experiment, Fr = 0.43; overall view.

Figure 39: Predicted (CFDSHIP-IOWA, Iowa) normalized wavefield elevations (Z/L) compared with experiment, Fr = 0.43; zoomed view at bow and stern.

CFDSHIP-IOWA (NSWCCD)

Predictions were also made by researchers at NSWCCD using the CFDSHIP-IOWA code. Results are provided in Figure 40 for the overall wave field for the baseline computational grid (i.e., no Chimera grid refinement). Again, there appears to be reasonable prediction of the development of the Kelvin wake in the region where the experimental measurements are available. A more detailed view of the bow region in Figure 41 shows qualitatively good prediction of the wave heights. The shoulder wave that develops from the transom appears fairly well represented, but the rooster tail that develops in the stern wake is predicted to begin further aft than in the experimental measurements and the wave topology is somewhat broader in the computations. A more quantitative comparison of the wave height predictions is provided in a later section.

Figure 40: Predicted (CFDSHIP-IOWA, NSWC) normalized wavefield elevations (Z/L) compared with experiment, Fr = 0.43; overall view.
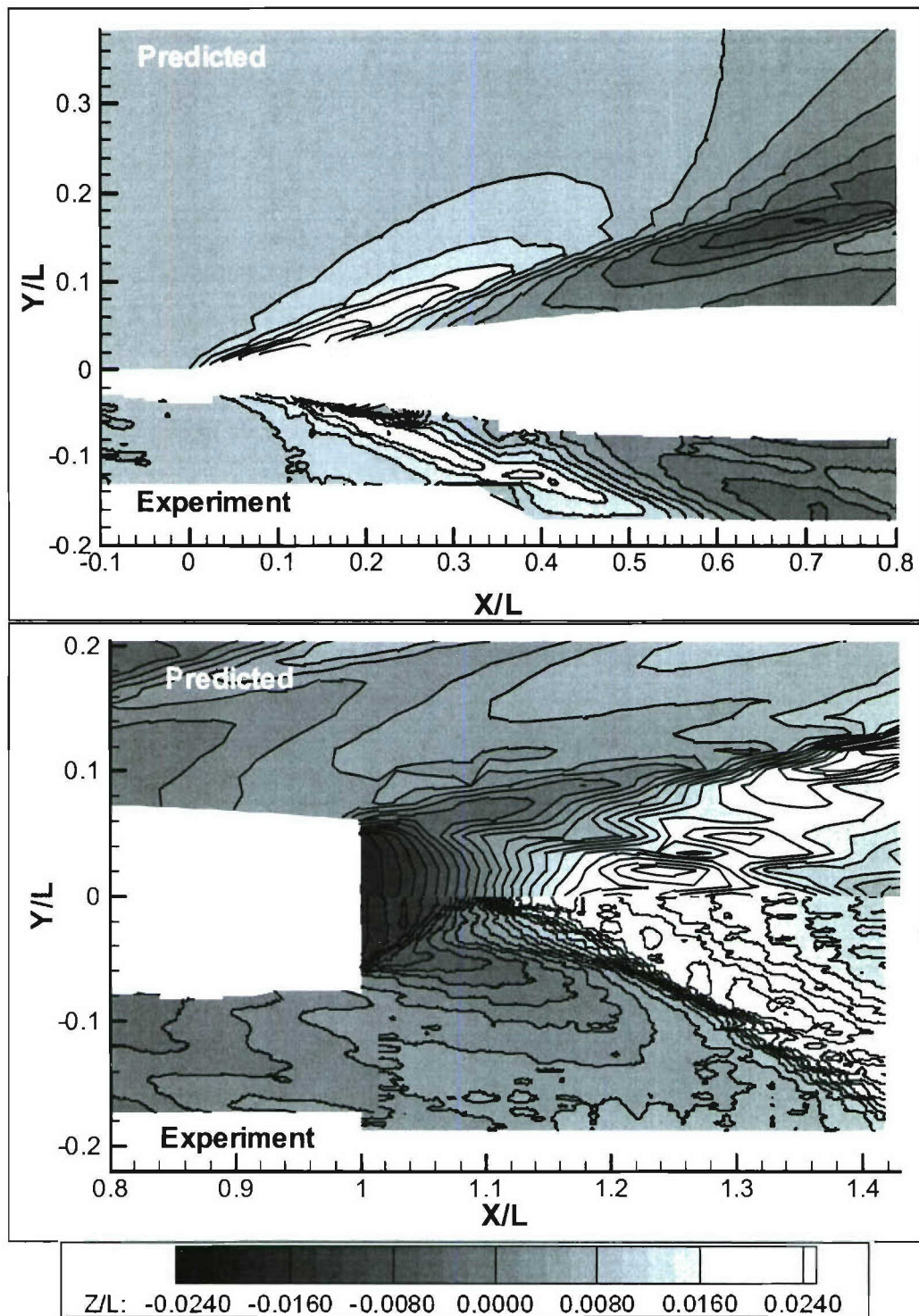
Figure 41: Predicted (CFDSHIP-IOWA, NSWC) normalized wavefield elevations (Z/L) compared with experiment, Fr = 0.43; zoomed view at bow and stern section.

CFDSHIP-IOWA (NSWCCD) with Chimera Grid Refinement

The predictions of the overall wave field with the addition of the Chimera refinement block are shown in Figure 42. A comparison of Figure 40 using only the baseline grid and Figure 42 with the addition of the Chimera refinement block shows an enhanced prediction of the bow wake and the resulting wave train. A more detailed view of the bow and stern regions is shown in Figure 43. No Chimera refinement blocks were included in the stern region; hence, there was no improvement in the prediction of the stern wake. More detailed quantitative comparisons of the predicted and measured wave heights are provided in a later section.

Figure 42: Predicted (CFDSHIP-IOWA, NSWC) normalized wavefield elevations (Z/L) compared with experiment, Fr = 0.43; overall view.
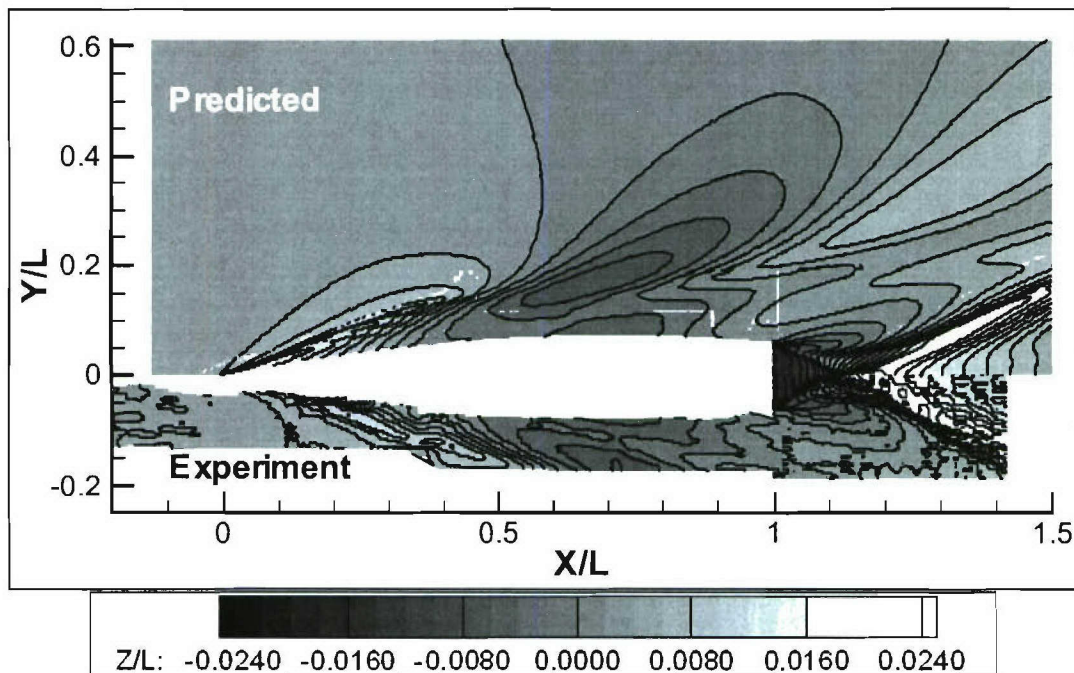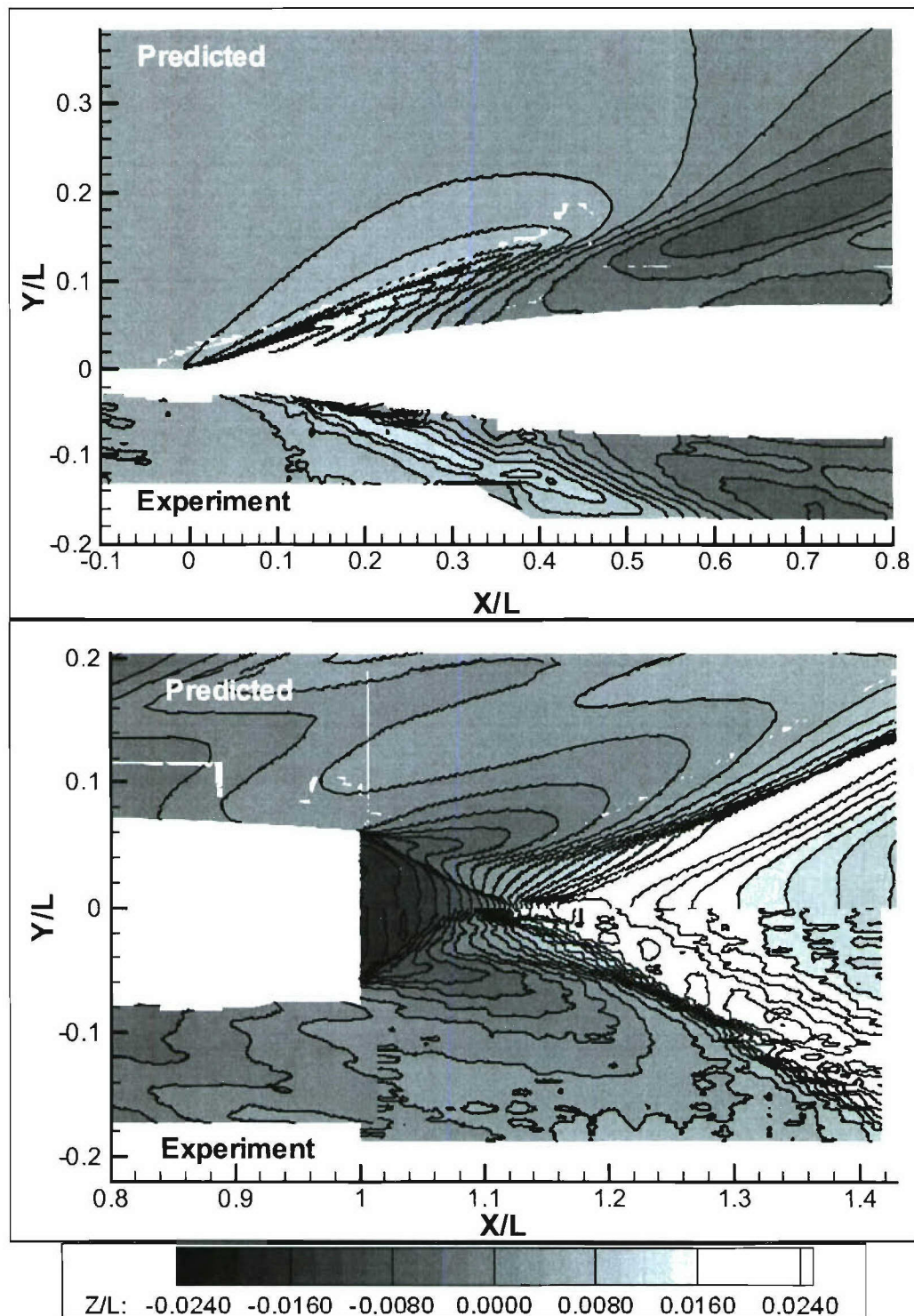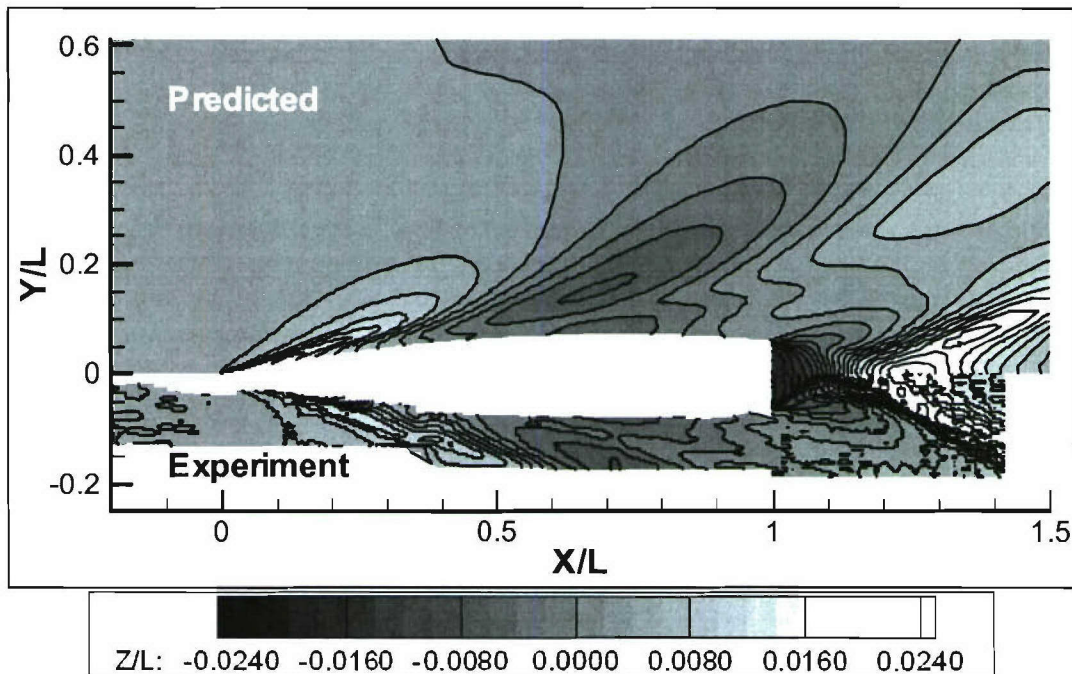
Figure 43: Predicted (CFDSHIP-IOWA, NSWC) normalized wavefield elevations (Z/L) compared with experiment, Fr = 0.43; zoomed view at bow and stern section.

Fluent

The overall wave field predicted using the commercial solver Fluent is shown in Figure 44. The results indicate a relatively good overall prediction of the Kelvin wake for the region captured in the experiments. A more detailed view of the bow and stern regions is provided in Figure 45. The bow region appears fairly well predicted. The stern region shows good prediction of the shoulder wave that develops from the transom. The rooster tail is predicted to begin further aft, but the topology appears relatively well represented. A more detailed quantitative comparison of the predicted and measured wave heights in provided in a later section.

Figure 44: Predicted (Fluent) normalized wavefield elevations (Z/L) compared with experiment, Fr = 0.43; overall view.

Figure 45: Predicted (Fluent) normalized wavefield elevations (Z/L) compared with experiment, Fr = 0.43; zoomed view at bow and stern section.
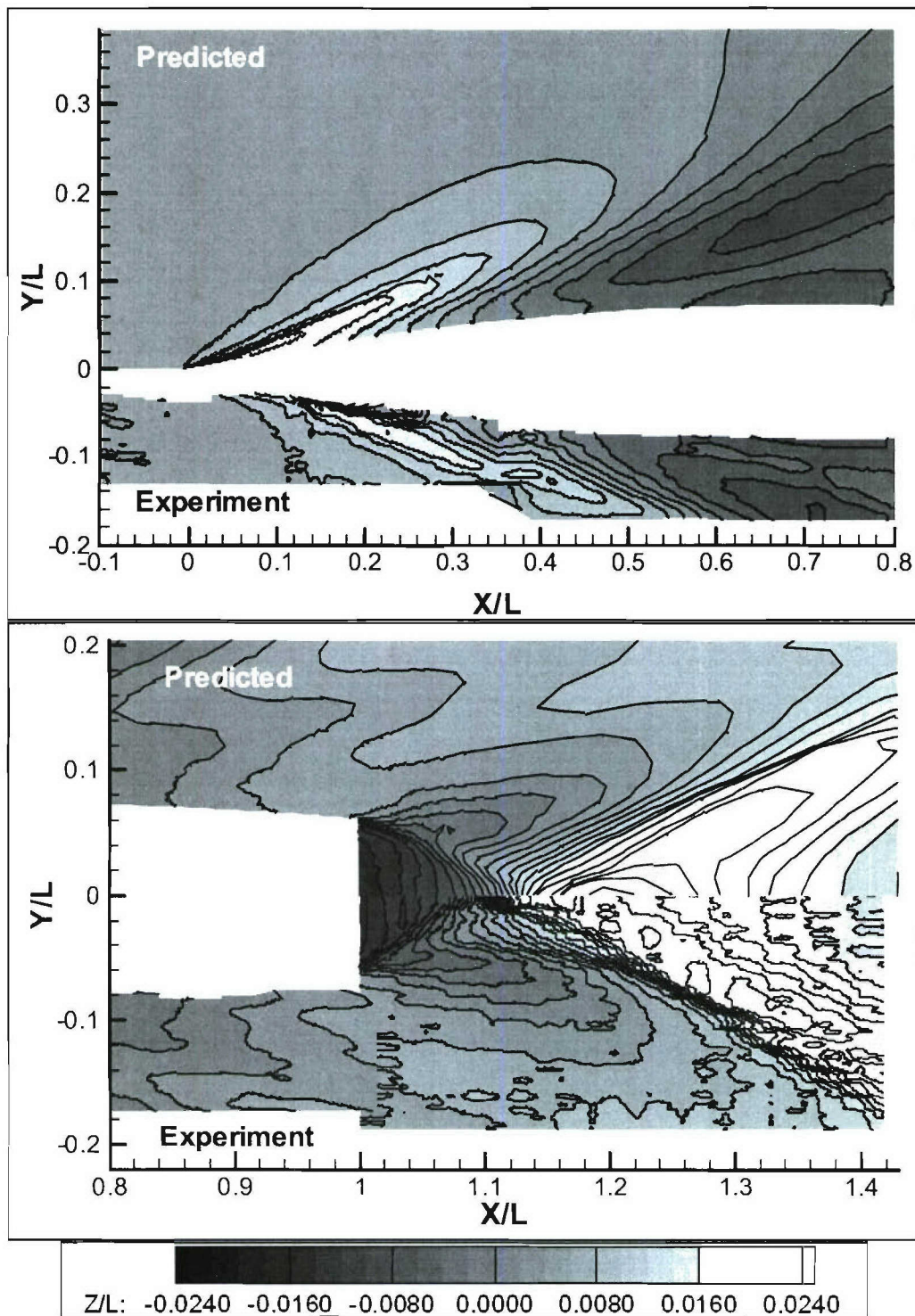
Figure 47: Predicted (Comet) normalized wavefield elevations (Z/L) compared with experiment, Fr = 0.43; zoomed view at bow and stern section.

NFA

The overall normalized wave field predictions using NFA version 2.0 [10,8] are shown in Figure 48. The results show a good prediction of the bow wake and an overall good representation of the stern wake. A more detailed view of the bow and stern regions is shown in Figure 49. A comparison of the bow region shows qualitatively good prediction of the bow wave. The stern region predictions show very good agreement with the stern wake topology, both for the shoulder wave from the edge of the transom and the rooster tail phenomenon in the stern wake.

Figure 48: Predicted (NFA) normalized wavefield elevations (Z/L) compared with experiment, Fr = 0.43; overall view.
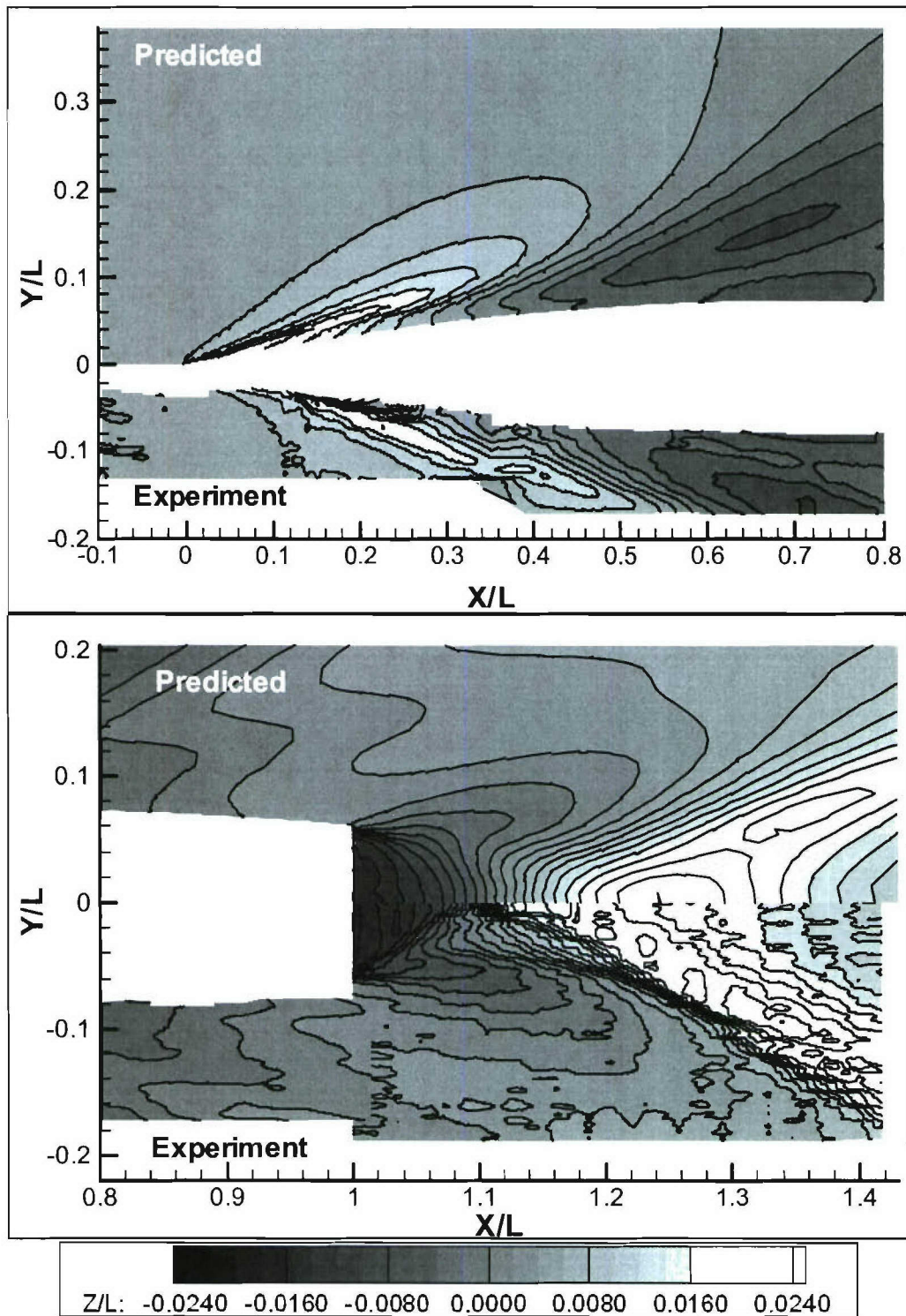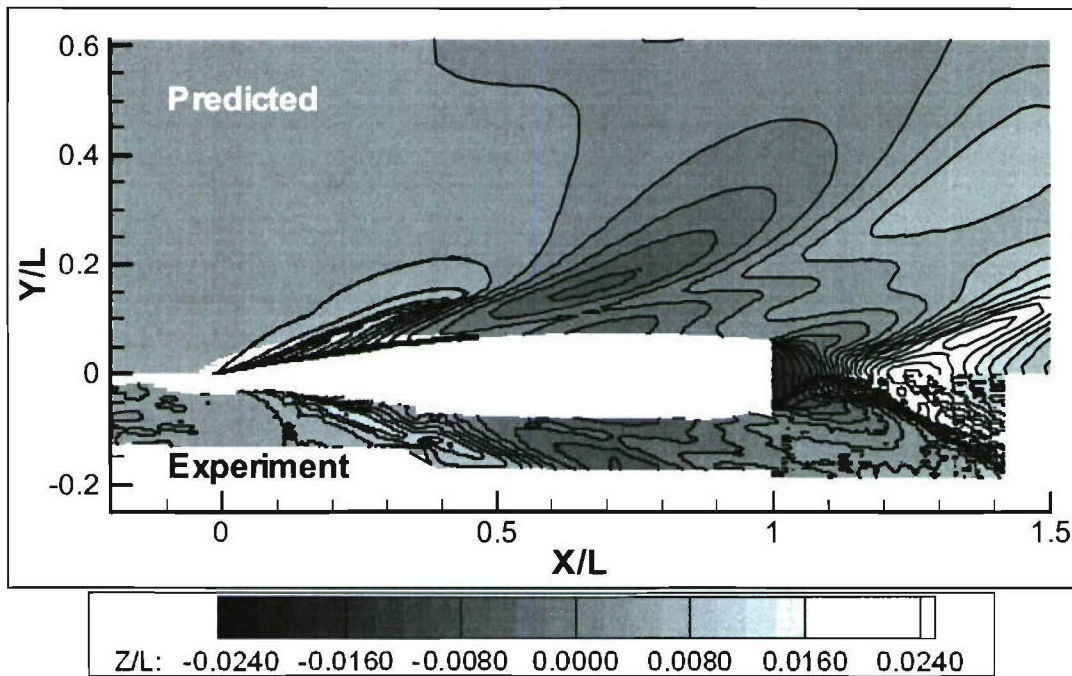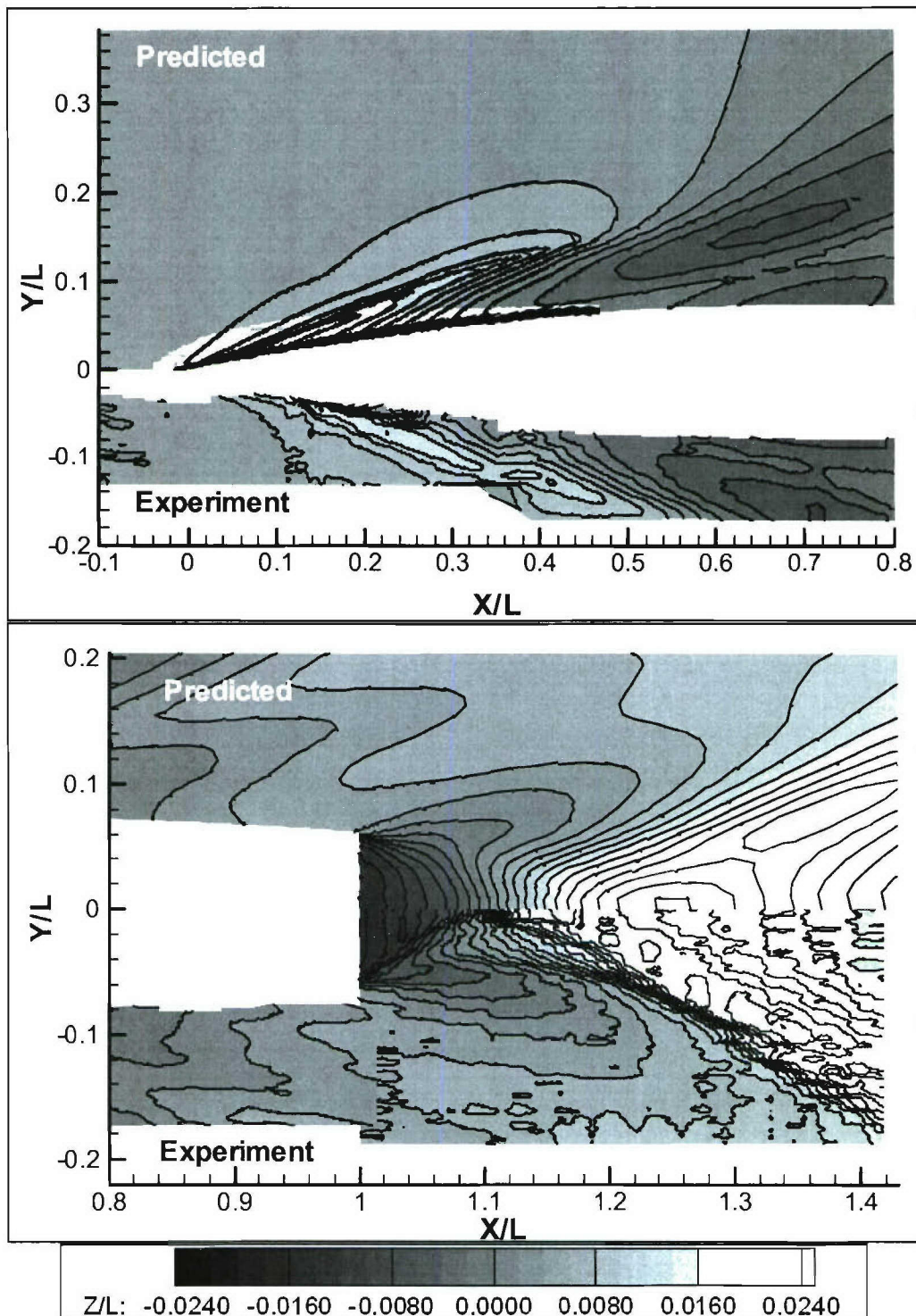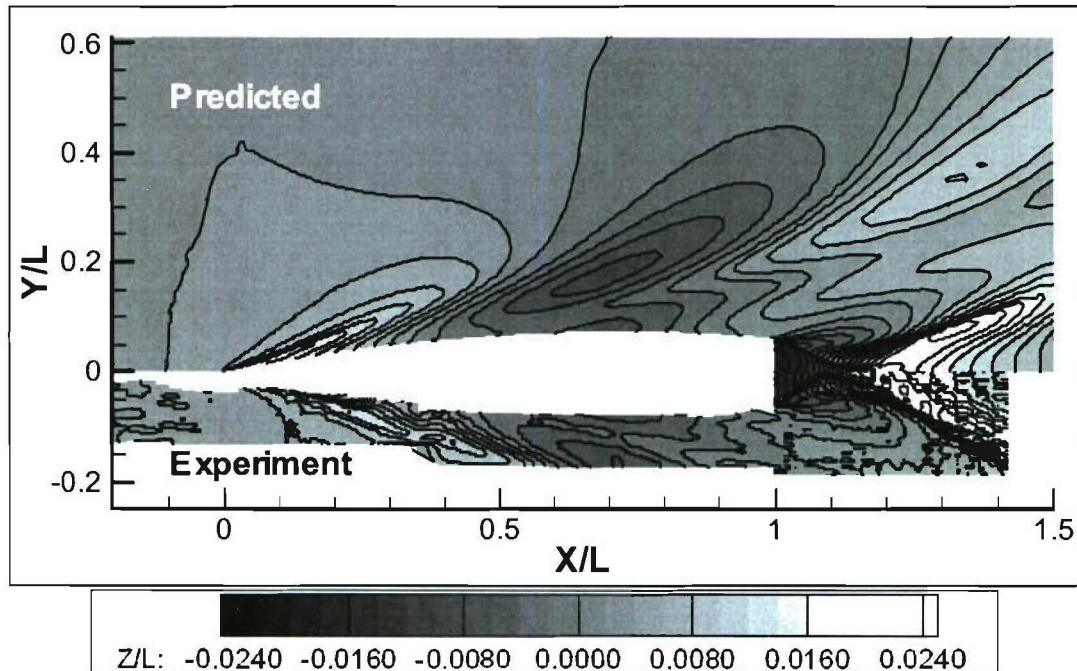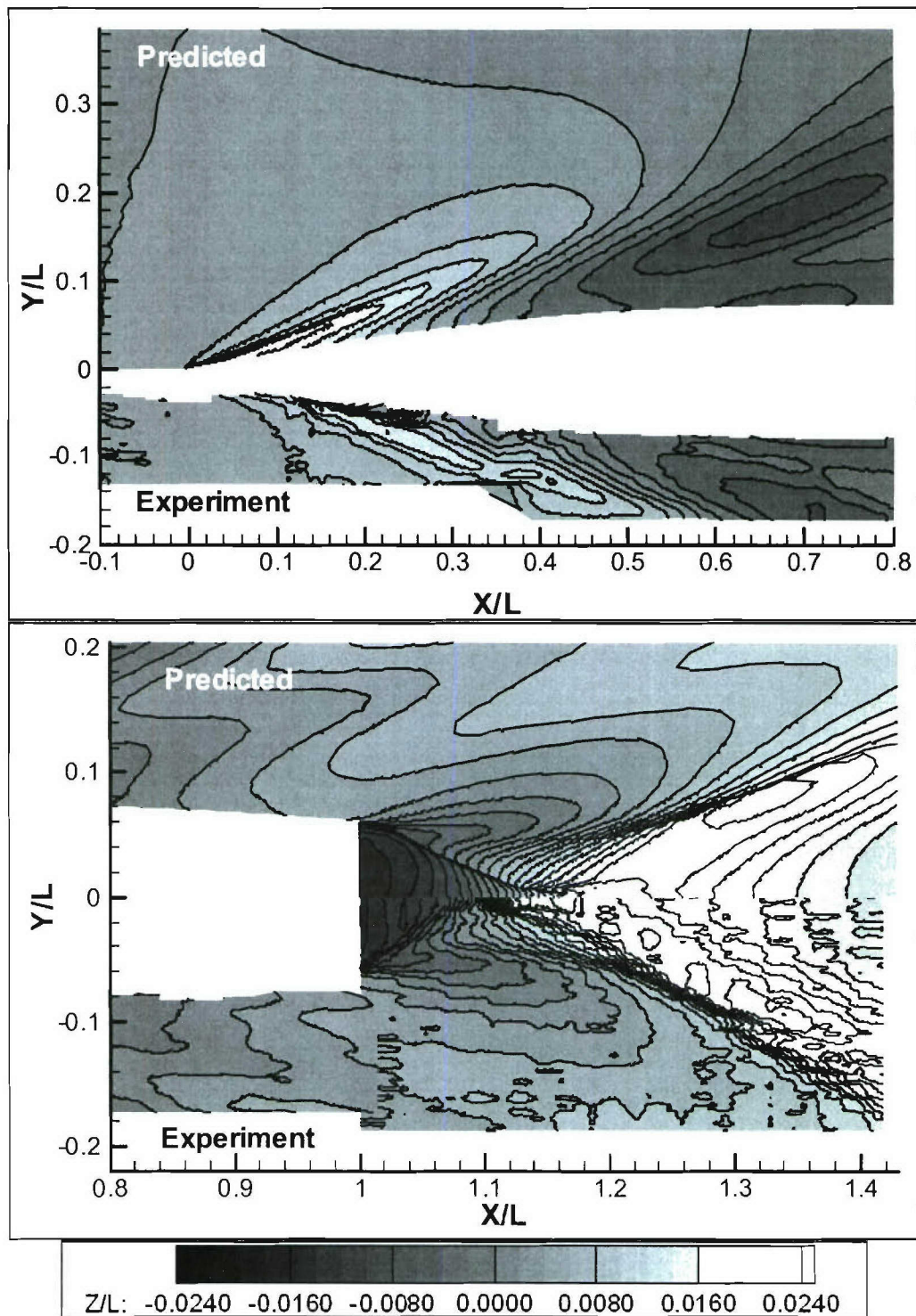
Figure 49: Predicted (NFA) normalized wavefield elevations (Z/L) compared with experiment, Fr = 0.43; zoomed view at bow and stern section.
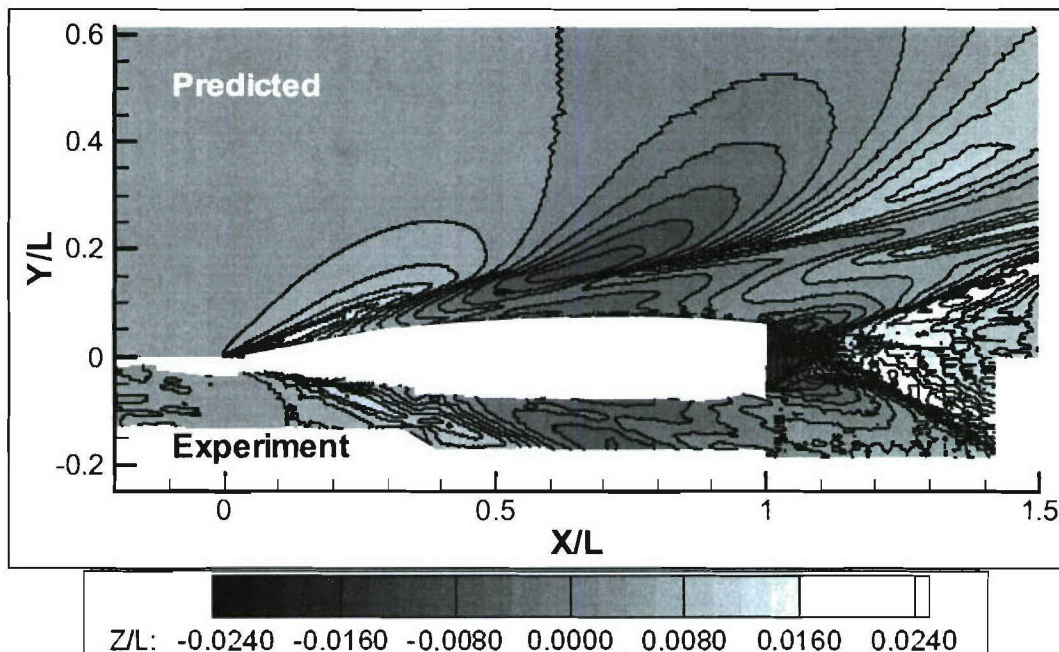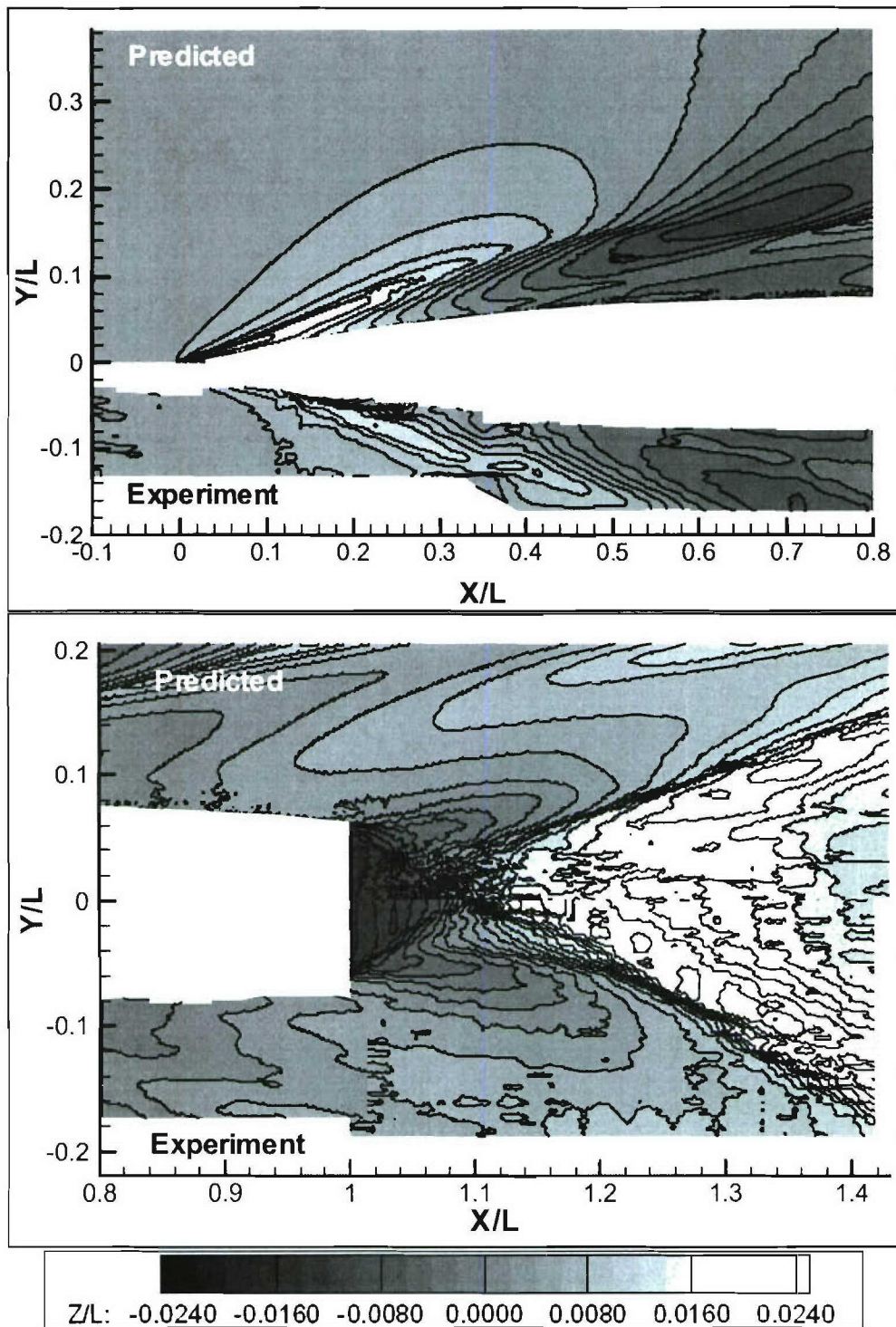
Fr = 0.43 (Full-Scale Speed = 18.0 knots) Wavecuts

This section provides a more quantitative comparison of the wave height predictions of the various solution methods for Fr = 0.43. The wave elevations were recorded in the experiments using capacitance probes at four transverse locations away from the ship hull centerline. These locations were at y/B_T = 0.86, 1.50, 2.0, and 2.5 where B_T is the maximum beam of the model: 0.84 m (2.74 ft).

The comparisons between the measured and predicted wave cuts using the Das Boot program[7,8] are shown in Figure 50 for all four transverse locations. The predictions overall agree well with the experimental measurements, although the first wave aft of the transom stern (x/L ~ 1.3) is over predicted for y/B_T = 0.86. The maximum wave elevation is under predicted for the further transverse locations, but overall the wave elevations are well quite well predicted.

The predictions made by the University of Iowa researchers[9,8] using CFDSHIP-IOWA are compared with the measured wave heights in Figure 51. The results indicate that the code does a good job in predicting the wave elevations of the bow wave as it proceeds out away from the ship model. The first wave crest just aft of the transom is also well predicted for the first two transverse locations closest to the ship model. At the further transverse locations, the stern wave is under predicted, but overall the code does a good job predicting the wave elevations for all four wave cut locations. The computational domain size, however, was limited to a fairly small region downstream from the ship model; hence, it is not possible to make comparisons with the experiment at regions greater than a ship length downstream from the transom stern (i.e., at locations greater than x/L = 2).

The predicted wave heights made by NSWCCD using the CFDSHIP-IOWA code are shown in Figure 52 for the baseline grid with no chimera grid refinement. The predictions show reasonable agreement of the bow wave and stern wave for y/B_T = 0.86, being only slightly under predicted; however, there is a divergence in the wave elevation at the farthest downstream section near x/L = 2. At the other wave cut locations, there is generally good agreement in the bow region, but a decreasing stern wave elevation. And the overall spatial resolution of the smaller details of the wave pattern get worse at the wave cut locations further away from the ship model. The predictions with the addition of the chimera grid refinement block are shown in Figure 53. The added grid resolution provides some improvement in the bow region, but, since there was no grid refinement at the stern, the remainder of the wave elevations appear unchanged. Also, as in the case of the Iowa predictions, the computational domain only went to x/L = 2 so no comparisons could be made farther downstream.

The wave elevations predicted using Fluent are shown in Figure 54. The code does a good job overall in predicting the wave elevations for all of the wave cut locations, with only perhaps a small phase shift in the bow region. Also, the maximum elevation of the stern wave peak is under predicted for y/B_T = 0.86, 1.50 and 2.0. The general wave topology is well represented at all of the wave cut locations, though at the further locations there is insufficient spatial resolution to capture some of the smaller wave

details. These predictions also do not exhibit the free surface height "sinking" that was evident in the lower Froude number predictions.

The Comet wave cut predictions are shown in Figure 55. The results show similar agreement to the Fluent results, with a good overall representation of the wave field, but under predicting the maximum stern wave height. Overall the code does a good job, but begins to lose the resolution of the smaller wave details in moving to the further wave cut locations. This again likely points out the lack of grid resolution moving away from the ship model.

The wave cuts predicted using the NFA Euler code[10,8] are compared with the experimental wave cuts in Figure 56. The results show an overall good agreement with the experimental measurements, although at all four wave cut locations, the downstream wave elevation tapers off to a fixed value after approximately $X/L = 2.25$. This is likely due to difficulties in setting an appropriate downstream boundary condition. Also, the computational domain is not sufficient to compare with the experimental measurements further downstream ($X/L > 2.5$). At the first transverse location, $y/B_T = 0.86$, the NFA predictions show very good agreement for the bow wave and the near-bow region, similar to the comet predictions, but with a slight phase shift. The stern wave is relatively well predicted, but the magnitude of the maximum wave height is under predicted, and again there is a small phase shift in the predictions. At $y/B_T = 1.50$ the NFA code predicts the locations of the smaller wave peaks, but the magnitude is over predicted near $x/L = 0.9$ and 1.25, and the stern wave maximum elevation is again under predicted. At the further wave cut locations the NFA code continues to have good agreement with the experimental measurements. Even at the furthest location from the ship model, $y/B_T = 2.50$, the wave elevations are very well predicted up to about $X/L = 2$.

DasBoot:
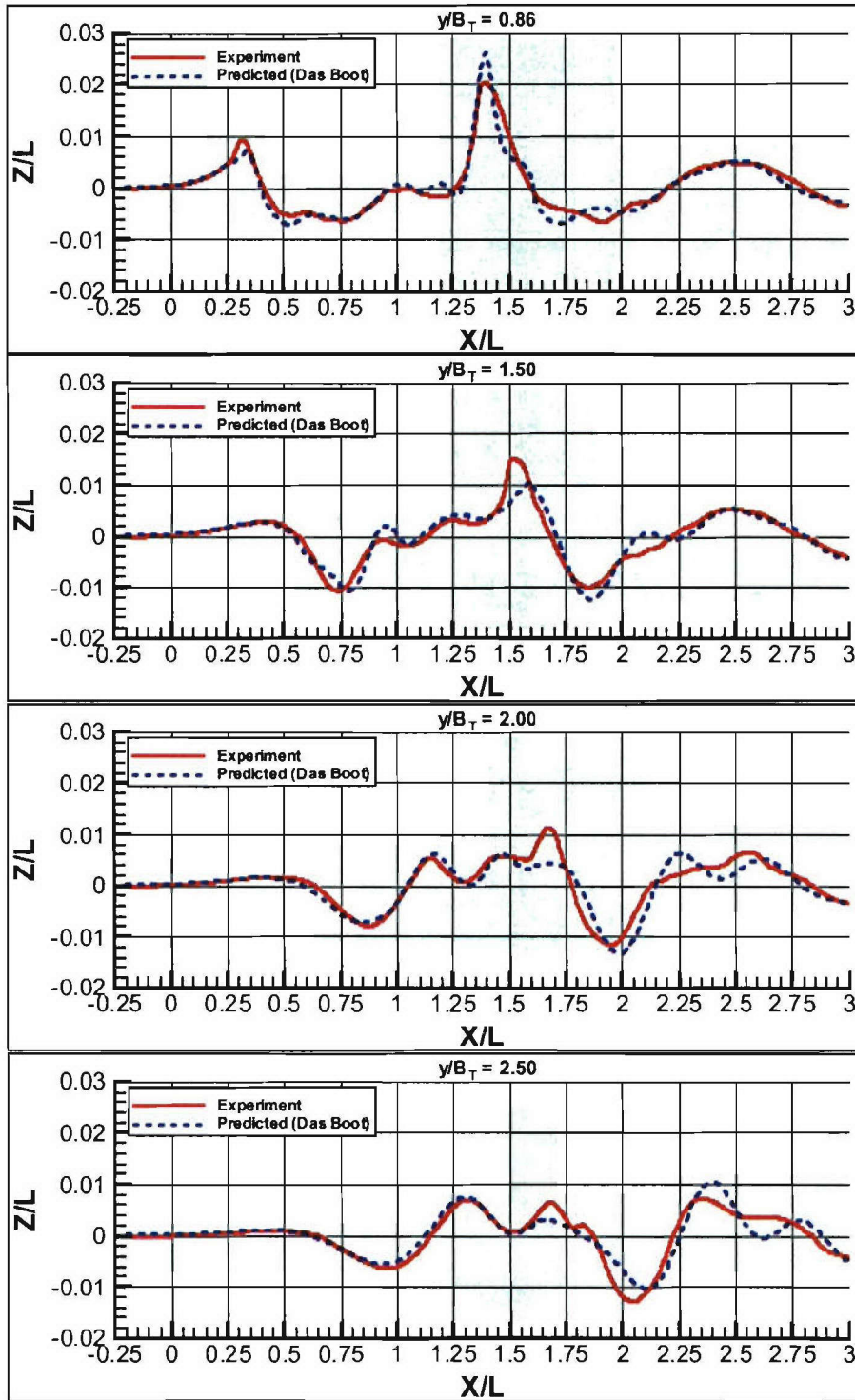
Figure 50: Predicted (Das Boot) and measured wavecuts for Model 5365, Fr = 0.43: (a) y/B = 0.86, (b) y/B = 1.50, (c) y/B = 2.0, and (d) y/B = 2.50.

CFDSHIP-IOWA (U. of Iowa)
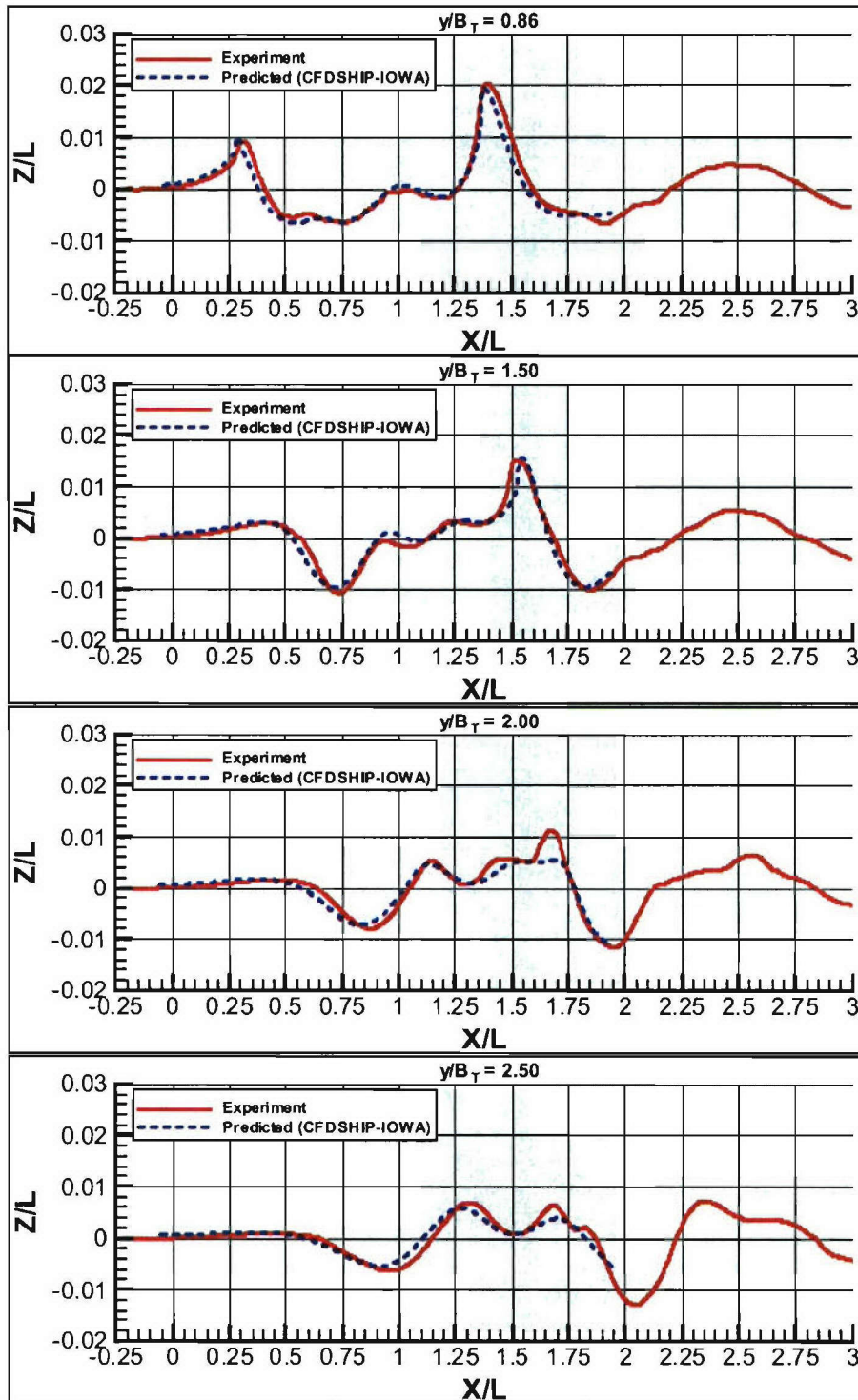
Figure 51: Predicted (CFDSHIP-IOWA, U. of Iowa) and measured wavecuts, Model 5365, Fr = 0.43: (a) y/B=0.86, (b) y/B=1.50, (c) y/B=2.0, (d) y/B=2.50.

CFDSHIP-IOWA (NSWCCD)
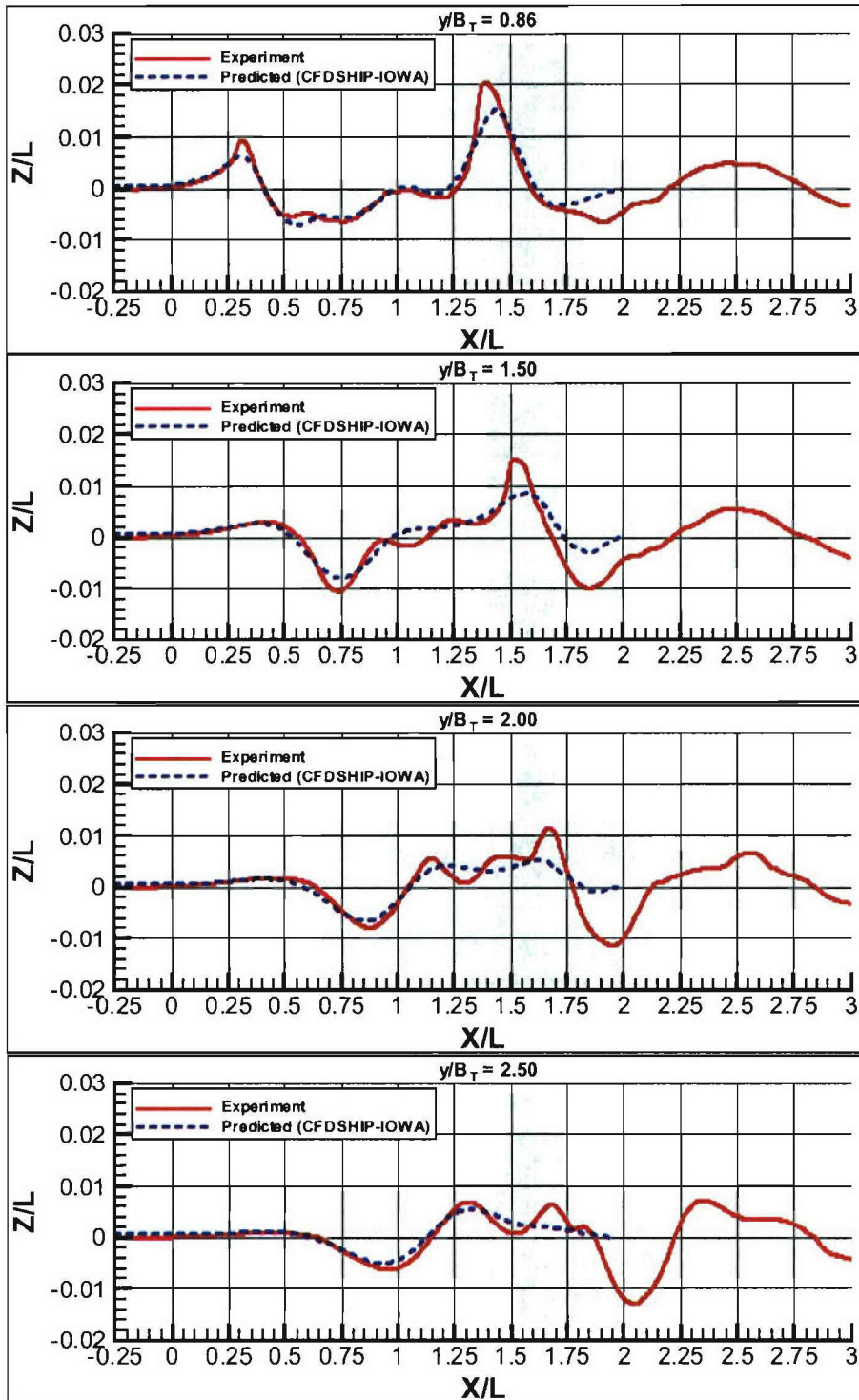
Figure 52: Predicted (CFDSHIP-IOWA, NSWCCD) and measured wavecuts, Model 5365, Fr = 0.43: (a) y/B=0.86, (b) y/B=1.50, (c) y/B=2.0, (d) y/B=2.50.

CFDSHIP-IOWA (NSWCCD) with Chimera Grid Refinement
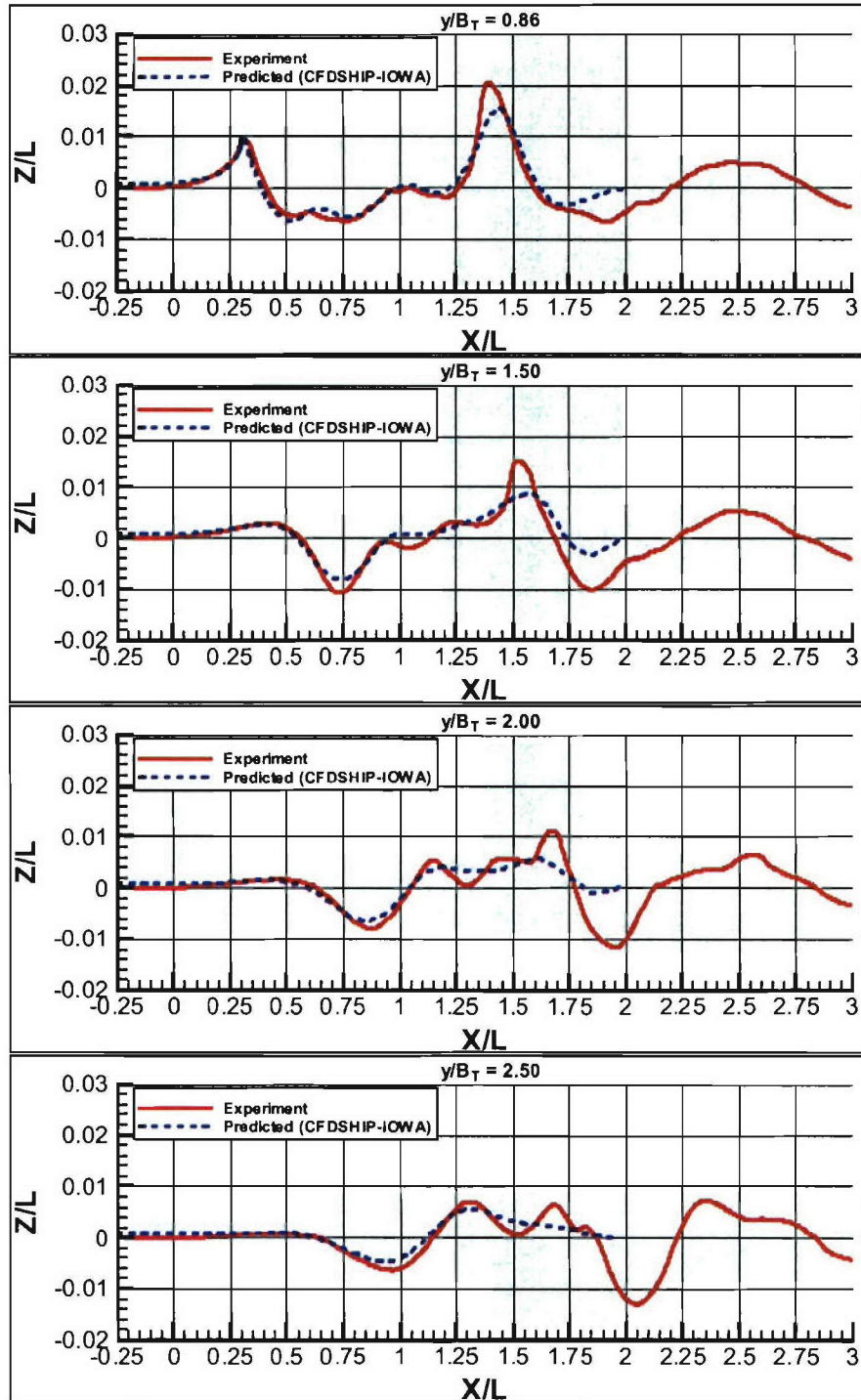
Figure 53: Predicted (CFDSHIP-IOWA, NSWCCD) with chimera grid refinement and measured wavecuts, Model 5365, Fr = 0.43: (a) y/B=0.86, (b) y/B=1.50, (c) y/B=2.0, (d) y/B=2.50.
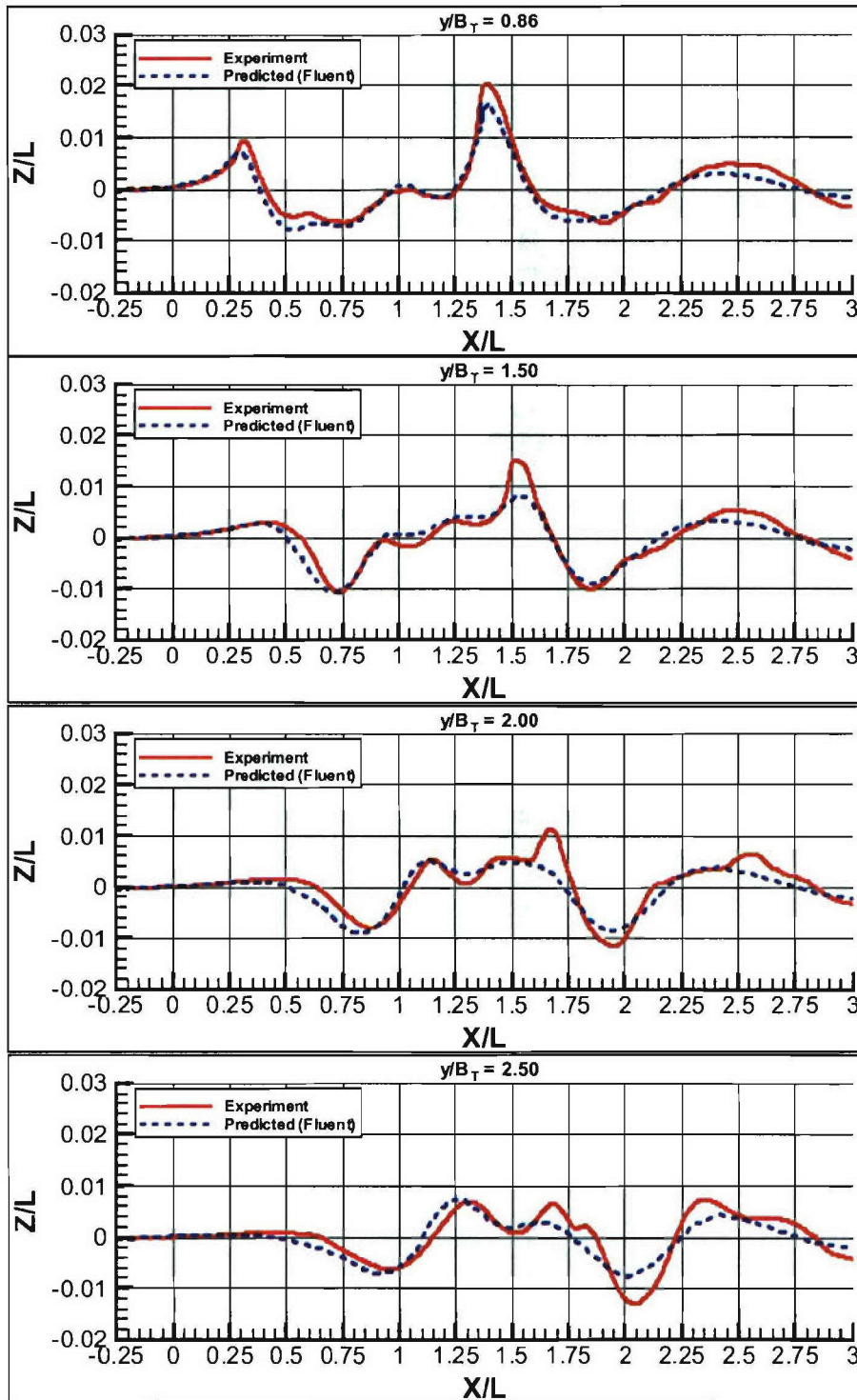
Fluent

Figure 54: Predicted (Fluent) and measured wavecuts for Model 5365, Fr = 0.43: (a) y/B = 0.86, (b) y/B = 1.50, (c) y/B = 2.0, and (d) y/B = 2.50.
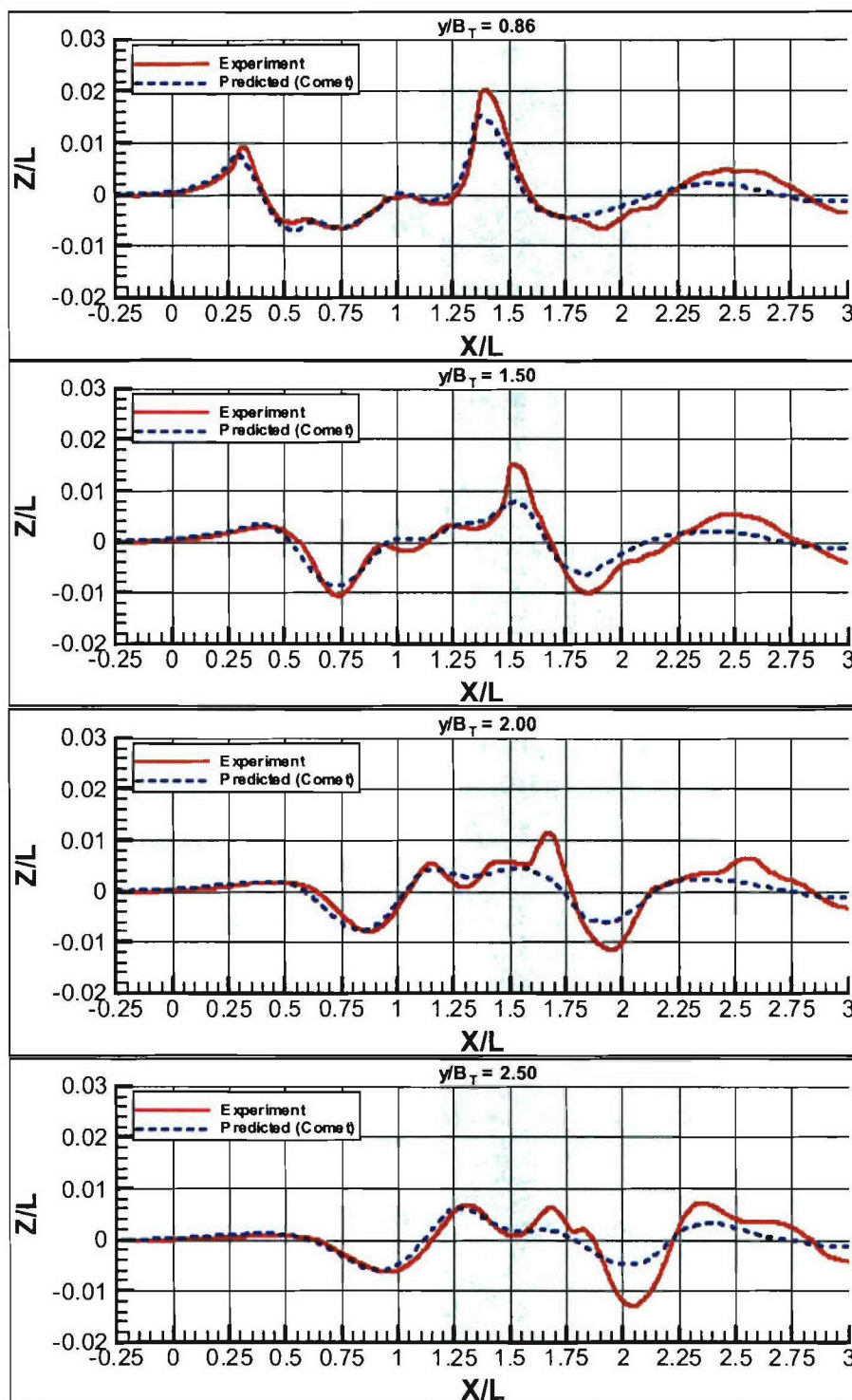
Comet

Figure 55: Predicted (Comet) and measured wavecuts for Model 5365, Fr = 0.43: (a) y/B = 0.86, (b) y/B = 1.50, (c) y/B = 2.0, and (d) y/B = 2.50.

NFA
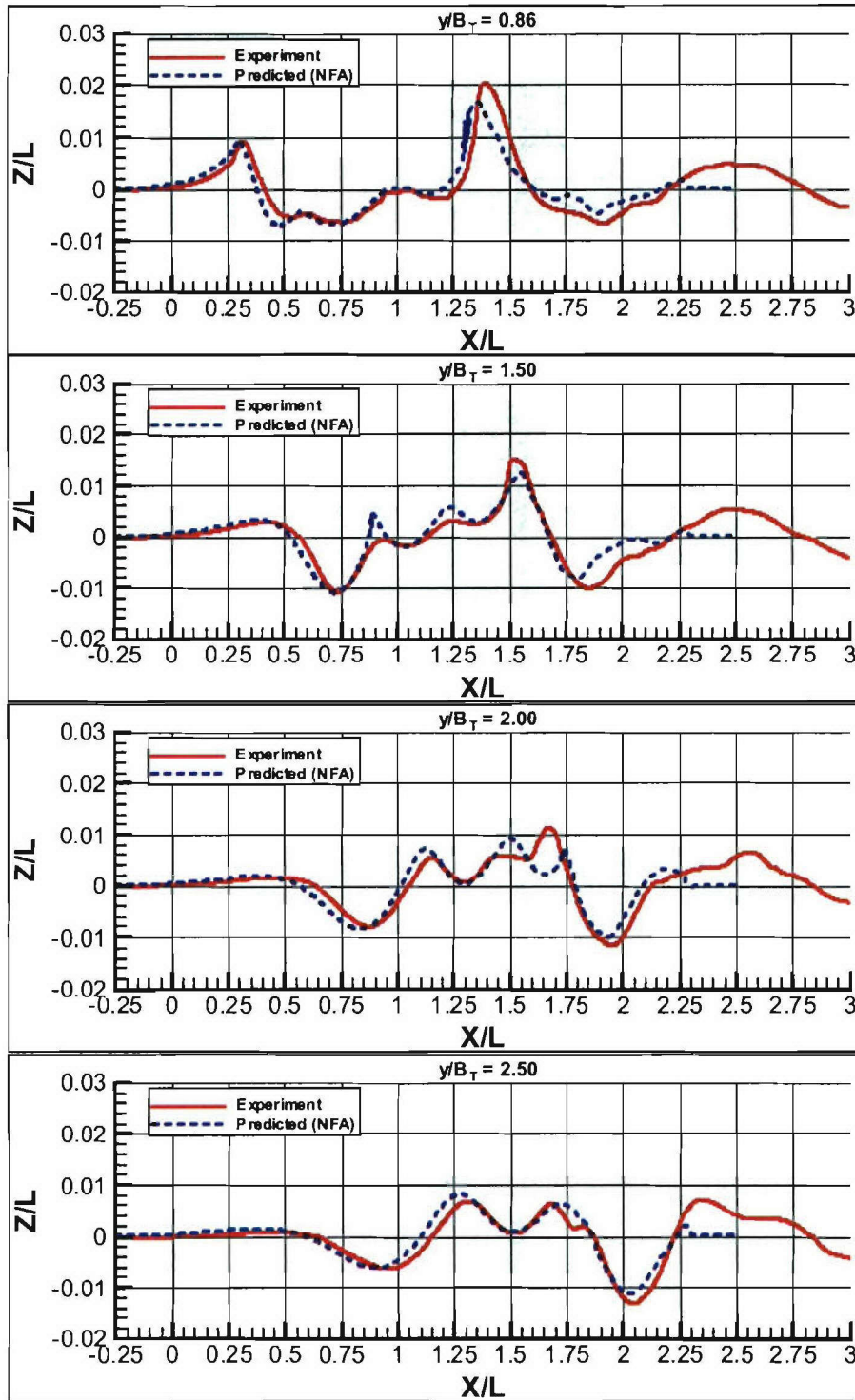
**Figure 56: Predicted (NFA) and measured wavecuts for Model 5365, Fr = 0.43:
(a) y/B = 0.86, (b) y/B = 1.50, (c) y/B = 2.0, and (d) y/B = 2.50.**

Fr = 0.43 (Full-Scale Speed = 18.0 knots) Summary

A summary of the observations regarding the predicted wave elevations and wavecuts by the different codes is given in Table 6. Again, these ratings are somewhat subjective, but it provides a reasonable way to evaluate the differences in the prediction methods.

Table 6: Summary of wave elevation and wavecut predictions (Fr = 0.43).

Case	Code	Bow Region	Stern Region	Wave Cuts
1	Das Boot w/Breaking Model	Looks Okay	Looks Okay	Looks Really Good
2	CFDSHIP-IOWA	Looks Good	Looks Good	Looks Really Good
3	CFDSHIP-IOWA (NSWC)	Looks Good	Looks Good	Looks Okay
4	CFDSHIP-IOWA w/Chimera	Looks Good	Looks Good	Looks Good/Okay
5	Fluent	Looks Good	Looks Good	Looks Good/Okay
6	Comet	Looks Good	Looks Good	Looks Okay
7	NFA v2.0	Looks Good	Looks Good	Looks Really Good

Resistance

As part of the tasking for the workshop, each of the participants also provided a prediction of the resistance (total drag force) on the hull for each ship speed. The results are summarized in Table 7 for Fr = 0.25 (full-scale speed = 10.5 knots) and in Table 8 for Fr = 0.43. The results from the 1979 DTMB test (reported in Jenkins, 1984)[6] and a previously unpublished set of data from a test at DTMB in 1992 are also included.

Table 7: Summary of predicted resistance (total drag force) for Fr = 0.25.

F_x (lbs)	Code
11.43	Das Boot
10.43	CFDSHIP-IOWA
11.38	CFDSHIP-IOWA (NSWC)
11.33	CFDSHIP-IOWA w/Chimera
9.56	Fluent
10.78	Comet
11.00	1979 (Interpolated)
7.73	Measurement (2004)

Table 8: Summary of predicted resistance (total drag force) for Fr = 0.43.

F_x (lbs)	Code
31.03	Das Boot
28.24	CFDSHIP-IOWA
31.76	CFDSHIP-IOWA (NSWC)
31.81	CFDSHIP-IOWA w/Chimera
28.46	Fluent
33.05	Comet
32.30	1979 (Interpolated)
21.98	Measurement (2004)

A comparison of the predicted and measured resistance is shown graphically in Figure 57. For the two ship speeds considered, it appears that the predictions made using Fluent and those made by the University of Iowa using CFDSHIP-IOWA have a slightly better prediction of the resistance. At the higher ship speed, the predictions made using Comet were slightly worse than the others.
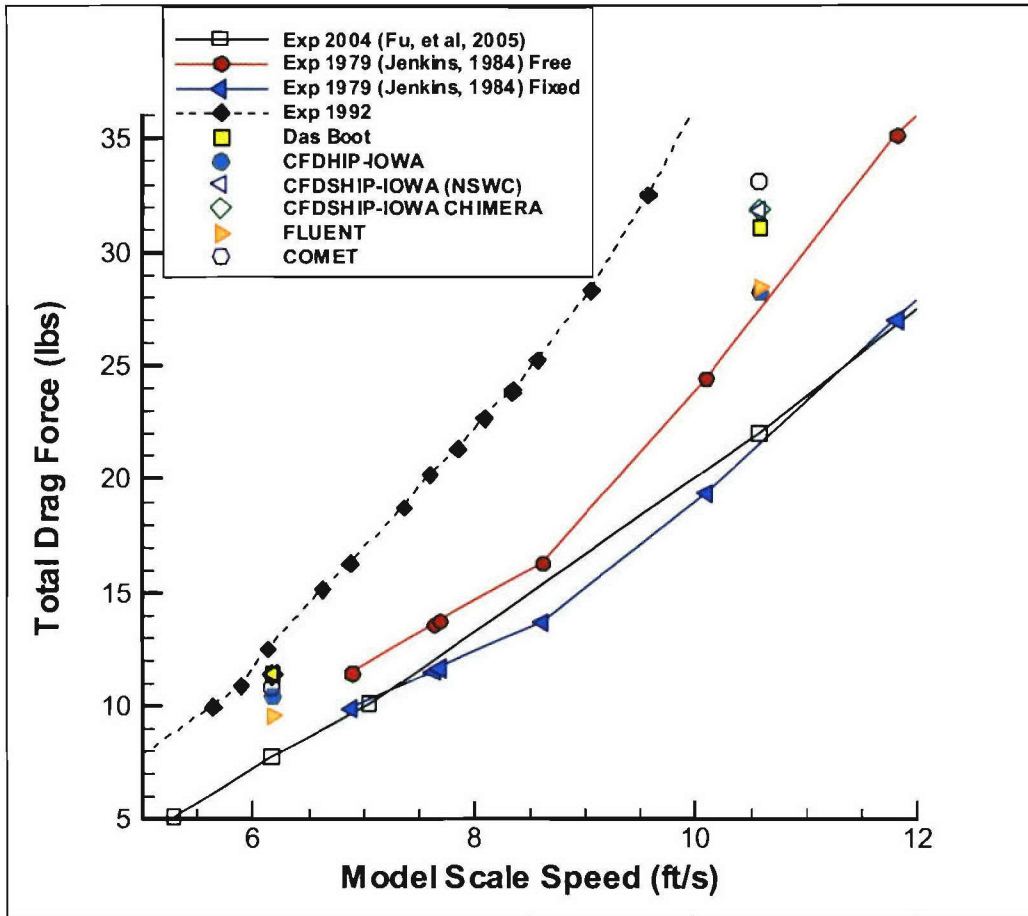
Figure 57: Comparison of predicted and measured resistance for Model 5365.

Sinkage, trim, and resistance were measured over a range of Froude numbers (0.14 to 0.82). The sinkage and trim are also in good agreement with Jenkins (1984)[6] as well as previously unpublished data acquired in 1992. This was shown in Fu *et al.* (2005)[1]. The measured total resistance is systematically less than the previously measured data, pointing to an error in calibration or possible stiction in the tow post/grasshopper. While an error in speed is another possible explanation, this seems unlikely, in that the wave cuts and sinkage and trim data are in good agreement with the 1979 Jenkins data[6].

Wave Breaking Predictions

One of the primary purposes of the workshop was to survey the current state-of-the-art in numerical prediction methods, to determine whether they are capable of predicting wave breaking. As stated previously, the codes that were examined fall into basically three groups: (1) inviscid flow methods with an additional model to handle wave breaking, (2) commercial and university codes using VOF interface capturing, and (3) university codes using level-set interface capturing methods. Some of the results from the workshop are highlighted in this section to show the capabilities of the different codes to predict the wave breaking phenomena.

Wave field predictions made by the University of Iowa researchers[9] using CFDSHIP-IOWA are shown in Figure 58 for the higher Froude number case (Fr = 0.43). Predictions made by NSWCCD are shown in Figure 59. Both of these figures demonstrate the ability of the CFDSHIP-IOWA code to predict overturning wave structures. This is a significant departure from previous interface tracking methods, which relied on adjusting the shape of the computational grid to match the fluid interface. With the interface tracking methods it is not possible to predict waves that turn over onto themselves, or even fairly steep waves for that matter. With the use of the level set method, there is no constraint on the computational grid, and the fluid interface is found to reside inside the fixed grid space, providing a more robust solution, and avoiding the limitations that would prevent the prediction of steep waves or overturning waves.
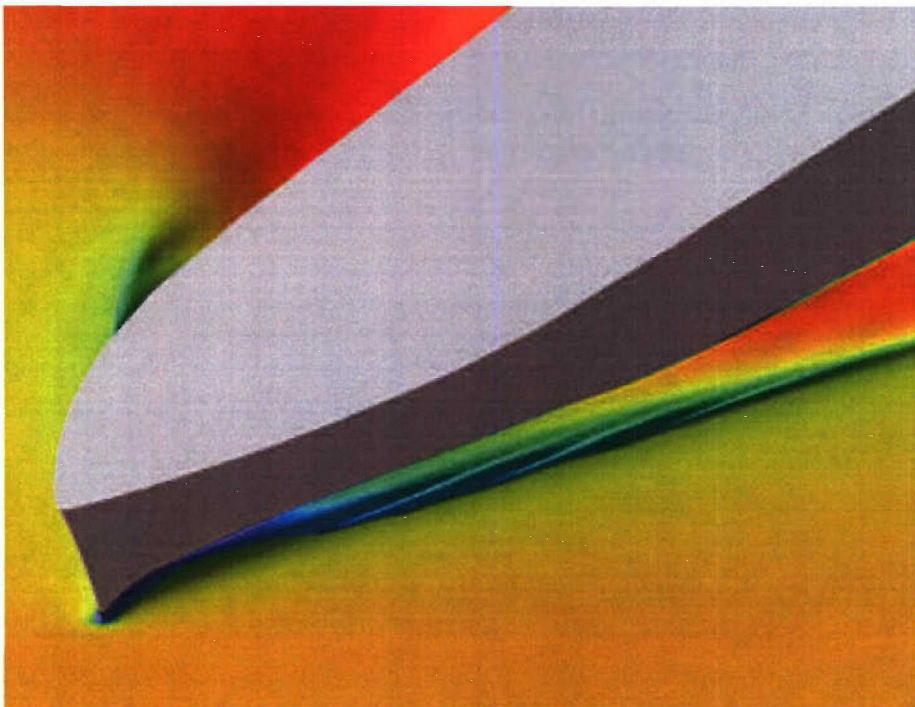
Figure 58: Free surface wave breaking predictions (Fr=0.43), CFDSHIP-IOWA (U. of Iowa).
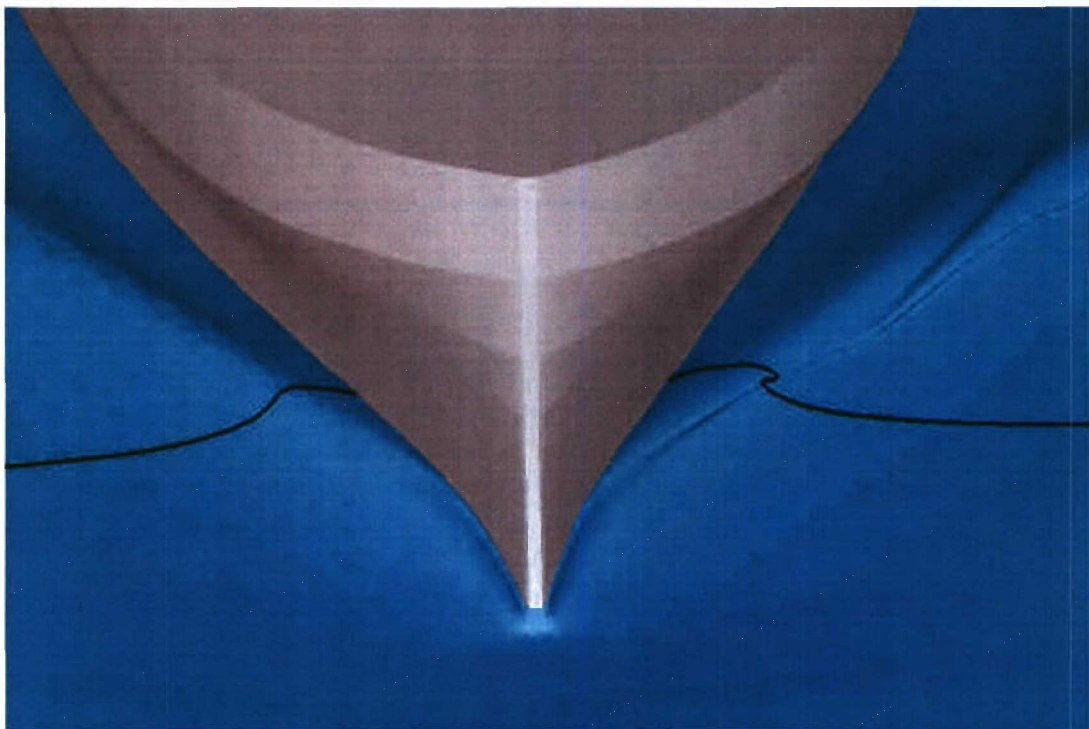
Figure 59: Free surface wave breaking predictions (Fr = 0.43), CFDSHIP-IOWA (NSWC), baseline grid (left) and with chimera grid refinement (right).

Figure 59 also includes a comparison of the baseline grid predictions with those made using chimera grid refinement. The black lines in the figure follow isoparms along the free surface to help distinguish the shape of the free surface. As shown in the figure, it is necessary to have sufficient grid resolution to be able to resolve the overturning wave structure. Without sufficient resolution the fluid interface in the overturning regions is simply smeared out and the wave does not turn over on itself, as shown on the left of the figure; however, this had little impact on the predicted resistance.

A similar grid comparison is shown in Figure 60 for predictions made using the commercial solver Comet for Fr = 0.43. The two commercial codes, Comet and Fluent, use the volume of fluid (VOF) method of interface capturing, as discussed previously. This method also does not have the limitations of the interface tracking methods which require manipulation of the grid topology to follow the fluid interface. As shown in the figure, the code is able to predict overturning waves, as shown on the right, provided that there is sufficient grid resolution. In the case of Comet, the added grid resolution can be added by the use of focused grid adaption, where the computational cells in a particular region of the flow are refined into smaller subdivisions as you approach the viscous surface (i.e., the ship hull).

All of these results indicate the ability of the interface capturing methods to predict the wave breaking phenomena. The primary requirement is to have sufficient spatial grid resolution, at least in the vicinity of the changes in the fluid interface, such

that the small changes in the interface shape can be resolved. If the computational grid is too coarse, then it is not possible to predict the changes in the shape of the fluid interface.

Figure 60: Free surface wave breaking predictions (Fr = 0.43), Comet, baseline grid (left) and with grid refinement (right).

SUMMARY AND OBSERVATIONS
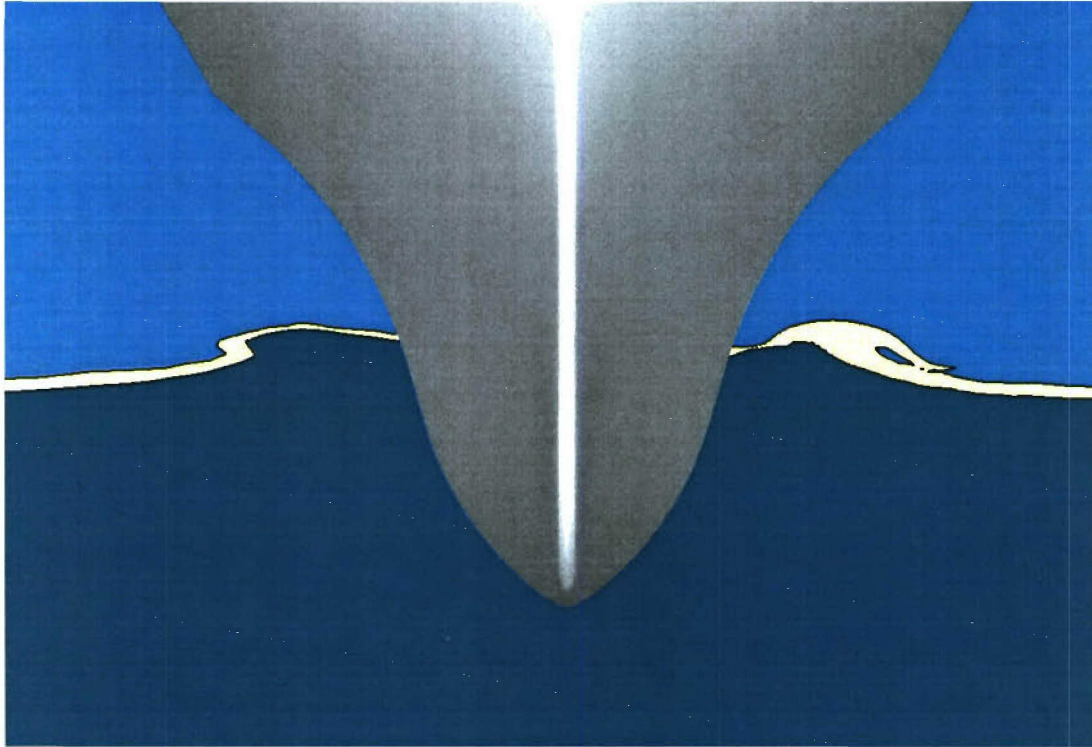
Detailed measurements and characterization of the wave field around Model 5365 were completed and used during the 2005 ONR Ship Wavebreaking Workshop, to evaluate the current capability of CFD codes to accurately predict the wave field and wave breaking generated from a ship at constant velocity. Detailed surface topography was measured at four speeds, corresponding to full-scale speeds of 5.4, 9.3, 13.3, and 15.4 m/s (17.7, 30.4, 43.5, and 50.6 ft/s), or 10.5, 18, 25.8 and 30 knots. Longitudinal wave cuts were also made at these speeds and were used to compute wave resistance for these four speeds. C_w was in good agreement with the results reported by Jenkins (1984)[6].

Sinkage, trim, and resistance were measured over a range of Froude numbers (0.14 to 0.82). The sinkage and trim are also in good agreement with Jenkins (1984) as well as previously unpublished data acquired in 1992. The measured total resistance is systematically less than the previously measured data, pointing to an error in calibration or possible stiction in the tow post/grasshopper. While an error in speed is another possible explanation, this seems unlikely, in that the wave cuts and sinkage and trim data are in good agreement with Jenkins (1984)[6]. Further details regarding the experimental measurements are provided in Fu, *et al* (2005)[1].

The computational predictions made as part of the workshop are presented for each of the two speed cases considered, which correspond to full-scale ship speeds of 10.5 and 18.0 knots, with corresponding Froude numbers of 0.25 and 0.43, respectively. These two cases were chosen as they represent both a displacement speed, submerged transom case and a dry transom, semi-planing case. The computations are compared with experimental measurements for the surface topography in regions close to the ship model, and for four separate longitudinal wave cut locations. An attempt has also been made in this report to provide a reasonable comparison of the different solution methods that were used for this workshop. This comparison includes the different numerical approaches, computational grid requirements, interface prediction schemes, and required computational resources to complete the calculations. It was found that each of the different solution methods has different advantages and disadvantages, and each has certain specific requirements for obtaining accurate solutions of a surface ship wave field.

A rating system was used to make some comparisons between the different prediction methods based on the comparisons with the experimental measurements for the wave field topography and longitudinal wave cuts. Though somewhat subjective, this provides a reasonable way to assess the capabilities of the different codes, as well as their relative strengths and weaknesses. The predicted total drag force on the model was presented and compared with previous model test data. Comparisons were also made of the necessary computational resources to achieve the solutions presented as part of the workshop. These three pieces together provide a means of assessing the different solution methods.

The single potential flow method, Das Boot, was extremely fast and provided reasonably good predictions of the longitudinal wave cuts to the furthest locations from the ship model, but had difficulties in the stern region at the lower speed. The Das Boot program uses an interface tracking method, and required the use of a breaking model in

76

order to handle the steepness of the waves. This is a well established method, however, for predicting wave heights in the farfield and can be done quickly. The NFA Euler code provided a lot of fine details in the wave field topography and reasonably good predictions of the wave cuts, but used extremely fine grids and enormous computational resources. The two sets of RANS solutions with CFDSHIP-IOWA using the level-set interface capturing method, and the two commercial RANS solvers, Fluent and Comet, using the volume of fluid method, provided reasonably good predictions of the wave field topography and the wave cuts for moderate computational costs. The commercial solvers also provide a large amount of flexibility and ease of use with well defined graphical user interfaces. It is also unclear based on all the comparisons, how much the wave field and longitudinal wave cut predictions influence the predicted total resistance. It could be argued that the Fluent results for the lower Froude number were the worst at predicting the wave cuts, but it provided the closest comparison for the total resistance to the current measurement.

One of the goals of the workshop was to assess the capabilities of numerical methods to predict the wave breaking phenomenon. It was clearly demonstrated that the interface capturing methods, either using the level-set method or volume of fluid method, are able to predict steep waves and waves that overturn onto themselves. This is a departure from previous interface tracking methods, which required that the computational grid be stretched and modified to conform to the fluid interface. With the interface tracking methods it is not possible to accurately resolve the motion of a steep wave or an overturning wave because the grid would become too skewed, and to overturn on itself would produce a singularity. The interface capturing methods are not bound by this limitation because the fluid interface location is determined within the fixed grid structure.

It was further demonstrated that in order to predict the wave breaking phenomenon it is necessary to have sufficient spatial grid resolution in order to predict the changes in the fluid interface shape. There are economical ways to achieve this without simply producing fine computational grids throughout the entire domain. The CFDSHIP-IOWA solutions take advantage of chimera grid refinement to provide better grid resolution in certain regions. The commercial solvers, Fluent and Comet, have grid adaption capabilities that are based on different methodologies to provide better spatial resolution either in restricted regions, or based on local solution results. The grid adaption capabilities in Fluent were not attempted during the time of this workshop, but it is anticipated that these types of methods would provide improved solutions for relatively minor computational cost increases.

Another issue that was not addressed in this workshop was the use of unstructured computational meshing techniques. For a reasonably smooth lined hull form without any appendages or propulsor, it is reasonable to use structured grid methods to define the hull form and the nearby fluid volume. With more complex hull shapes, and with the addition of appendages, however, unstructured mesh techniques become much more attractive and require significantly less time to develop a computational mesh for a given hull form. For these cases, there would seem to be an inherent advantage for the commercial solvers used here since they have the flexibility of using unstructured computational meshes as well. This coupled with region based or solution based grid adaption techniques would

seem to be the most robust and computationally economical way to provide accurate free surface predictions in the vicinity of surface ship hulls.

ACKNOWLEDGEMENTS

REFERENCES

1. Fu, T. C., Karion, A., Pence, A.M., Rice, J.R., Walker, D. & Ratcliffe, T., "Characterization of the Steady Wave Field of the High Speed Transom Stern Ship – Model 5365 Hull Form." Naval Surface Warfare Center, Carderock Division, Hydromechanics Directorate R&D Report, NSWCCD-50-TR-2005/046, August 2005, pp. 34.

2. Paterson, E. G., Wilson, R. V. and Stern, F., "General-Purpose Parallel Unsteady RANS Ship Hydrodynamics Code: CFDSHIP-IOWA," IIHR Report No. 432, Iowa Institute of Hydraulic Research, University of Iowa, November 2003.

3. Furey, D.A. and Fu, T.C., "Quantitative Visualization (QViz) Hydrodynamic Measurement Technique of Multiphase Unsteady Surfaces," 24th Symposium on Naval Hydrodynamics, Fukuoka, Japan, July 8-13, 2002.

4. Fu, T.C., Furey, D., Karion, A., Mutnick, I., Rice, J., Sur, T., and Walker, D. "Hydrodynamic Measurements of a Steady Wave During Various Breaking Conditions in the Circulating Water Channel," Naval Surface Warfare Center, Carderock Division, Hydromechanics Directorate R&D Report, NSWCCD-50-TR-2003/012, March 2003, pp. 30.

5. Karion, A., Sur, T., Fu, T.C., Furey, D., Rice, J., and Walker, D., "Experimental Study of the Bow Wave of a Large Towed Wedge," 8th International Conference on Numerical Ship Hydrodynamics, Busan, Korea. September 22-25, 2003.

6. Jenkins, D., "Resistance Characteristics of the High Speed Transom Stern Ship R/V Athena in the Bare Hull Condition Represented by DTNSRDC Model 5365," Ship Performance Dept. Research & Development Report, DTNSRDC-84/024, June 1984.

7. Wyatt, D. Das Boot presentation. ONR Ship Wavebreaking Workshop and Review. Reston, VA, April 4-5, 2004.

8. Fu, T. C., Overview Presentation. ONR Ship Wavebreaking Workshop and Review. Reston, VA, April 4-5, 2004.

9. Stern, F. and Wilson, R. CFDSHIP-IOWA presentation. ONR Ship Wavebreaking Workshop and Review. Reston, VA, April 4-5, 2004.

10. Dommermuth, D., O'Shea, T., and Wyatt, D., "Numerical Flow Analysis: NFA" presentation. ONR Ship Wavebreking Workshop and Review. Reston, VA, April 4-5, 2004.

Distribution

Copies

NAVSEA
1   05T   A. Reed (electronic)
1   DTIC

ONR
1   334   P. Purtell

DIVISION DISTRIBUTION
1   3442   TIC
1   5010   (w/o enclosure)
1   5060   D. Walden
1   5200   D. Hendrix, T. Ratcliffe D. Walker (w/o enclosure)
1   5400   J. Gorski, L. Mulvihil, R. Miller (electronic)
1   5400   W. Wilson
1   5600   T. Fu
1   5600   A. Fullerton , J. Rice (electronic)

SAIC
2   D. Wyatt, D. Dommermuth (electronic)

University of Iowa (IIHR)
2   F. Stern, P. Carrico (electronic)

University of Tennessee, Knoxville
1   R. Wilson (electronic)